

**SUBLIMATION GROWTH OF ALN BULK CRYSTALS AND HIGH-
SPEED CVD GROWTH OF SIC EPILAYERS, AND THEIR
CHARACTERIZATION**

by

PENG LU

B. S., Beijing University of Chemical Technology, 1999

M.S., Kansas State University, 2004

AN ABSTRACT OF A DISSERTATION

**Submitted in partial fulfillment of the
requirement for the degree**

DOCTOR OF PHILOSOPHY

**Department of Chemical Engineering
College of Engineering**

KANSAS STATE UNIVERSITY

Manhattan, Kansas

2006

ABSTRACT

The effects of process conditions on the material's properties were investigated for the sublimation growth of aluminum nitride and the epitaxial growth of silicon carbide. Since the mid 1990's, these semiconductors have made new types of high power electronics and short wavelength optoelectronics that were never before feasible.

The sublimation growth of AlN crystals on SiC seeds was carried out to produce high quality AlN bulk crystals. Si-face, 3.5 ° off-axis 6H-SiC (0001) and 8 ° off-axis 4H-SiC (0001) wafers were used as the substrates. An investigation of the initial growth demonstrated 1800 – 1850 °C was the optimum temperature for AlN growth. By optimizing the temperature gradient, large area AlN layer was deposited. Consecutive growths and continuous growth were performed to enlarge the crystal thickness. Single-crystalline AlN layers, each with a thickness of 2 mm and a diameter of 20 mm, were produced. X-ray diffraction confirmed the grown AlN had good crystal quality. Approximately 3 – 6 at% of Si and 5 – 8 at% of C were detected in the crystals by x-ray photoelectron spectroscopy, which came from the decomposition of SiC seeds and the degradation of the graphite components in the furnace. Molten KOH/NaOH etching revealed the dislocation density decreased from 10^8 cm^{-2} to 10^6 cm^{-2} as the AlN layer thickness increased from 30 μm to 2 mm.

Epitaxial growth of SiC was carried out in a chemical vapor deposition system. High-quality 6H-SiC and 4H-SiC homoepitaxial films were produced at growth rates up to 80 $\mu\text{m/hr}$ by using a novel single precursor, methyltrichlorosilane (MTS). Inclusions of 3C-SiC were circumvented by employing 8 ° mis-orientated substrates. Adjusting the

H₂/Ar flow ratio in the carrier gas effectively changed the C/Si ratio in the gas phase due to the reaction between H₂ and the graphite heater; thereby, influencing surface roughness and dislocation density. Low H₂/Ar ratios of 0.1 and 0.125 produced smooth surfaces without step-bunching. Higher H₂/Ar ratios of 0.2 and 0.33 enhanced the conversion of basal plane dislocations into threading edge dislocations, and reduced the density of basal plane dislocations to approximately 600 cm⁻².

**SUBLIMATION GROWTH OF ALN BULK CRYSTALS AND HIGH-
SPEED CVD GROWTH OF SIC EPILAYERS, AND THEIR
CHARACTERIZATION**

by

PENG LU

B. S., Beijing University of Chemical Technology, 1999

M.S., Kansas State University, 2004

A DISSERTATION

**Submitted in partial fulfillment of the
requirement for the degree**

DOCTOR OF PHILOSOPHY

**Department of Chemical Engineering
College of Engineering**

KANSAS STATE UNIVERSITY

Manhattan, Kansas

2006

Approved by:

Major Professor

Dr. James H. Edgar

ABSTRACT

The effects of process conditions on the material's properties were investigated for the sublimation growth of aluminum nitride and the epitaxial growth of silicon carbide. Since the mid 1990's, these semiconductors have made new types of high power electronics and short wavelength optoelectronics that were never before feasible.

The sublimation growth of AlN crystals on SiC seeds was carried out to produce high quality AlN bulk crystals. Si-face, 3.5 ° off-axis 6H-SiC (0001) and 8 ° off-axis 4H-SiC (0001) wafers were used as the substrates. An investigation of the initial growth demonstrated 1800 – 1850 °C was the optimum temperature for AlN growth. By optimizing the temperature gradient, large area AlN layer was deposited. Consecutive growths and continuous growth were performed to enlarge the crystal thickness. Single-crystalline AlN layers, each with a thickness of 2 mm and a diameter of 20 mm, were produced. X-ray diffraction confirmed the grown AlN had good crystal quality. Approximately 3 – 6 at% of Si and 5 – 8 at% of C were detected in the crystals by x-ray photoelectron spectroscopy, which came from the decomposition of SiC seeds and the degradation of the graphite components in the furnace. Molten KOH/NaOH etching revealed the dislocation density decreased from 10^8 cm^{-2} to 10^6 cm^{-2} as the AlN layer thickness increased from 30 μm to 2 mm.

Epitaxial growth of SiC was carried out in a chemical vapor deposition system. High-quality 6H-SiC and 4H-SiC homoepitaxial films were produced at growth rates up to 80 $\mu\text{m/hr}$ by using a novel single precursor, methyltrichlorosilane (MTS). Inclusions of 3C-SiC were circumvented by employing 8 ° mis-orientated substrates. Adjusting the

H₂/Ar flow ratio in the carrier gas effectively changed the C/Si ratio in the gas phase due to the reaction between H₂ and the graphite heater; thereby, influencing surface roughness and dislocation density. Low H₂/Ar ratios of 0.1 and 0.125 produced smooth surfaces without step-bunching. Higher H₂/Ar ratios of 0.2 and 0.33 enhanced the conversion of basal plane dislocations into threading edge dislocations, and reduced the density of basal plane dislocations to approximately 600 cm⁻².

TABLE OF CONTENTS

LIST OF FIGURES	ix
LIST OF TABLES	x
ACKNOWLEDGEMENTS	xi
DEDICATION	xii
CHAPTER 1 INTRODUCTION	1
1.1 Bulk Crystal Growth of AlN	1
1.2 Epitaxial Growth of SiC	3
CHAPTER 2 LITERATURE REVIEW OF ALUMINUM NITRIDE	6
2.1 Structures & Properties of AlN	6
2.2 Applications of AlN	10
2.3 Crystal Growth of AlN	12
CHAPTER 3 LITERATURE REVIEW OF SILICON CARBIDE	23
3.1 Structures & Properties of SiC	23
3.2 Applications of SiC	28
3.3 Crystal Growth of SiC	30
CHAPTER 4 EXPERIMENTAL & CHARACTERIZATION	35
4.1 Sublimation Growth of AlN	35
4.2 Epitaxial Growth of SiC	40
4.3 Wet Chemical Etching	44
Characterization Techniques	45
REFERENCES	49

PAPER I	Nucleation of AlN on SiC substrates by seeded sublimation growth (Accepted by the Journal of Crystal Growth)	61
PAPER II	Bulk AlN crystal growth on SiC seeds and defects study (Submitted to the Material Research Society Symposium Proceeding)	83
PAPER III	Seeded growth of AlN on SiC substrates and defect characterization (unpublished)	98
PAPER IV	High-speed homoepitaxy of SiC from methyltrichlorosilane by chemical vapor deposition (Journal of Crystal Growth, Vol. 285 (2005) 506)	120
PAPER V	The influence of the H ₂ /Ar ratio on surface morphology and structural defects in homo-epitaxial 4H-SiC films grown with methyltrichlorosilane (Accepted by the Journal of Applied Physics)	141

LIST OF FIGURES

Figure 2.1 Wurtzite AlN crystal structure

Figure 2.2 Schematic drawing of the AlN primitive unit cell indicating (a) Al-polar and (b) N-polar structures.

Figure 2.3 (a) Polycrystalline AlN boule grown at 1930 °C for a total of 130 hours, (b) predominantly c-plane AlN wafer cut radially and polished from the AlN boule, and (c) cross sectional AlN wafer cut axially and polished from the AlN boule.

Figure 3.1 The tetragonal bonding of a carbon atom with four nearest silicon neighbors.

Figure 3.2 Three possible relative positions, A, B, and C, in close-packed crystal structure, from the view perpendicular to *c*-axis.

Figure 3.3 The [1120] plane of the 3C-, 2H-, 4H-, and 6H-SiC polytypes.

Figure 3.4 Schematic images of the relationship between growth modes and polytypes of layers grown on 6H-SiC: (a) 3C-SiC is grown by two-dimensional nucleation, and (b) homoepitaxy of 6H-SiC is achieved owing to step-flow growth.

Figure 4.1 (a) Schematic and (b) photograph of the resistively heated graphite furnace.

Figure 4.2 Temperature profile inside the furnace at 60% of power output.

Figure 4.3 The lifetime of a graphite-heating element at different growth temperatures.

Figure 4.4 (a) A schematic of the CVD system, (b) photograph of the vertical quartz reactor, and (c) photograph of the entire system.

Figure 4.5 AFM images of (a) as received 6H-SiC wafer and (b) 6H-SiC after etched in H₂ at 1600 °C for 15 mins.

LIST OF TABLES

Table 2.1 Properties of wurtzite AlN at room temperature.

Table 2.2 Advantages and disadvantages of MOCVD, MBE and HVPE

Table 3.1 Structural and physical properties of SiC at room temperature

Table 3.2 Electrical properties of SiC

Table 3.3 SiC properties and potential applications

ACKNOWLEDGEMENTS

I would like to first express my sincere thanks to my major advisor, Dr. James H. Edgar, for his kindness of introducing me to the field of wide bandgap semiconductors, guidance and valuable suggestions in research, constant support throughout my graduate study and assistance in composing this dissertation. Without his patience and encouragement, I would have not been able to complete this work.

Acknowledgements extend to Dr. L.T. Fan and Dr. Larry A. Glasgow in Chemical Engineering, Dr. Jingyu Lin in Physics, and Dr. Robby in Computing and Information Science for their time and efforts on reviewing this work. I really appreciate the collaborations from Dr. Keith L. Hohn's group for x-ray photoelectron spectroscopy, Dr. Hongxing Jiang and Dr. Jingyu Lin's group for photoluminescence measurements, Dr. Douglas S. McGregor's group for scanning electron microscopy, Dr. Zlatko Sitar's group in North Carolina State University for high resolution x-ray diffraction measurements, and Dr. Jharna Chaudhuri's group in Texas Tech University for x-ray diffraction measurements.

Additional appreciation goes to my colleagues, Dr. Bei Liu, Dr. Dejin Zhuang, Dr. Zheng Gu, Ms. Chundi Cao and Ms. Li Du for their support and help. The professional help from Mr. David Threewit was indispensable.

The financial support from the National Science Foundation through grant number DMR-0408874 is greatly appreciated.

Finally, special thanks to my parents and my lovely wife for their support and encouragement through all my endeavors.

DEDICATION

To My Family

CHAPTER 1 INTRODUCTION

Aluminum nitride (AlN) and silicon carbide (SiC) are two very unique materials in semiconductor industry and research. Their crystal structures, physical properties and electrical properties make them attractive for fabrication of optical and electrical devices. In this present work, the progress made in bulk crystal growth of AlN and the epitaxial growth of SiC are reported. In addition, the methods of characterizing their crystal quality, surface morphology, and defects density are also discussed.

1.1 Bulk Crystal Growth of AlN

Group III nitrides, GaN, AlN and InN, are recognized as superior semiconductor materials for short wavelength optoelectronic devices and high temperature, high power, and high frequency electronic devices, which have potential markets of billions dollars. GaN and its alloys with AlN and InN, are excellent candidate materials for violet, blue and green light emitting diodes (LEDs) due to their direct and wide band gaps (GaN 3.4 eV, AlN 6.2 eV, and InN 0.85 eV) [1]. GaN forms solid solutions with AlN and InN allowing the specification of the band gap, which is essential for defining the emission wavelengths of the LEDs. The spectrum of GaN based LEDs can be varied from ultra violet (200 nm for pure AlN) to infrared (1460 nm for pure InN) [2]. This flexibility in tailoring of emission wavelengths makes LEDs practical for many applications including red and green LEDs for traffic signals, white LEDs for conventional light sources, and UV LEDs for military, medical, and biotechnology sensors. The advantages of the solid

state LEDs compared with other light sources include high luminous efficiency, low maintenance, small volume, quick response speed and long life.

GaN is also suitable for short wavelength (UV to green spectral region) laser diodes (LDs). Switching to short wavelength LDs increases the storage capacity of optical discs and enhances the resolution of laser scanners and printers compared to traditional GaAs based LDs.

Group III nitrides are also employed in high power and temperature electronics such as switches because of their remarkable physical properties, such as good thermal conductivities, large dielectric breakdown voltages, high electron drift velocities in large electric fields, huge current carrying capacities, and good physical and chemical stabilities [2].

Due to the lack of native bulk crystals, GaN based devices are typically deposited on foreign single crystal substrates, such as sapphire and silicon carbide (SiC), by metal organic chemical vapor deposition (MOCVD), molecular beam epitaxy (MBE), and hydride vapor phase epitaxy (HVPE). The mismatch in lattice constant and thermal expansion coefficient generates high density of dislocations, typically $10^8 - 10^{11} \text{ cm}^{-2}$ [3], in nitride layer. The high dislocation densities cause many problems such as increased device threshold voltage and reverse bias leakage currents, depleted sheet charge carrier concentration in heterostructure field effect transistors, reduced charge mobility and thermal conductivity, and degraded *pn* junction abruptness [3].

Native crystals are an appealing alternative to foreign substrates. For example, AlN bulk crystals are an ideal substrate for the growth of III-nitride epilayers and heterostructures. The advantages of single crystal AlN substrates include: small mismatch

in lattice constant and thermal expansion coefficient with GaN; chemical compatibility; steps on isomorphic substrates without leading to stacking mismatch boundary (SMB); polar surface; and less contamination from substrates due to high stability and the absence of foreign elements. Compared to GaN bulk crystals, AlN is an even better substrate for high Al-content AlGaIn epitaxy (essential for short-wavelength emitters and detectors), where lattice matching is a critical factor to avoid dislocations and cracks.

In this work, the sublimation growth of AlN bulk crystals was studied. Since single crystalline AlN wafers are not commercialized, AlN bulk crystals were deposited on foreign substrates, 4H-SiC or 6H-SiC. 4H- and 6H-SiC have similar crystal structures and small lattice mismatch with AlN, and high quality wafers are commercially available, therefore, they are the suitable substrates for AlN bulk crystal growth. The growth was carried out in a temperature range of 1800 – 1950 °C and at a pressure of 800 torr in ultra high purity (UHP) nitrogen. First, the nucleation of AlN on SiC substrate was investigated to explore the initial growth mechanism of AlN; second, large area (up to 20 mm in diameter) AlN layers were grown by optimizing the growth temperature and temperature gradient; and third, single-crystalline AlN layers, each with a diameter of 20 mm and a thickness of 0.5 – 2 mm, were successfully achieved by long period growth and consecutive growth.

1.2 Epitaxial Growth of SiC

Silicon carbide (SiC) is an excellent candidate for high-power, high-frequency and high-temperature electronic devices because of their remarkable properties including wide bandgap, high breakdown field, high thermal conductivity, and high electron

saturation drift velocity [4]. In contrast to the group III nitrides, SiC is an indirect band gap semiconductor, therefore SiC is only used for electronic devices and not for optoelectronic devices. A major advantage of SiC over GaN is that single-crystalline wafers of 4H- and 6H-SiC are commercially available. Thus, no heteroepitaxy is required, thereby avoiding many problems that plague GaN.

SiC based devices such as switching and rectifying devices can be operated at higher voltages, higher current densities and more duty cycles than Si based devices. For the same power level, SiC power devices can be much smaller than Si devices. Due to its large band gap, high thermal conductivity and good stability, SiC is attractive for electronic devices that can operate at high temperatures (exceeding 300 °C), much higher than silicon-based devices.

SiC epitaxial growth is usually performed by chemical vapor deposition (CVD). The conventional technique, which uses silane (CH_4) and propane (C_3H_8) as the precursors, can only produce the growth rate less than 10 $\mu\text{m/hr}$. Rates are limited in part by gas phase homogeneous nucleation of Si, due to the irreversible decomposition of silane. Consequently, with these precursors it is not practical to deposit uniform and thick ($>150 \mu\text{m}$) epilayers, which are required for high voltage, high power SiC transistors.

In this present work, an alternative chemistry was examined, to achieve higher growth rates. Epitaxial layers of 4H- and 6H-SiC were grown with a single precursor methyltrichlorosilane, CH_3SiCl_3 (MTS), a reactant widely employed to deposit polycrystalline 3C-SiC protective layers on graphite, but rarely used in epitaxy. In the present study, 4H- and 6H-SiC homo-epitaxial layers were deposited with high growth rate up to 80 $\mu\text{m/hr}$. Crystal quality was characterized by x-ray diffraction rocking curves

(XRC), Raman spectroscopy, and photoluminescence (PL). Molten KOH/NaOH eutectic etching was employed to explore the surface and structural defects. Micropipes, threading screw dislocation (TSD), threading edge dislocation (TED) and basal plane dislocation (BPD) were observed and their densities were measured. Based on the etching results, the growth process was modified to produce the epilayer with a low dislocation density in the order of 10^4 cm^{-2} .

CHAPTER 2 LITERATURE REVIEW OF ALUMINUM NITRIDE

2.1 Structures & Properties of AlN

At ambient conditions, the wurtzite structure for AlN is thermodynamically stable [1]. The wurtzite structure has a hexagonal unit cell and thus two lattice constants, a and c , as illustrated in Fig. 2.1. The space grouping for the wurtzite structure is $P6_3mc$ [2], the same as that of the hexagonal (4H and 6H polytypes) SiC. Each unit cell contains 6 atoms of each type. The wurtzite structure consists of two interpenetrating hexagonal close packed (HCP) sublattices, each with one type of atom, offset along the c -axis by $5/8$ of the cell height ($5/8 c$) [1]. Wurtzite AlN has ABABAB... repeated bilayers stacking sequence along $\langle 0001 \rangle$ direction, hence it is 2H polytype denoted by Ramsdell notation, which is a number followed by a letter [3]. In c -plane (0001), AlN is 3-fold symmetric. The number of dangling bonds for the atoms on single bilayer steps is different and repeated every 120 degrees [3]. This is the reason why the III-nitride films will form stacking mismatch boundary (SMB) on a non-isomorphic substrates such as SiC [3].

The wurtzite structure is non-centrosymmetric, and thus AlN possesses different properties along different $\langle 0001 \rangle$ polar directions [5]. The basal plane (i.e. the (0001) plane of AlN crystals can be either Al or N polar [6]. The polarity of AlN can be defined with respect to the relative positions of the Al atom and N atom in the $\{0001\}$ bilayer. As the crystal surface is approached from the bulk along the c -direction, if the long bond goes from the nitrogen atom to the Al atom, the crystal is nitrogen polar. If instead the long bond goes from the Al atom toward the nitrogen atom, the crystal is Al polar [6], as

illustrated in Fig. 2.2. The polarity of AlN significantly affects its surface and bulk properties [7-14] as well as its electrical and optical properties [15-19].

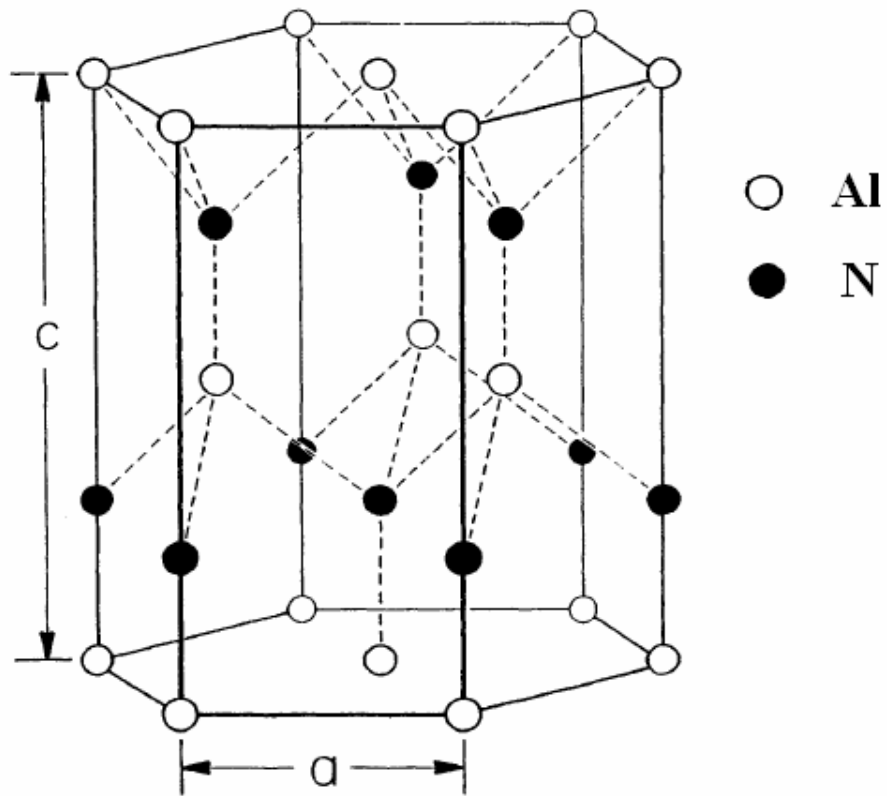


Fig. 2.1 Wurtzite AlN crystal structure [1]

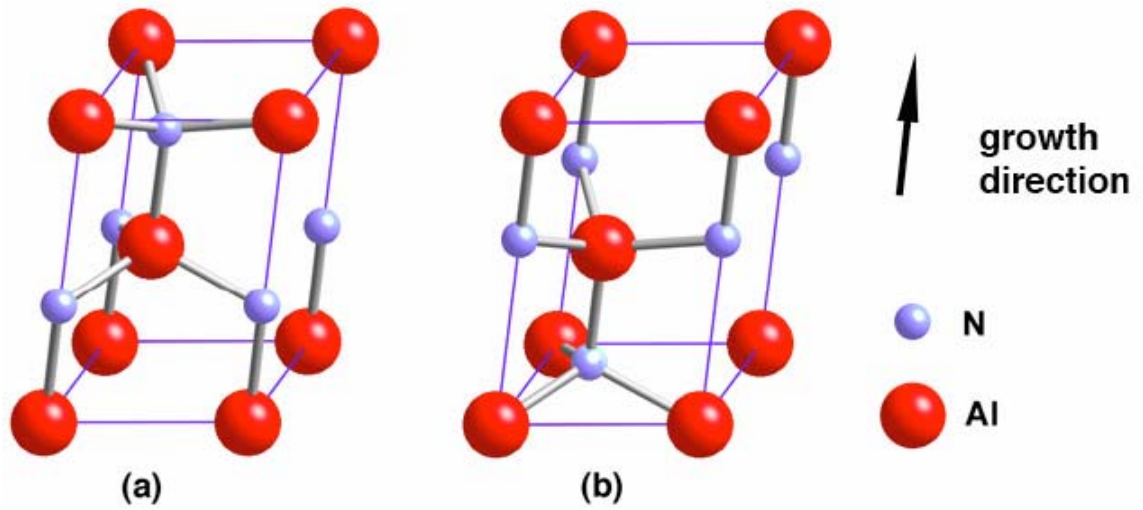


Fig. 2.2 Schematic drawing of the AlN primitive unit cell indicating (a) Al-polar and (b) N-polar structures [5][20].

The large difference of ionic natures between Al atoms and nitrogen atoms results in high bond energy in AlN crystals, which consequently results in its wide bandgap and high thermal and chemical stability. Table 2.1. summarizes some structural, physical and electrical properties of AlN [21-30].

Table 2.1 Properties of wurtzite AlN at room temperature

Properties	Value	Reference
Lattice constant (bulk crystal, nm)	$a = 0.31106, c = 0.4979$	[21]
Density (g/cm ³)	3.28	[22]
Melting point	2800 °C at 100 atm	[23]
Heat capacity (J/mol K)	29.83	[21]
Thermal conductivity (bulk crystal) (W/cm K)	2.85	[24]
Thermal expansion coefficient (linear) $\times 10^{-6}\text{K}^{-1}$	$a = 2.9, c = 3.4$	[21]
Percentage change in lattice constants (300 – 1400 K)	$\Delta a/a_0: 0.6415$ $\Delta c/c_0: 0.5349$	[25]
Bulk modulus (GPa)	201	[26]
Young's modulus (GPa)	344.83	[27]
Refractive index	2.15 ± 0.5	[28]
Dielectric constant	$\varepsilon(0) : 8.5 \pm 0.2$ $\varepsilon(\infty) : 4.68, 4.84$	[28]
Band gap (bulk crystal, eV)	6.2	[29]
Electrical resistivity (Ω cm)		
Undoped	10^7 to 10^{13}	[30]
n-, p-type	400, 10^3 to 10^5	

2.2 Applications of AlN

The principle application for AlN bulk crystals will be as an ideal substrate for III-nitrides (GaN, InN) epitaxy. Heterostructure deposited on AlN substrates have a wide range of applications in high temperature/high power microelectronics and optoelectronic devices.

Due to the high equilibrium nitrogen pressure over GaN and its high melting point (~ 2300 °C), growing bulk GaN crystals via high nitrogen pressure solution (HNPS) is extremely difficult, requiring high system pressure (above 10 kbar) and high temperature (up to 1700 °C) [6]. Although the recent development in another approach, hydride vapor phase epitaxy (HVPE) [6], can successfully produce bulk crystals of GaN, the high dislocation density ($10^8 - 10^{10}$ cm⁻²) impedes its application in device fabrication.

Most of the GaN devices to date have been fabricated heteroepitaxially on commercially available foreign substrates, such as sapphire and SiC. The large lattice mismatches between the epilayers and substrates caused high dislocation density in heteroepitaxial GaN, typically in the range of $10^8 - 10^{11}$ cm⁻² [31, 32]. Such high dislocation densities, combined with other defects including micropipes, inversion domain boundaries, and stacking faults, increase the device threshold voltage; reverse bias leakage currents; deplete sheet charge carrier concentrations in heterostructure field effect transistor; degrade *pn* junction abruptness; and reduce the charge mobility and thermal conductivity, and thus significantly reduce the efficiency, shorten the lifetime and increase the cost of GaN based devices [33]. Furthermore, the thermal expansion mismatch between substrate and epilayer introduces stress resulting in cracks in the epilayer.

As an ideal substrate for GaN based devices, the advantages of AlN include: a small lattice constant mismatch ($\sim 2.4\%$ in a-axis [3]) and a small difference in thermal expansion coefficient with GaN; chemical compatibility; steps on isomorphic substrates without leading to SMBs; polar surface; and less contamination from substrates due to the substrate and the epilayer contain the same elements. Compared to GaN bulk crystals, AlN is even a better substrate for high Al-content AlGaN epitaxy (essential for short-wavelength emitters and detectors), where a lattice matching is a critical factor to avoid dislocations and cracks [3, 6]. The number of reports on the applications of bulk AlN crystals is increasing and includes its use in the fabrication AlGaN LEDs [34], high quality GaN epilayers [35, 36], AlGaN/GaN HFET devices [37], deep UV emitters, and multi- quantum well structures [38-40].

In addition to being a good substrate for epitaxy of GaN, AlN finds its own applications in surface acoustic wave (SAW) devices and short wavelength LEDs/LDs, where good piezoelectric properties and higher bandgap energies are preferred [6]. Moreover, AlN is a good substrate for certain electronic devices, such as field effect transistors (FET) because its high resistivity (on the order of $10^{11} \sim 10^{13} \Omega\cdot\text{cm}$ [41-44]) simplifies the device isolation process. The high electrical resistivity of AlN makes it attractive as insulating films for metal insulator semiconductor or as passivating layers [45, 46].

2.3 Crystal Growth of AlN

2.3.1 Growth Methods

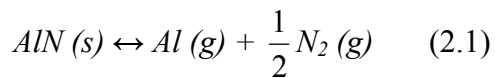
Metal organic chemical vapor deposition (MOCVD) [47-53], molecular beam epitaxy (MBE) [54-57], and HVPE [58-60] are the most studied epitaxial growth techniques for depositing AlN epitaxial layers. MOCVD can produce high quality AlN thin films on foreign substrates (SiC, Sapphire) with high throughput and low cost. In addition to a high growth rate (on the order of 1 ~ 10 $\mu\text{m/hr}$), MOCVD provides uniform coverage of non-planar shapes, and the layer thickness can be monitored *in situ*. Combined with the epitaxial lateral overgrowth (ELO) technique, MOCVD can produce GaN films with dislocation densities as low as 10^6 cm^{-2} [61]. MBE has the advantages of better control of growth parameters, relatively low growth temperature, no hydrogen carrier gas involved, and *in situ* characterization [6]. However, due the low growth rate (less than 10 $\mu\text{m/hr}$), MOCVD and MBE are only capable of growing epitaxial thin films, but not bulk crystals. Moreover, the large mismatch in lattice constants and the thermal expansion coefficients between AlN and foreign substrates (SiC and sapphire) generates a high density of dislocations ($10^9 \sim 10^{10} \text{ cm}^{-2}$ [62, 63]) and cracking in AlN films. HVPE is successful in producing free-standing GaN bulk crystals with high growth rate (10 ~ 100 $\mu\text{m/hr}$). The synthesis of freestanding AlN crystals by HVPE is complicated and is only in the initial states of development. The complications from excessive impurity incorporation, originating from the reactions between AlCl_3 and quartz reactor wall, and severe homogeneous gas phase reactions have hindered the development of AlN HVPE [6]. Table 2.2. summarizes the advantages and disadvantages of MOCVD, MBE and HVPE.

Table 2.2 Advantages and disadvantages of MOCVD, MBE and HVPE [6]

Growth Technologies	Advantages	Disadvantages
MOCVD	<p>High growth rate and throughput</p> <p>Low dislocation density (using ELO)</p> <p>Atomically sharp interface</p> <p>Uniform coverage and large area growth</p> <p>Scalable for mass production</p>	<p>Lack of precise <i>in situ</i> characterization</p> <p>Need large quantities of NH₃</p> <p>Thin film growth only</p>
MBE	<p>Precise control of Growth parameters</p> <p>Relative low growth temperature</p> <p>No hydrogen involved</p> <p>Atomically sharp interfaces</p> <p>In situ characterization</p> <p>High purity growth environment</p>	<p>Require ultra high vacuum</p> <p>Low throughput and growth rate</p> <p>Thin film growth only</p> <p>High dislocation density</p>
HVPE	<p>Very high growth rate</p> <p>Bulk crystal growth</p> <p>Simple growth technique</p>	<p>High dislocation density</p> <p>Complicated reactions in vapor phase</p>

For AlN, the sublimation-recondensation method (abbr. Sublimation) is so far the most successful bulk crystal growth technique. In semiconductor industry, single crystal boules are typically grown from melts, e.g. Si. Due to its high melting temperature and large dissociation pressure at the melting point [64], bulk crystal growth of AlN from the melt is impossible. Other growth methods including vaporization [65] and solution routes [66] have been studied and proved impractical. Recently, Schlessner *et al.* [67, 68] achieved bulk AlN crystal growth via a vaporization method using high purity aluminum (Al) metal and ultra high purity (UHP) nitrogen as source materials. Transparent *c*-plates, each with the size up to $10 \times 5 \text{ mm}^2$, were grown at $2100 \text{ }^\circ\text{C}$ with a growth rate of 5 mm/hr [67]. The high growth rate was attributed to the higher Al vapor pressure over pure Al metal than AlN. However, longer-term growth was impeded by the formation of a nitride layer over the metallic Al source, which gradually decreased the Al vapor pressure [67].

Sublimation growth of AlN involves physical vapor transport (PVT), as developed by Slack *et al.* [69, 70] in 1970's. In a sublimation process, AlN source material decomposes to gaseous Al and nitrogen at an elevated temperature, and are subsequently transported through a temperature gradient to a region held at a lower temperature than the source, where they recrystallize into crystals. This process follows the reaction:



To effectively enhance and control the growth rate, nitrogen is used as the process gas during growth and is independently controlled [6]. Although the sublimation process has a lower growth rate than that in the vaporization and solution routes, it has advantages of

long-term growth capability and easy implementation of the process. To date, several research groups have demonstrated bulk growth of AlN by sublimation. [71-77]

2.3.2 AlN Crystal Growth by Sublimation

The process of sublimation growth consists of several steps: sublimation of the source materials; mass transport in the bulk gas phase; adsorption on the growth surface; surface diffusion; and surface desorption [71]. Various factors, including growth temperature, ambient gas pressure, mass transport, growth kinetics, impurity incorporation, and thermodynamics, influence the resulting crystals. Sublimation growth of AlN is challenging because of its high process temperature, absence of appropriate substrate/seeding materials, and lack of chemically/physically stable crucible materials. Recent progress in AlN sublimation growth is summarized below.

2.3.2.1 The Effects of Temperature and Pressure

Temperature is the most important factor controlling the crystal growth habit [72, 73]. Sublimation of AlN is feasible over a wide range of temperatures starting from 1850 °C [72], but stable growth of well-faceted crystals is possible only at temperatures exceeding 2100 °C [73]. However, according to thermodynamic calculations, the growth temperature should not exceed 2493 °C, where the formation of liquid aluminum on nucleation surface is inevitable [69, 73]. By investigating self-nucleation on the crucible walls, Epelbaum *et al.* [74] found that the natural growth habit of AlN crystals are highly dependent on temperature: six-sided prismatic needles (in transparent and almost colorless), columnar rhombohedral crystals (in translucent and dark yellow), and thick

faceted crystals (in dark-amber) were obtained at relatively lower (2050 °C), medium (2150 °C), and higher temperatures (2250 °C), respectively [74]. Similar results were also observed by Tanaka *et al.* [75].

Pressure is another influential parameter in sublimation growth. Generally, lowering the total pressure leads to higher sublimation rate. At extreme condition, e.g. ultra high vacuum, the mass transport of reactive species switches from diffusion to drift, resulting in several orders of magnitude higher growth rate [76]. However, in AlN growth, N₂ has extremely low sticking coefficient at the crystal surface, which means only small fraction of the N₂ arriving at the surface incorporates into the crystal; the rest desorbs from the surface [77]. The availability of nitrogen atoms at the growing surface will be the rate-control step [77]. Thus, excess N₂ has to be provided and system pressure needs to be kept over 100 torr to enhance AlN growth [77]. Moreover, under supersaturation conditions (low pressure and high temperature), the relative high Al vapor mole fraction will degrade the performance of furnace fixture due to the volatile nature of aluminum vapor [3].

2.3.2.2 Self-Seeding Growth of AlN

In self-seeding growth, crystals are allowed to nucleate without any attempt to control their orientation. The AlN source materials sublime at elevated temperature, transport to the cooler end of the crucible, recondense, and crystallize as single crystals [3, 6]. Ideally, only one nucleus forms at the coldest point of the crucible in the initial stage, providing a perfect nucleation site for subsequent growth. In practice, numerous nuclei form, each of which may lead to single crystal grains at the initial stage of the

growth. With growth, these grains merge together and form a polycrystalline layer of AlN. As the layer grows thicker, some grains preferentially expand in the c -plane and grow over smaller grains. Eventually one or several single crystal grains will dominate the growing surface, as the crystal boule grows thick enough.

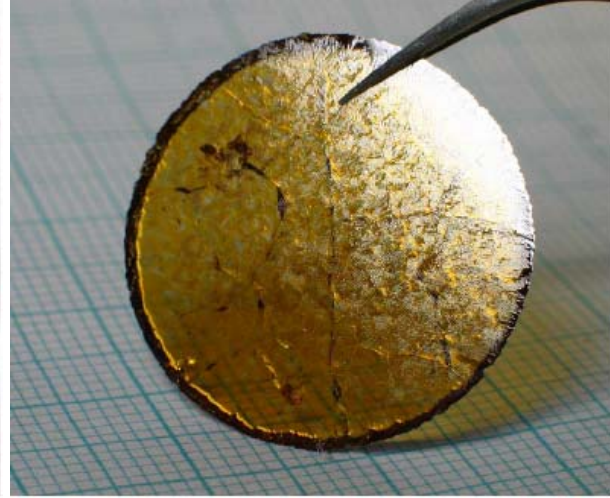
In comparison with seeded growth on foreign substrates (SiC or sapphire), self-seeding growth produces crystals with higher quality since the process avoids the stress-causing lattice mismatch and difference in thermal expansion coefficient. Furthermore, self-seeded growth also precludes the dislocations inherited from the foreign substrates. The growth temperature, and thus the growth rate, is higher than those in seeded growth, as substrate decomposition is not a concern in self-seeding growth.

At KSU, polycrystalline AlN boules, each with 15 – 20 mm long and 20 – 25 mm in diameter, were produced at 1930 °C with growth for a total 120 – 150 hours [78]. On the top of the boule, the maximum size of a single grain is $5 \times 5 \text{ mm}^2$, as shown in Fig. 2.3.(a). A predominantly c -plane polycrystalline AlN wafer and a cross sectional AlN wafer were cut and polished from AlN boules are shown in Fig. 2.3. (b) and (c), respectively [78].

Bikermann *et al.* [79] also reported an unpolished AlN wafer having single crystalline grains up to $5 \times 5 \text{ mm}^2$. Most recently, Zhuang *et al.*[80] demonstrated a AlN boule with single grain size up to $13 \times 15 \text{ mm}^2$ by repeated growth on a polycrystalline AlN seed cut from polycrystalline AlN boule.



(a)



(b)



(c)

Fig. 2.3 (a) Polycrystalline AlN boule grown at 1930 °C for a total of 130 hours, (b) predominantly c-plane AlN wafer cut radially and polished from the AlN boule, and (c) cross sectional AlN wafer cut axially and polished from the AlN boule [78].

2.3.2.3 Seeded Growth of AlN on SiC

Since single crystalline AlN wafers are not commercially available, seeded growth of bulk AlN is usually performed on SiC seeds. SiC has a good thermal stability and a small *a*-lattice constant mismatch (0.96% for 6H-SiC and 1.2% 4H-SiC) [81] with AlN. Large area (up to 100 mm in diameter) and high quality single crystalline 4H- and 6H-SiC (0001) wafers are commercialized, providing high quality seeds for AlN. The crystal orientation and polarity are more easily controlled with seeding compared to self-seeding growth.

Employing SiC as a seed to grow AlN was first reported by Campbell and Chang [82] in the 1960's. Twenty years later, Balkas *et al.* [83] grew single crystalline hexagonal AlN platelets ($2 \times 2 \text{ mm}^2$) on 6H-SiC substrates in a SiC-coated graphite crucible. A growth rate of 0.5 mm/hr was demonstrated in a temperature range of 2150 – 2250 °C. The AlN was contaminated with Si, C and O, and had a high density of screw dislocation and cracks [83]. The cracking was caused by thermal expansion mismatch between AlN and SiC, which was also reported by others [84]. Edgar and co-workers [71, 77, 85-89] designed a novel sublimation sandwich technique and utilized a tungsten resistively heating reactor to grow AlN on SiC. A MOCVD layer of AlN/SiC alloy was deposited on SiC substrate prior to pure AlN growth to compensate the thermal expansion and lattice mismatch. Though cracks and stress were not completely eliminated, a freestanding AlN crystal ($4 \text{ mm} \times 6 \text{ mm}$) was obtained after 100 hours growth [85]. The growth temperature, and thus the growth rate, was kept low to prevent the decomposition of SiC.

Liu *et al.* [81] summarized the major problems of seeded growth AlN on SiC: (1) cracks in AlN film are common due to the higher thermal expansion coefficient of AlN compared to SiC and the low critical shear stress of SiC; (2) SiC decomposition during the growth introduces Si and C into the AlN, or even worse forms an AlN and SiC alloy instead of pure AlN; and (3) achieving two dimensional growth on Si face (0001) is difficult since the growth is prompted by steps associated with screw dislocations.

Epelbaum *et al.* [90] reported similar observations of three-dimensional growth of AlN on Si-face on-axis (0001) 6H-SiC. However, they produced fully coalesced AlN layers by employing a slightly off-axis substrate, where the step-flow growth mode was achieved [90].

Most recently, Dalmau *et al.* [91] obtained 3 mm thick single crystal AlN layers on Si-face, on-axis 6H-SiC (0001) and off-axis 4H-SiC (0001) by “two-step growth”. First a fully coalesced AlN layer was grown at a low temperature around 1850 °C with a growth rate of 10 – 30 $\mu\text{m/hr}$, covering the SiC substrate. Then the temperature was raised 100 – 200 °C to achieve a high growth rate of 70 $\mu\text{m/hr}$. As-grown surface were characterized by sharp hexagonal hillocks [91]. Mokhov *et al.* [92] employed a similar procedure and successfully grew a 10-12 mm thick single crystal AlN layer on Si-face, SiC substrates. Wang *et al.* [93] and Balakrishnan *et al.* [94] carried out the AlN growth on C-face SiC substrates, and 650 μm and 300 μm thick AlN layers were obtained respectively. They claimed that C-face SiC can produce AlN layers with smoother surface [93] and higher growth rate [94] than Si-face SiC.

2.3.2.4. Chemical Stability of the Crucible

The sublimation growth of AlN requires high process temperatures in a range of 1800 – 2300 °C. Such extreme temperatures, combined with the chemically aggressive nature of Al vapor, severely limit the choice of crucible materials. Schlessner *et al.* [95] summarized the requirements of an ideal crucible material for AlN sublimation growth: (1) refractory and compatible with extreme temperatures; (2) inert to chemically aggressive Al vapor; (3) a negligible source of contamination to the growth progress; (4) re-usable for multiple growth runs; (5) relatively inexpensive, and (6) manufacturable in various shapes and dimensions.

Some promising candidate materials includes boron nitride (BN) and the nitrides/carbides of refractory transition metals (W, Ta, Nb, Zr) due to their high melting points and relatively low vapor pressure at high temperature.

BN has been extensively investigated as crucible material for AlN growth [67, 68, 96]. Crystals grown in BN were colorless and transparent, and the growth rate was anisotropic [96, 97]. Depending on growth temperature, crystals habits include whiskers, hexagonal platelets, and prisms. Some crystals had striations running along the growth directions, probably due to the boron incorporation [96, 97]. Compositional analysis by glow-discharge mass spectrometry (GDMS) shows about 100 ppm boron in grown crystals compared to only 2.5 ppm in the sintered AlN powder source [97].

The most successful crucible materials for AlN growth were all carried out in crucibles made of refractory transition metals (such as W [78]) and their carbides (such as TaC) [91, 97]. AlN growth is isotropic and its crystals are well faceted [97]. AlN nucleates in a much higher density on tantalum carbide (TaC) compared with BN, rapidly

forming a continuous deposit [96]. Prismatic needles and hexagonal hillocks were obtained in TaC and niobium carbide (NbC) coated graphite crucible [94]. However, crucibles made of nitrides or carbides suffer severe cracking, which was caused by the diffusion of aluminum and nitrogen along the grain boundaries and/or mismatch of thermal expansion coefficients [95-97].

Schlesser *et al.* [95] developed a successful process to manufacture TaC crucibles: sinter TaC powders into crucible shapes at high temperature yielding better than 96% dense TaC crucibles without measurable open porosity. The resulting crucibles were successfully re-used in multiple growth runs and had an average lifetime exceeding 200 hours.

Tungsten (W) is also a suitable crucible material for AlN growth. Gu *et al.* [78] obtained AlN boules in 15 mm long and 25 mm in diameter with low W contamination (< 20 ppm). Crystals grown in W crucible usually have an amber color, as shown in Fig. 2.3, presumably due to nitrogen vacancies or aluminum vacancies [69]. Though it was reported that W is prone to grain boundary attack by aluminum [69], the W crucible used in our group remains good shape after long growth times (> 100 hours). No Al was detected by scanning auger microscopy (SAM) in a piece of crushed W crucible [98]. Nevertheless, SiC seeded growth of AlN is not viable in a W crucible and heating-element furnace, since the sublimed Si reacts with W forming low melting point eutectic alloy, that ruins the crucible [90].

Based on the discussion above, TaC and W might be the best crucible materials for AlN sublimation growth with considering of lifetime and contamination.

CHAPTER 3 LITERATURE REVIEW OF SILICON CARBIDE

3.1 Structures & Properties of SiC

Silicon carbide (SiC) is the only chemically stable compound containing only silicon and carbon. Its crystalline structure consists of the close-packed stacking of double layers of Si and C atoms [97]. The basic unit of SiC is a covalently bonded tetrahedron of Si atoms with a C at its center or vice versa, i.e. either CSi_4 or SiC_4 [87], as illustrated in Fig. 3.1. The bonding of silicon and carbon atoms is 88% covalent and 12% ionic with a distance between the Si and C atoms of 1.89 Å [99]. The distance between the nearest Si atoms is approximately 3.08 Å.

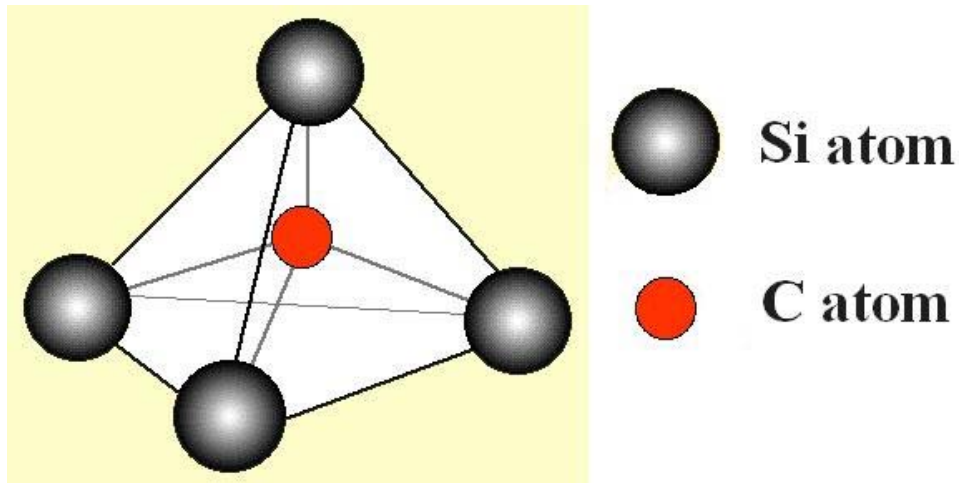


Fig. 3.1 The tetragonal bonding of a carbon atom with four nearest silicon neighbors.

SiC exists in more than 250 polytypes – one-dimensional variations of the stacking sequence of close packed biatomic planes [100]. The various polytypes are distinguished by the stacking order between the succeeding double layers of carbon and silicon atoms.

The stacking of the double layers follows one of three possible relative positions which are arbitrarily labeled A, B and C, as illustrated in Fig. 3.2.

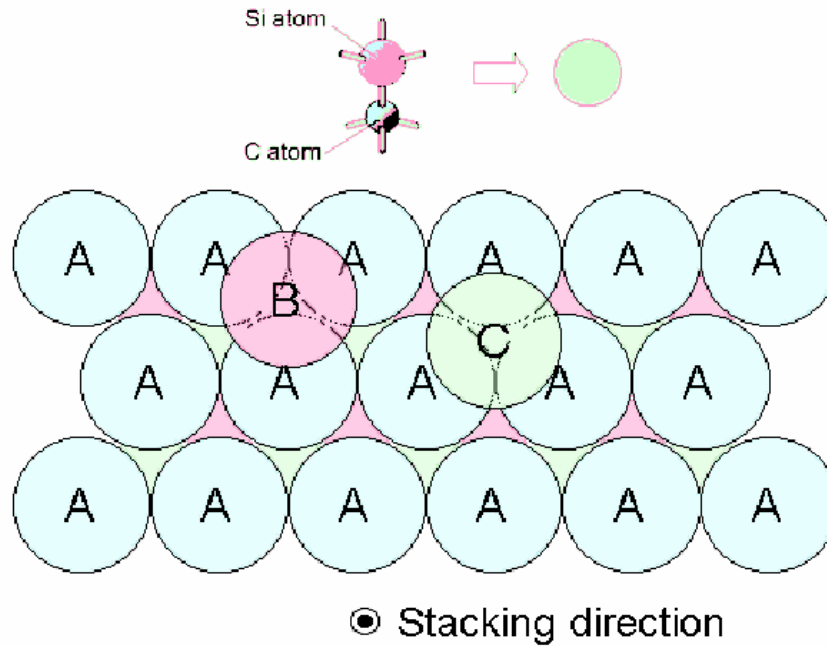


Fig. 3.2 Three possible relative positions, A, B, and C, in close-packed crystal structure, from the view perpendicular to c -axis.

The various polytypes are denoted by the Ramsdell notation consisting of a number followed by a letter [99]. The number represents the number of double layers in the stacking sequence before the sequence is repeated and the letter represents crystal structure: C – cubic, H – hexagonal and R – rhombohedral. The most common polytypes of SiC are 3C, 2H, 4H and 6H. 3C-SiC has the zincblende structure with a repeated sequence of ABC, while 2H-, 4H- and 6H-SiC have the hexagonal structure with repeated sequences of AB, ABAC, ABCACB, respectively. A distinct difference of the cubic polytype compared to the hexagonal polytypes is the absence of rotation in the stacking sequence. Thus the 3C structure proceeds in a straight line and hexagonal structures proceed in a zigzag pattern [101]. By observing the SiC crystal perpendicular

to the c -axis, the stacking sequence can be projected [87] as shown in Fig. 3.3. The height of the unit cell, c , varies with the different polytypes hence the ratio c/a also differs from polytype to polytype. The measured c/a ratios are approximately 1.641, 3.271 and 4.098 for the 2H-, 4H- and 6H-SiC polytypes, respectively, very close to the ideal values ($\sqrt{8/3}$, $2\sqrt{8/3}$ and $3\sqrt{8/3}$) [87]. The structural and physical properties of SiC in different polytypes are summarized in Table 3.1.

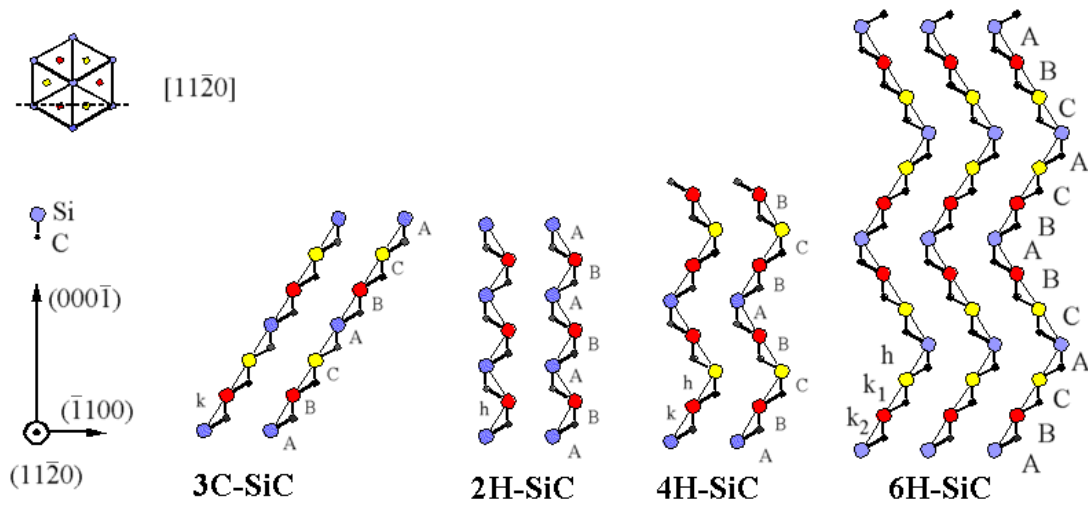


Fig. 3.3 The $[11\bar{2}0]$ plane of the 3C-, 2H-, 4H-, and 6H-SiC polytypes [100].

Each polytype has a unique set of electronic properties associated with its crystal structure. The bandgaps of the different polytypes at liquid helium temperature range from 2.39 eV (for 3C) to 3.33 eV (for 2H) [87]. The electrical properties of 3C, 4H- and 6H-SiC are summarized in Table 3.2.

Table 3.1 Structural and physical properties of SiC at room temperature

Properties	Polytype	Value	Reference
Lattice constant (Å)	3C	$a = 4.3596$	[103]
	4H	$a = 3.0730, c = 10.053$	
	6H	$a = 3.0806, c = 15.1173$	
Percentage change in lattice constants (300 –1400 K)	3C	$\Delta a/a_0: 0.5140$	[104]
	6H	$\Delta a/a_0: 0.4781$ $\Delta c/c_0: 0.4976$	
Density (g/cm ³)	3C	3.166	[105]
	6H	3.211	
Melting point (°C)	3C	2793	[106]
Thermal conductivity (W/cm K)	3C	3.2	[105]
	4H	3.7	
	6H	3.6	
Heat capacity (J/g K)	6H	0.71	[107]
Linear thermal expansion coefficient ($\times 10^{-6} \text{ K}^{-1}$)	3C	3.9	[108]
	6H	4.46 <i>a</i> -axis 4.16 <i>c</i> -axis	
Young's modulus (GPa)	3C	440	[109]
Refractive index (ordinary ray)	3C	2.6916 at the rate of $\lambda = 498 \text{ nm}$	[110]
	4H	2.6980 at the rate of $\lambda = 498 \text{ nm}$	
	6H	2.6894 at the rate of $\lambda = 498 \text{ nm}$	

Table 3.2 Electrical properties of SiC

	3C	4H	6H	Reference
Energy band gap (eV) (T < 5K)	2.39	3.26	3.02	[111]
Charge carrier mobilities (cm ² /V s) (300 K)				[111]
Electrons	800	1000	400	
Holes	40	115	101	
High breakdown electric field (V/cm)	2.1×10^6	2.2×10^6	2.4×10^6	[111]
High saturation drift velocity (cm/s)	2.0×10^7	2.0×10^7		[111]
Static dielectric constant	9.72		9.66	[111]
Electrical resistivity (undoped) (Ω cm)		$10^2 - 10^3$		[112]

3.2 Applications of SiC

4H- and 6H-SiC are the most important polytypes as they are excellent candidates for high-power, high-frequency and high-temperature devices because of their remarkable properties including wide bandgap, high breakdown field, high thermal conductivity, and high electron saturation drift velocity [113, 114]. Single-crystalline boules of 4H- and 6H-SiC are commercially available, which are produced by sublimation in the modified Lely process developed by Tairov and Tsvetkov [115]. The devices fabricated on 4H- and 6H-SiC have the advantages over their Si based counterparts including: higher operating voltages, higher current densities, more duty cycles, much smaller size and the ability to operate in harsh environments [116]. The applications of SiC and the related electrical properties are summarized in Table 3.3.

Because of these advantages, the military envisions incorporating increasing numbers of SiC-based devices into their systems. Their ultimate goal is to produce all electric ships and combat vehicles, and more electric aircraft; all with improve reliability, speed, and efficiency. The recent progress made in crystal growth, processing and fabrication yields will lower the price of SiC devices leading to their incorporation into commercial electronics.

Table 3.3 SiC properties and potential applications [117]

Wide Energy Bandgap

- High temperature operation of electronic devices, electromechanical actuators in airplanes, and sensors for deep-well drilling
- Radiation resistant devices
- Ultra-low leakage devices

High Breakdown Electric Field

- High voltage/high power switching diodes, transistor, thyristors, and surge suppressors
- High power MOSFETs for power applications in space
- High device packing in ICs

High Thermal Conductivity

- High power densities with good heat dissipation
- High integration density

High Saturated Electron Drift Velocity

- Microwave power transistors for radar
- Fast switching diodes

3.3 Crystal Growth of SiC

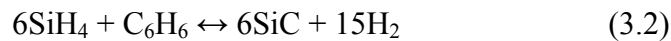
3.3.1 Bulk Crystal Growth of SiC

Bulk crystals of SiC were first commercialized in early 90's. Large boules of 6H-SiC were grown by a sublimation [118 – 120], which was first introduced by Lely in 1955 [121]. In the original Lely process, nucleation and crystal growth occurred randomly, and the resulting crystals were small and irregularly shaped. In the modified process, the sublimation growth of SiC was significantly improved by introducing single crystal SiC seed to control the crystal orientation, and by reducing the operating pressure of the reactor to increase the mass transport rate between the source material and the growing crystal. Carter *et al.* [122] modified the process, which produced 6H- and 4H-SiC wafers up to 4 inch in diameter.

3.3.2 Epitaxial Growth of SiC

SiC epitaxy has been mostly performed by chemical vapor deposition (CVD). CVD has advantages in controlling epilayer's thickness, uniformity, and precisely impurity doping [123].

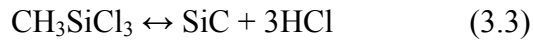
A common deposition system is based on the reaction of silane (SiH₄) with a hydrocarbon such as propane or benzene in the following simplified reactions [124]:



In most of the studies of SiC epitaxy, the first reaction was employed: silane (SiH₄) and propane (C₃H₈) as the precursors, since propane is less toxic than benzene. Epitaxial films of 4H- and 6H-SiC have been deposited on commercial 4H- and 6H-SiC wafers,

respectively, in cold wall reactors [123, 125-128]. However, the growth rate of the current technology is typically less than 10 $\mu\text{m/hr}$. Rates are limited in part by gas phase homogeneous nucleation of Si, due to the irreversible decomposition of silane. Consequently, with these precursors it is not practical to deposit uniform and thick ($>150 \mu\text{m}$) epilayers, which are required for high voltage, high power SiC transistors.

Another commonly used reaction in SiC deposition is the decomposition of methyltrichlorosilane, CH_3SiCl_3 (MTS) [124]:



MTS is widely employed to deposit polycrystalline 3C-SiC on graphite substrates as a protective coating against oxidation and etching [129-133]. In contrast, its use for SiC epitaxy is rare. Gorin *et al.* [134, 135] employed MTS to grow single crystal 3C-SiC platelets ($3\text{mm} \times 5\text{mm} \times 1.5 \text{mm}$) on graphite substrates at 1650–1750 $^\circ\text{C}$. Very high-quality crystals were produced at extremely high growth rates of 500 $\mu\text{m/hr}$. Zelenin *et al.* [136] deposited 6H-SiC epitaxial films on small misoriented ($0.5 - 2^\circ$) 6H-SiC (0001) substrates. 3C-SiC inclusions and 6H-SiC stacking faults were evident in their films. They made no attempt to maximize the growth rate.

Compared to the combination of silane and propane, there are several advantages of MTS. First, MTS has low thermal stability. Its decomposition begins at less than 600 $^\circ\text{C}$ and above 750 $^\circ\text{C}$ its equilibrium is completely shifted toward the formation of SiC [134]. Second, MTS contains chlorine, and HCl is produced as the reactant decomposes. The presence of HCl during SiC epitaxy can produce a more regular step and terrace structure, decrease the surface supersaturation, and reduce undesired nucleation sites for 3C-SiC [137, 138]. Third, it is a liquid, making it inherently safer than the gas sources

more typically used. Lastly, inexpensive but high-purity MTS is available, making it suitable for semiconductor synthesis. The disadvantage of MTS is the ratio of Si/C cannot be adjusted.

The simultaneous deposition of mixed polytypes is generally to be avoided in SiC epitaxy. 3C-SiC incorporates into 6H- or 4H-SiC epilayer forming inversion domain boundaries. One method to reduce this problem is to raise the growth temperature to 1800 °C to avoid 3C-SiC [139-141], since 3C polytype is unstable at high temperatures (> 1600 °C). Another solution, “step-controlled epitaxy”, was developed by Matsunami *et al.* [123] who employed a wafer with a misorientated cut off *c*-plane as a substrate. 3C free 6H-SiC film was deposited at 1500 °C on misorientated 6H-SiC substrate.

During SiC chemical vapor deposition, adsorbed species migrate on a surface and are incorporated into a crystal at steps and/or kinks where the potential is low. However, nucleation can also take place on terrace when the supersaturation is sufficiently high. On well-oriented {0001} faces, the terrace width is relatively huge and the step density low. Crystal growth may initially occur on terraces through two-dimensional nucleation due to the high supersaturation on the surface [123]. The polytype of SiC formed is highly dependent on the growth temperature. At a low temperature range, 1300 – 1500 °C, 3C-SiC is generated on the substrate. As the stacking sequence of 6H-SiC is ABCACB..., the growing 3C-SiC can take two possible stacking sequences of ABCABC...and ACBACB..., as shown in Fig. 3.4 (a). On misorientated substrates, the step density is high, and the terrace width narrow enough for adsorbed species to reach steps. At a step, the incorporation site is uniquely determined by bonds from the step, as shown in Fig. 3.4 (b). Therefore, homoepitaxy can be achieved through the lateral growth from steps (step-

flow growth), inheriting the stacking sequence of the substrates [123]. Powell *et al.* [142] found that homoepitaxy of 6H-SiC is possible even on substrates with a low tilt angle of 0.2 ° and 3C-SiC nucleation takes place at defect sites on the surface. Tairov *et al.* [119] observed stable homoepitaxy without 3C-SiC on mis-orientated substrates in a wide temperature range of 1600 – 2200 °C. The improvement of 6H-SiC film quality has also been reported in liquid phase epitaxy (LPE) [143] [144]. Thus, the use of misorientated substrates is a key technique in high quality SiC epitaxial growth.

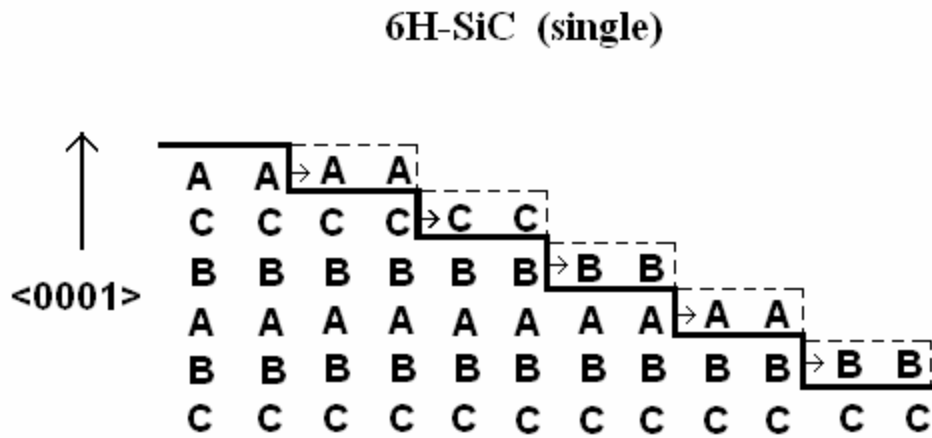
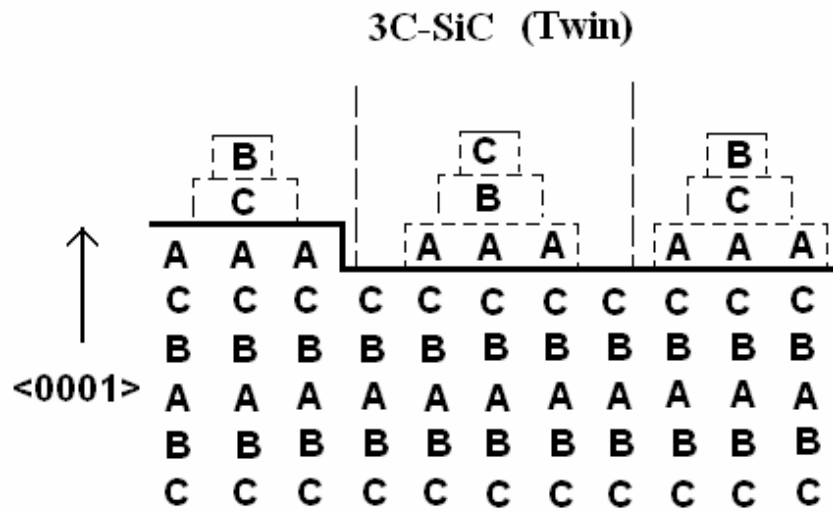


Fig. 3.4 Schematic images of the relationship between growth modes and polytypes of layers grown on 6H-SiC: (a) 3C-SiC is grown by two-dimensional nucleation, and (b) homoepitaxy of 6H-SiC is achieved owing to step-flow growth.

CHAPTER 4 EXPERIMENTAL AND CHARACTERIZATION

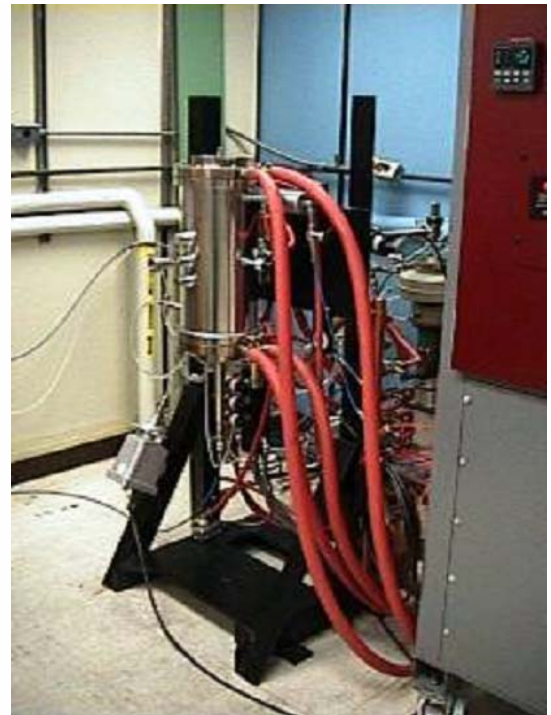
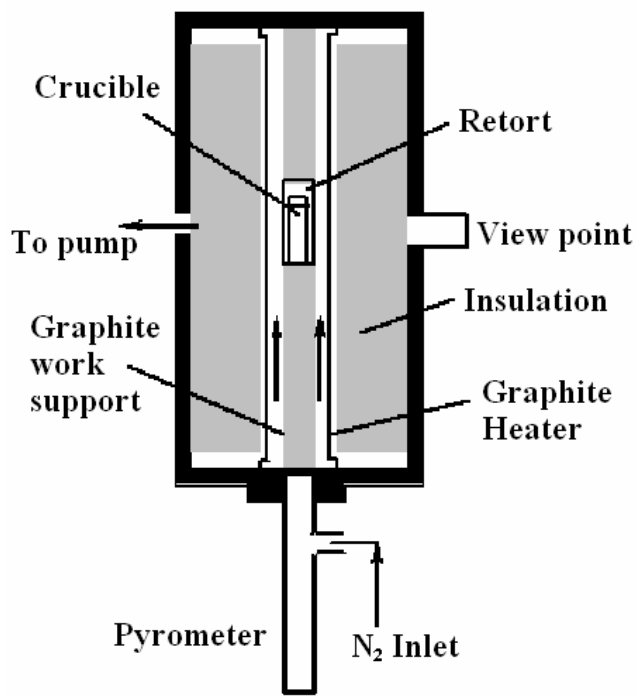
4.1 Sublimation Growth of AlN

4.1.1 Sublimation System

In this study, bulk AlN crystals were grown by the sublimation-recondensation (abbr. sublimation) technique. A resistively heated graphite furnace was used to perform the sublimation growth. The main components of the furnace consisted of a growth chamber, a graphite heating element, thermal insulation, a vacuum system, and a temperature and pressure control system. A schematic and a photograph of the furnace are shown in Fig. 4.1 (a) and (b), respectively.

In the growth chamber, a crucible was contained within a concentric graphite retort sitting together on a cylindrical graphite work support. The vertical temperature profile of the growth chamber was measured in separate experiments by an optical pyrometer focused on a movable target placed at different axial positions [94]. The shape of the graphite heater and its material grade determined the axial temperature distribution. Fig. 4.2 [94] shows the temperature profile inside the furnace measured at 60% power output. An axially uniform high temperature zone 2 centimeters long was located in the middle of the heating element. Temperature variations were less than 2 °C in this high temperature zone. By varying the height of the work support, different temperature gradients were obtained. The seed and source material were enclosed in the crucible, and positioned at this zone. The nucleation surface, where the AlN recondensed, was about 5 to 10 mm above the sublimation surface with temperature decrease less than 10 °C. The

critical parameters were growth temperature and temperature difference between the sublimation surface and nucleation surface.



(a)

(b)

Fig. 4.1 (a) Schematic and (b) photograph of the resistively heated graphite furnace.

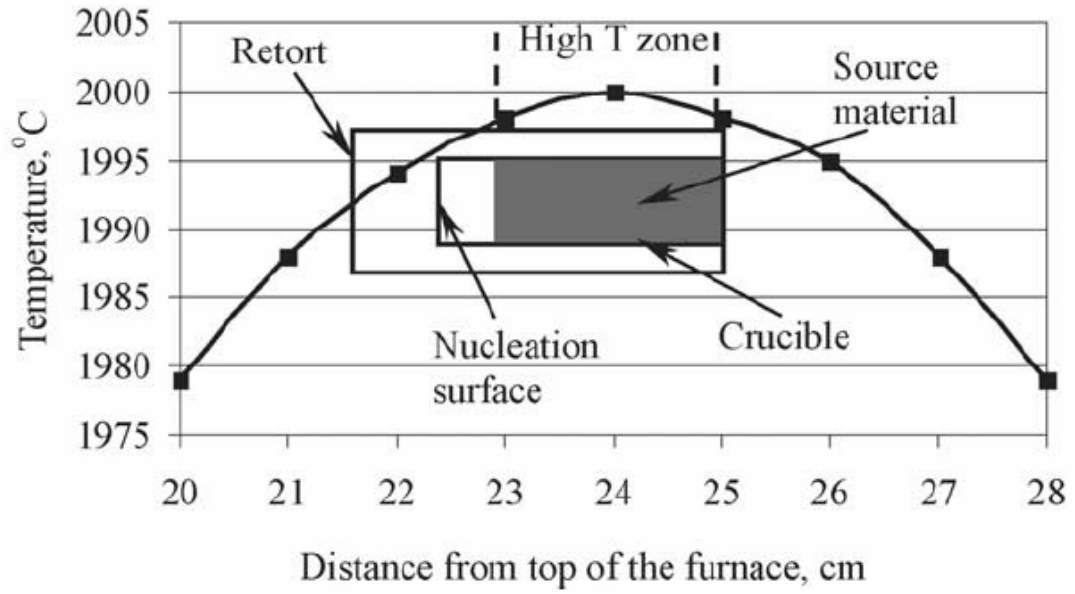
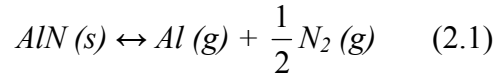


Fig. 4.2 Temperature profile inside the furnace at 60% of power output [94].

4.1.2 Growth Procedure and Condition

AlN seeded growth on SiC substrates was explored. During the sublime process, the AlN source material vaporized into Al and N₂ gases at the hot zone following the forward direction of the reaction (2.1). The gases transported to the cooler zone recrystallize into AlN crystals on SiC substrates following the reverse direction of the reaction (2.1).



The AlN source was Tokuyama grade F AlN powder with elemental analysis of oxygen concentration less than 0.9 wt % and carbon concentration less than 0.04 wt %. Prior to growth, the fresh AlN powder was baked at 1900 °C for 4 hours decreasing the oxygen concentration to less than 0.1 wt % [94].

The SiC substrate was held 3 – 5 mm above the surface of the source either by sintered AlN pieces or adhered directly to the top of the crucible. The substrate temperature was 10 °C – 15 °C lower than the source temperature. The growth temperatures reported in this work refer to the AlN source temperature. Si-face, 4H-SiC (0001) with an 8 ° mis-orientation toward (11 $\bar{2}$ 0) and on-axis 6H-SiC (0001) were employed as substrates. As-received wafers were cut into the sizes of 15 × 15 mm² – 25 × 25 mm² pieces and cleaned in organic solvents in the sequence of trichloroethylene, acetone and methanol, rinsed with DI water and dried with nitrogen.

The growth temperature was limited in the range of 1700 °C – 1900 °C to prevent the decomposition of SiC seeds. During the growth, ultra high purity (UHP) nitrogen continuously flowed through the furnace and the system pressure was kept at 800 torr to keep the graphite heater free from oxygen attack. Under continuously nitrogen flow, the lifetime of graphite heating element was tremendously increased from 400 – 500 hours to

over 1000 hours. However, the main compounds, i.e. heat insulation and the heating element of the furnace are made of graphite, thus the insulation and the heating element are etched during the growth due to the reaction between the carbon and nitrogen, especially when the process temperature is higher than 2000 °C. Therefore, the heat insulation needs to be replaced for ever year. The estimation of life time of a heating element versus different growth temperature is summarized in Fig. 4.3.

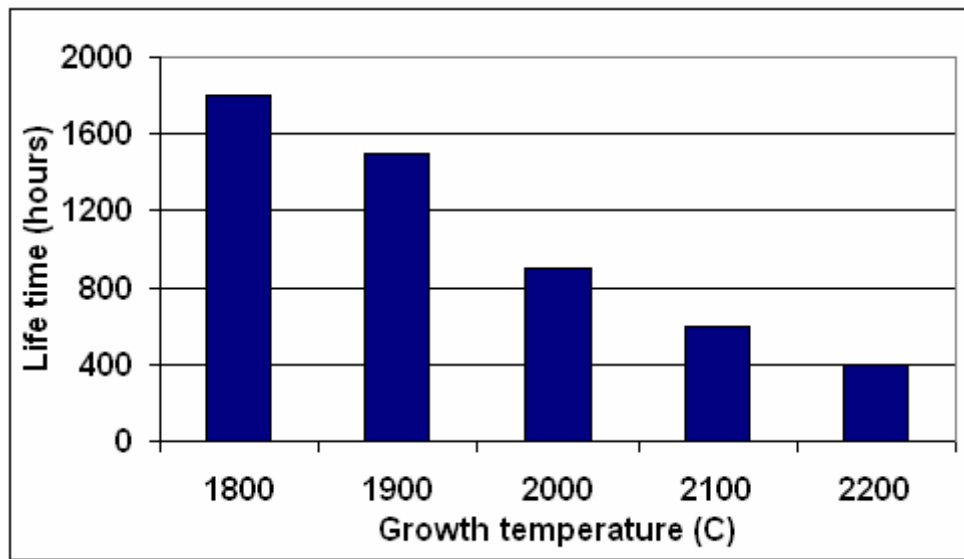
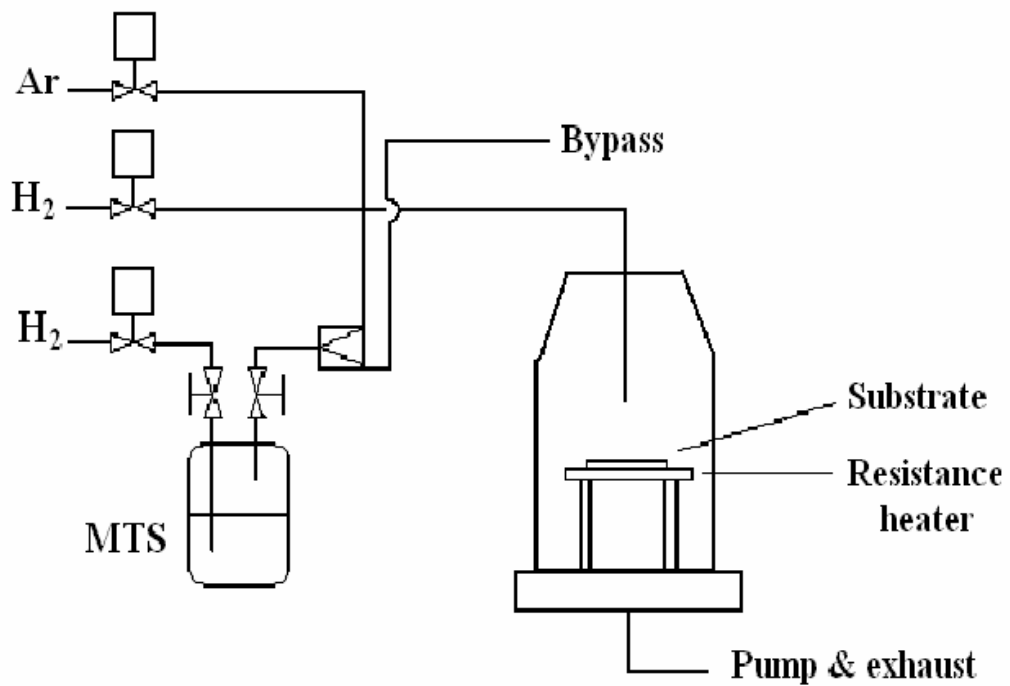


Fig. 4.3 The lifetime of a graphite-heating element at different growth temperatures.

4.2 Epitaxial Growth of SiC

4.2.1 Chemical Vapor Deposition System

Epitaxial growth of SiC was performed in a customer made chemical vapor deposition (CVD) system. The main components of the CVD consisted of a vertical quartz reactor, a resistively heated graphite susceptor, a gas manifold, a pyrex bubbler, a vacuum system and a temperature and pressure control system. A schematic of the system, a photograph of the vertical quartz reactor, and a photograph of the entire CVD system are shown in Fig. 4.4 (a), (b) and (c), respectively.



(a)

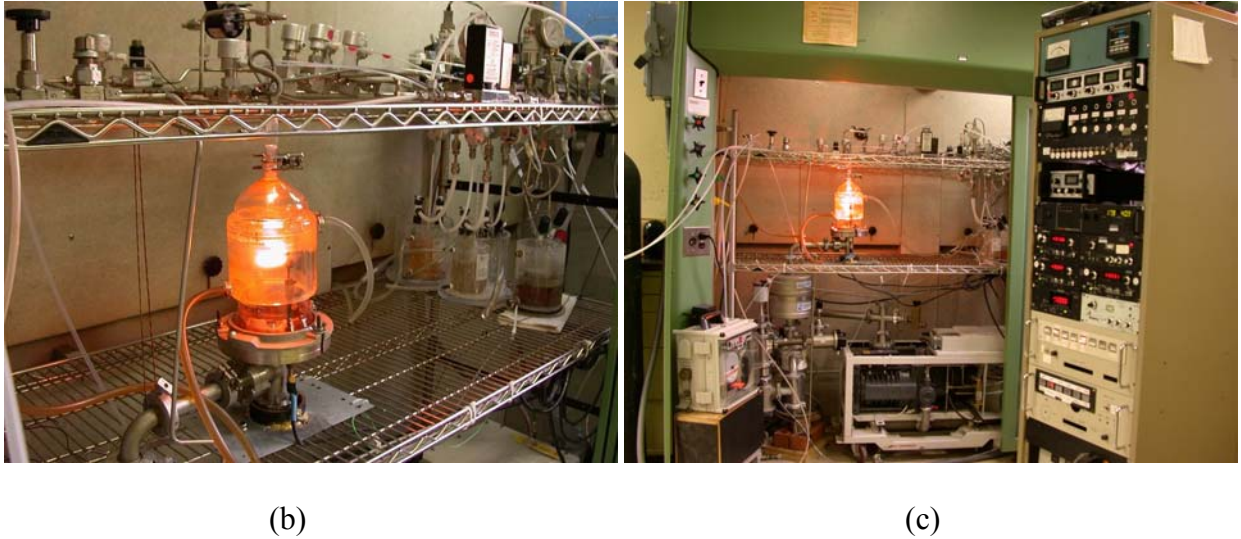
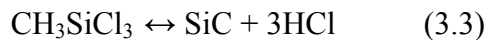


Fig. 4.4 (a) A schematic of the CVD system, (b) photograph of the vertical quartz reactor, and (c) photograph of the entire system.

4.2.2 Growth Procedure and Condition

Methyltrichlorosilane, CH_3SiCl_3 (MTS), was used as a single precursor to growth SiC thin films. The decomposition of MTS in hydrogen provides both the silicon and carbon needed for the formation of SiC. The overall reaction is



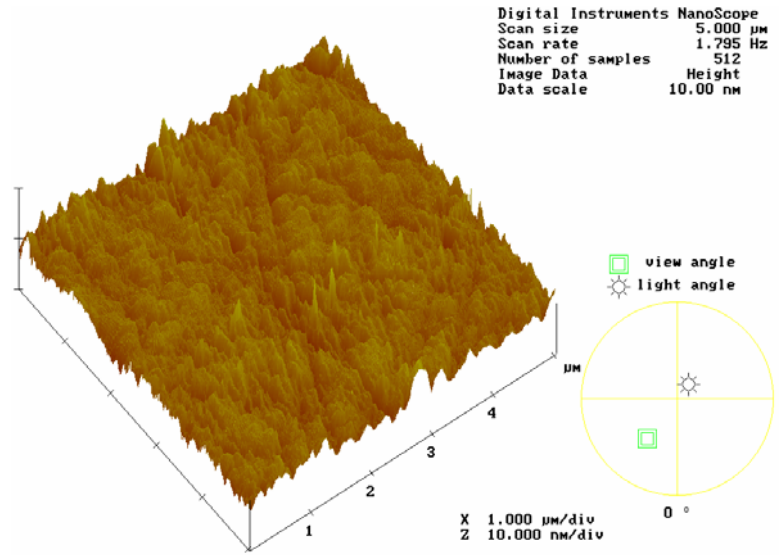
At room temperature, MTS is a liquid, thus it was contained in the pyrex bubbler, which was held in an ice bath to maintain a constant vapor pressure of 6.67×10^3 Pa [134].

Hydrogen was the carrier gas for MTS. The main carrier gas was a mixture of Ar and H_2 . Although H_2 does not participate in the main reaction as given by reaction 3.3, it appears to take part in the intermediate stages and sharply decrease the amount of free carbon in the resulting films [134, 136]. Nevertheless, H_2 can also react with the graphite susceptor at high temperature to generate hydrocarbons making the Si/C ratio uncontrollable; therefore Ar was also used as a dilution gas to minimize this reaction.

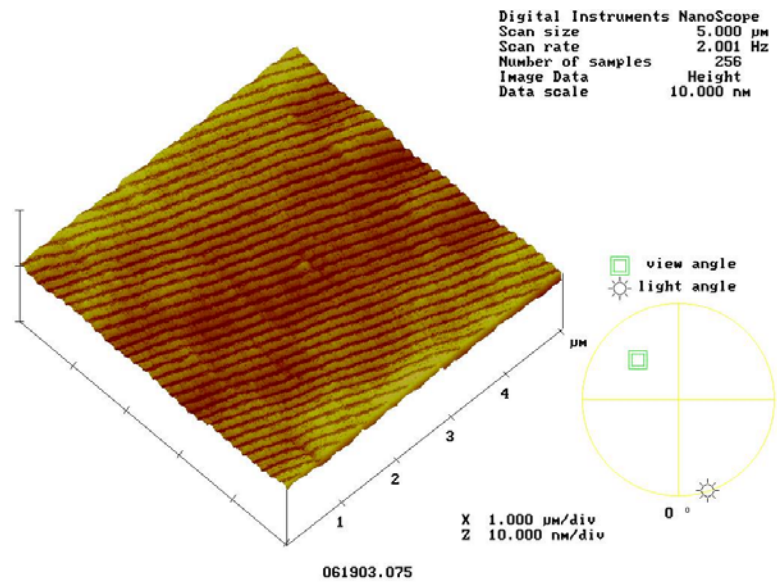
Commercial *n*-type 6H- and 4H-SiC (0 0 0 1) wafers with different misorientations were employed as substrates. The offset angles included on-axis, 3.5 ° and 8 ° off-axis toward (11 $\bar{2}$ 0). 1 × 1 cm² substrates were placed on a resistively heated graphite susceptor. The films were deposited on the Si face. Before loaded into the reactor, the substrate was cleaned in organic solvents in the sequence of trichloroethylene, acetone and methanol, rinsed with DI water and dried with nitrogen.

Proper preparation of the substrate surface is critical for high quality epilayer and eliminating 3C-SiC inclusions. SiC wafers as received from the manufacturer typically have a high density of scratches and subsurface polishing damages, as shown in the AFM image Fig. 4.4 (a). This damage increases the roughness of the deposited epilayer and act as nucleation sites for the formation of 3C-SiC inclusions on 4H- and 6H-SiC polytypes. The scratches and damage can be removed by an *in situ* hydrogen etching: at the beginning of each experiment, the substrate was brought to 1600 °C and etched by H₂ for 15 min to produce a uniform step and terrace structure on the substrate surface. A well-prepared 6H-SiC substrate is shown in an AFM image, Fig. 4.5 (b).

After etching the temperature was adjusted to the growth temperature, and the MTS vapor was admitted into the reactor. Films were deposited over the temperature range from 1300 to 1700 °C at a pressure of 100 Torr nominally for 1 hour. The effects of growth temperature and growth rate, polytypes of the grown epilayers, and dislocation type and density were investigated.



(a)



(b)

Fig. 4.5 AFM images of (a) as received 6H-SiC wafer and (b) 6H-SiC after etched in H_2 at 1600 °C for 15 mins.

4.3 Wet Chemical Etching

Wet chemical etching is an effective method to characterize defects in crystalline materials. Defect-selective etching produces etch pits or hillocks on a crystal surface due to the different etch rate at defects, which are caused by chemical and structural inhomogeneities such as stress surrounding the dislocations and the decoration of defects by impurities. When a new etchant or a new etching system has been carefully calibrated with other more sophisticated techniques, e.g. scanning electron microscopy (SEM), transmission electron microscopy (TEM), atomic force microscopy (AFM), one can estimate the defect density in crystalline material by measuring the etch pits density (EPD) [6]. Estimation of dislocation density by defect-selective etching has advantages of being low cost, simple, and capable of examining large sample areas, and not requiring any specific sample geometry. In addition, etching of group III nitrides in aqueous KOH solution was effective in identifying crystal polarity.

4.3.1 Etching Procedure of AlN

Aqueous KOH solution (45 wt %) and molten KOH / NaOH eutectic alloy (59 wt % KOH / 41 wt % NaOH) etchings were undertaken to identify the crystal polarity, the types of defects, and to estimate the defect density in AlN. Before etching, all AlN samples were cleaned with hydrochloric acid (HCl) for 10 minutes to remove any impurities on the surface. This step does not etch AlN. Etchings in aqueous KOH were performed at 60 °C for 10 minutes. The N-polarity surface forms hexagonal hillocks after etching at this condition, while the more inert Al-polarity regions remain unchanged [6]. The molten KOH/NaOH eutectic was contained in a platinum crucible held in an

aluminum plate. A quartz cover helped to reduce heat loss and stabilize the temperature. The optimum etching condition was determined as at 300 – 310 °C for 5 – 8 minutes. In molten KOH/NaOH, both the N-polarity and the Al-polarity are etched: the N-polarity forms hexagonal hillocks and the Al-polarity forms hexagonal etch pits. The type and the density of dislocations were revealed by the shape and density of the etch pits [6].

4.3.2 Etching Procedure of SiC

Molten KOH / NaOH eutectic alloy (59 wt % KOH / 41 wt % NaOH) etching was undertaken to identify the types of defects and estimate the defect density in SiC epilayers. The etching of SiC was carried out in the same set up as for etching AlN. The optimum etching condition was determined as at 440 – 460 °C for 5 – 8 minutes, since SiC is more chemically stabilized than AlN.

4.4 Characterization Techniques

4.4.1 X-ray Diffraction

In x-ray diffraction (XRD), a pattern produced by the diffraction of x-rays through the closely spaced lattice of atoms in a crystal is recorded and then analyzed to reveal the nature of that lattice. XRD is commonly used to characterize the orientation and quality of crystalline material. In this study, XRD measurements were conducted using a XDS 2000 diffractometer (Scintag Inc.) with Cu radiation (40kV × 30 mA) and Ge and Si (Li) solid state x-ray detectors cooled by liquid nitrogen. Slits controlled the intensity and spot size of the x-ray beam on the sample. The x-ray tube divergent slit was 2 mm and the detector reference slit was 0.2 mm. The divergence of the x-ray beam was about 10% to obtain the

high-resolution beam. The scanning step width was 0.02° in a continuous mode. The scan rate was $0.5^\circ \text{ min}^{-1}$.

4.4.2 Scanning Electron Microscopy

Scanning Electron Microscopy (SEM) is the best known and most widely used surface analytical technique. The primary electron beam bombards the sample surface and generates many low secondary electrons. The intensity of these secondary electrons is largely governed by the surface topography of the sample; thus, the surface morphology can be revealed by analyzing the intensity of secondary electrons as a function of position of the scanning primary electron beam. A Hitachi 4700-S SEM was used in this study to observe the sample surface.

4.4.3 Raman Spectroscopy

Raman spectroscopy is an effective tool for structural characterization of a semiconductor. Since it is sensitive to strain and crystal structure changes, it can be used to detect stress and to characterize the crystalline quality. In addition, Raman spectroscopy is capable of determining the sample composition and free carrier concentration. When a light is scattered from the surface of a sample, the scattered light mainly contains the same wavelengths that were incident on the sample. However, scattered light of different wavelengths, representing the interaction of incident light with optical phonons (Raman scattering), is also detectable, though their intensity is low. By measuring the intensities of such Raman scattered light, a Raman spectrum is generated. The Raman system used in this study was performed with SPEX Triplemate with CCD

detector, Mitutoyo Microscope with 100 X objective, and 10mW of 514.5 nm laser light. The spatial resolution was 0.7 μm lateral and 15 μm in depth.

4.4.4 Photoluminescence

Photoluminescence (PL) is a nondestructive technique to detect optical transitions in semiconductors, which are associated with impurities or point defects. When a semiconductor is excited by an optical source – a laser with energy higher than the semiconductor bandgap – for example, electron hole pairs (EHPs) are generated. By measuring the intensities of photons emitted by the radiative recombination of EHPs, the presence of specific impurities is determined. Though identifying impurities in the semiconductors by PL is simple, the measurement of the impurity concentrations is more difficult, and the samples need to be cooled to temperatures near liquid helium to minimize the thermally activated nonradiative recombinations. In this study, the PL at 1.6K was excited by the 351 nm line of an Ar^+ ion laser. The band edge emission was analyzed by a 0.25-m double-grating spectrometer and detected by a GaAs photomultiplier tube.

4.4.5 X-ray photoelectron spectroscopy

X-ray photoelectron spectroscopy (XPS) was developed in the mid 1960s by K. Siegbahn and his research group. The phenomenon is based on the photoelectric effect outlined by Einstein in 1905 where the concept of the photon was used to describe the ejection of electrons from a surface when photons impinge upon it. For XPS, Al $K\alpha$ (1486.6eV) or Mg $K\alpha$ (1253.6eV) are often the photon energies of choice. Other X-ray lines can also be chosen such as Ti $K\alpha$ (2040eV). The XPS technique is highly surface specific

due to the short range of the photoelectrons that are excited from the solid. The energy of the photoelectrons leaving the sample is determined using a CHA and this gives a spectrum with a series of photoelectron peaks. The binding energy of the peaks is characteristic of each element. From the peak areas (with appropriate sensitivity factors) to the composition of the materials surface can be determined. The shape of each peak and the binding energy can be slightly altered by the chemical state of the emitting atom. Hence XPS can provide chemical bonding information as well. XPS is not sensitive to hydrogen or helium, but can detect all other elements. XPS must be carried out in ultra high vacuum conditions.

REFERENCES

1. J.H. Edgar, in: J.H. Edgar (Ed.), Properties of Group III Nitrides Inspec/IEEE, 1994, p. 3.
2. R.R. Siergiej, R.C. Clarke, S. Siram, A.K. Agarwal, R.J. Bojko, A.W. Morse, V. Balakrishna, M.F. MacMillan, A.A. Burk Jr., C.D. Brandt, Mater. Sci. Eng. B61/62 (1999) 9.
3. L. Liu, in Growth of AlN Bulk Crystals by Sublimation, Dissertation, 2002, p. 14.
4. G.L. Harris, in: G.L. Harris (Ed.), Properties of Silicon Carbide Inspec/IEEE, 1995, p. viii.
5. R.F. Dalmau, in Aluminum Nitride Bulk Crystal Growth in a Resistively Heated Reactor, Dissertation, 2005, p. 28.
6. D.J. Zhuang, in Wet Etching Studies of AlN Bulk Crystals and Their Sublimation Growth by Microwaves, Dissertation, 2004, p. 8.
7. S. Keller, B.P. Keller, Y.F. Wu, B. Heying, d. Kapolnek, J.S. Speck, U.K. Mishra, S.P. Denbaars, Appl. Phys. Lett. 68, (1996) 1525.
8. A. Bykhovski, B. Gelmont, M. Shur, J. Appl. Phys. 74 (1993) 6734.
9. M. Seelmann-Eggebert, J.L. Weyher, Ho Obloh, H. Zimmermann, A. Rar, and S. Porowski, Appl. Phys. Lett. 71 (1997) 2635.
10. J.L. Rouviere, J.L. Weyher, M. Seelmann-Eggebert, and S. Porowski, Appl. Phys. Lett. 73 (1998) 668.
11. M. Sumiya, K. Yoshimura, K. Ohtsuka, and S. Fuke, Appl. Phys. Lett. 76 (2000) 2098.

12. E.C. Piquette, P.M. Bridger, Z.Z. Bandic, and T.C. McGill, *J. Vac. Sci. Technol. B*, 17 (2000) 1740.
13. B. Daudin, J.L. Rouviere, and M. Arlery, *Appl. Phys. Lett.* 69 (1996) 2480.
14. L.K. Li, M.J. Jurkovic, W.I. Wang, J.M. Van Hove, and P.P. Chow, *Appl. Phys. Lett.* 76 (2000) 1740.
15. S.F. Chichibu, A. Setoguchi, A. Uedono, K. Yoshimura, and M. Sumiya, *Appl. Phys. Lett.* 78 (2001) 28.
16. G.A. Martin, A. Botchkarev, A. Rockett, and H. Morkoc, *Appl. Phys. Lett.* 68 (1996) 2541.
17. U. Karrer, O. Ambacher, and M. Stutzmann, *Appl. Phys. Lett.* 77 (2000) 2012.
18. H. Morkoc, R. Cingolani, and b. Gil, *Solid-State Electron.* 43 (1999) 1909.
19. V. Kirlyuk, A.R.A. Zauner, P.C.M. Christianen, J.L. Weyher, P.R. Hageman, and P.K. Larsen, *Appl. Phys. Lett.* 76 (2000) 2355.
20. R. Dalmau, R. Schlessler, and Z. Sitar, *Phys Stat. Sol. (c)* 2, (2005) 2036.
21. S. Krukowski, M. Leszczynski, S. Porowski, in: J.H. Edgar, S. Strite, I. Akasaki, H. Amano, C. Wetzel (Ed), *Properties, Processing and Applications of Gallium Nitride and Related Semiconductors*, Inspec/IEE, Stevenage, UK, 1999, p. 21.
22. L.M. Sheppard, *Ceram. Bull.* 69 (1990) 1801.
23. W. Class, NASA-CR-1171 (1968) [Chem. Abstr. 69 (1968) 99062f].
24. G.A. Slack, *J. Phys. Chem. Solids* 34 (1973) 321.
25. R.R. Reeber, K. Wang, *Mater. Res. Soc. Symp.* 622 (2000) T6.35.1.
26. K. Tsubouchi, K. Sugai, M. Mikoshiba, in: R. McAvoy (Ed.), *Ultrasonics Symp. Proc. Chicago 1981*, IEEE, New York, 1981, p. 375.

27. J.F. Shackelford, W. Alexander, CRC Materials Science and Engineering Handbook, 3rd Edition, CRC Press, Boca Raton, 1999, p. 508.
28. S. Strite, H. Morkoc, J. Vac. Sci. Technol. B 10 (1992) 1237.
29. G.A. Slack, T.F. McNelly, J. Crystal. Growth 34 (1976) 263.
30. D.K. Gaskill, L.B. Rowland, K. Doverspike, in: J.H. Edgar (Ed.), Properties of Group III Nitrides, Inspec/IEE Stevenage, UK 1994, p. 101.
31. D. Kapolnek, X.H. Wu, B. Heying, S. Keller, B.P. Keller, U.K. Mishra, S.P. Denbaars, and J.S. Speck, Appl. Phys. Lett. 67 (1995) 1541.
32. F.A. Ponce, B.S. Krusor, J.S.M. Jr., W.E. Plano, and D.F. Welch, Appl. Phys. Lett. 67 (1995) 410.
33. S. Mahajan, Acta Mater. 48 (2000) 137.
34. T. Nishida, T. Makimoto, H. Saito, and T. Ban, Appl. Phys. Lett. 84 (2004) 1002.
35. G. Tamulaitis, I. Yilmaz, M.S. Shur, R. Gaska, C. Chen, J. Yang, E. Kuokstis, A. Khan, S.B. Schujman, and L.J. Schowalter, Appl. Phys. Lett. 83 (2003) 3507.
36. G. Tamulaitis, I. Yilmaz, M.S. Shur, R. Gaska, C. Chen, J. Yang, E. Kuokstis, A. Khan, J.C. Rojo, and L.J. Schowalter, Mat. Res. Soc. Symp. Proc. 743 (2003) L3.34.
37. X. Hu, J. Deng, N. Pala, R. Gaska, M.S. Shur, C. Chen, J. Yang, G. Simin, M.A. Khan, J.C. Rojo, L.J. Schowalter, Appl. Phys. Lett. 82 (2003) 1299.
38. J.C. Rojo, L.J. Schowalter, G. Slack, K. Morgan, J. Barani, S. Schujman, S. Biswas, B. Raghothamachar, M. Dudley, M. Shur, R. Gaska, N.M. Hohnson, and M. Kneissl, Mat. Res. Soc. Symp. Proc. 772 (2002) K1.1.
39. X. Hu, R. Gaska, C. Chen, J. Yang, E. Kuokstis, A. Khan, G. Tamulaitis, I. Yilmaz, M.S. Shur, J.C. Rojo, L.J. Schowalter, Mat. Res. Soc. Symp. Proc. 743 (2003) L6.30.

40. R. Gaska, C. Chen, J. Yang, E. Kuokstis, A. Khan, G. Tamulaities, I. Yilmaz, M.S. Shur, J.C. rojo, and L.J. Schowalter, *Appl. Phys. Lett.* 81 (2002) 4658.
41. J. Edwards, K. Kawab, G. Stevens, and R.H. Tredgold, *Solid State comm.* 3 (1965) 99.
42. G.A. Cox, D.O. Cummins, K. Kawabe, and R.H. Tredgold, *J. Phys. Chem. Solids* 28 (1967) 35.
43. S. Yoshida, S. Misawa, Y. Fujii, S. Takada, H. Hayakawa, S. Gonda, and A. Itoh, *J. Vac. Sci. Technol.* 16 (1979) 990.
44. W.M. Yim, E.J. Stofko, P.J. Zanzucchi, J.I. Pankove, M. Ettenberg, and S.L. Gilbert, *J. Appl. Phys.* 44 (1973) 292.
45. B. Liu, in *Growth of Aluminum Nitride Bulk Crystals by Sublimation*, Dissertation, p. 13.
46. O. Ambacher, *Growth and Applications of Group III-Nitrides*, *J. Phys. D*, 31 (1998) 2653.
47. T.L. Chu, D.W. Ing, and A.J. Noreika, *Electrochem. Technol.* 6 (1968) 56.
48. W.M. Yim, E.J. Stofko, P.J. Zanzucchi, J.I. Pankove, M. Ettenberg, and S.L. Gibert, *J. Appl. Phys.* 44 (1973) 292.
49. T.L. Chu, and R.W. Kelm, Jr. *J. Electrochem. Soc.* 122 (1975) 995.
50. A. Sazler, P. Kung, C.J. Sun, E. Bigan, and M. Razeghi, *Appl. Phys. Lett.* 64 (1994) 339.
51. P. Kung, A. Saxler, X. Zhang, d. Walker, T.C. Wang, I. Ferguson, and M. Razeghi, *Appl. Phys. Lett.* 66 (1995) 2958.

52. J.D. Hartman, A.M. Roskowski, Z.J. Reitmeier, K.M. Tracy, R.F. Davis and R.J. nemanich, *J. Vac. Sci. Technol. A* 21 (2003) 394.
53. H.M. Liaw, R. Doyle, P.L. Fejes, S. Zollner, A. Konkar, K.J. Linthicum, T. Gehrke, R.F. Davis, *Solid-State Electron*, 44 (2000) 747.
54. S. Yoshida, S. Misawa, and A. Itoh, *Appl. Phys. Lett.* 26 (1975) 461.
55. S. Winsztal, B. Wauk, H. Majewska-Minor, and T. Niemyski, *Thin Solid Films*, 32 (1976) 251.
56. H.U. Baier and W. Mönch, *J. Appl. Phys.* 68 (1990) 586.
57. S.A. Nikishin, N.N. Faleev, V.G. Antipov, S. Francoeur, L. Grave de Peralta, G.A. Seryogin, M. Holtz, T.I. Prokofyeva, S.N.G. Chu, A.S. Zubrilov, V.A. Elyukhin, I.P. Nikitina, Y. Melnik, V. Dmitriev, and H. Temkin, *Mat. Res. Soc. Symp. Proc.* 595 (1999) W 8.3.
58. M. Albrecht, I.P. Nikitina, A.E. Nikolaev, Y.V. Melnik, V.A. Dmitriev, and H.P. Strunk, *Phys. Stat. Sol. A* 176 (1999) 453.
59. A. Nikolaev, I. Nikitina, A. Zubrilov, M. Mynbaeva, Y. Melnik, and V.A. Dmitriev, *Mat. Res. Soc. Symp. Proc.* 595 (2000) W 6.5.
60. A.M. Tsaregorodtsev and A.N. Efimov, *Tech. Phys. Lett.* 22 (1996) 130.
61. T. Kunisato, Y. Nomura, H. Ohbo, T. Kano, N. Hayashi, M. Hata, T. Yamaguchi, M. Shono, M. Sawada, and A. Ibaraki, *Phys. Stat. Sol. C* 7 (2003) 2063.
62. T. Shibata, K. Asai, S. Sumiya, M. Mouri, M. Tanaka, O. Oda, H. Katsukawa, H. Miyake, and K. Hiramatsu, *Phys. Stat. Sol. C* 7 (2003) 2023.
63. Y. Wu, A. Hanlon, J.F. Kaeding, R. Sharma, P.T. Fini, S. Nakamura, and J.S. Speck, *Appl. Phys. Lett.* 84 (2004) 912.

64. I. Grzegory, J. Jun, M. Bockowski, S. Krukowski, M. Wroblewski, B. Lucznik, and S. Porowski, *J. Phys. Chem. Solids*. 56 (1995) 639.
65. J. Pastrnák and L. Roscovková, *Phys. Stat. Sol.* 7 (1964) 331.
66. C.O. Dugger, *Mat. Res. Bull.* 9 (1974) 331.
67. R. Schlessler, R. Dalmau, R. Yakimova and Z. Sitar, *Mat. Res. Symp. Proc.* 693 (2002) I 9.4
68. R. Schlessler and Z. Sitar. *J. Crystal Growth* 234 (2002) 349.
69. G. A. Slack and T.F. McNelly, *J. Crystal Growth* 34 (1976) 263.
70. G. A. Slack and T.F. McNelly, *J. Crystal Growth* 42 (1977) 560.
71. L. Liu and J.H. Edgar, *J. Crystal Growth* 220 (2000) 243.
72. L. Liu, B. Liu, Y. Shi and J.H. Edgar, *MRS Internet J. Nitride Semicond. Res.* 6 (2001) 7.
73. B.M. Epelbaum, M. Bickermann and A. Winnacker, private communication.
74. B.M. Epelbaum, C. Seitz, A. Magerl, M. Bickermann, and A. Winnacker, *J. Crystal Growth* 265 (2004) 577.
75. M. Tanaka, S. Nakahata, K. Sogabe, H. Nakata and M. Tobioka, *Jpn. J. Appl. Phys.* 36 (1997) L1062.
76. S.Y. Karpov, D.V. Zimina, Y.N. Makarov, E.N. Mokhov, A.D. Roenkov, M.G. Ramm and Y.A. Vodakov, *Phys. Stat. Sol. A*.176 (1999) 435.
77. L. Liu and J.H. Edgar, *J. Electrochem. Soc.* 149 (2002) G12.
78. Z. Gu, L. Du, J.H. Edgar, N. Nepal, J.Y. Lin, H.X. Jiang, R. Witt, *J. Crystal Growth*, in press.
79. M. Bickermann, B.M. Epelbaum and A. Winnacker, *Phys. Stat. Sol. C* 7 (2003) 1993.

80. D. Zhuang, Z.G. Herro, R. Schlessler, Z. Sitar, J. Crystal Growth 287 (2006) 372.
81. L. Liu, J.H. Edgar, Mater. Sci. Eng, R37 (2002) 61.
82. R.B. Campbell and H.-C. Chang, U.S. Govt. Res. Develop. Fed. Sci. Tech. Inform., (AD-815895) (1969) 164.
83. C.M. Balkas, Z. Sitar, T. zheleva, L. Bergman, R. Nemanich and r.F. Davis, J. Crystal Growth 179 (1997) 363.
84. W.L. Sarney, L. Salamanca-Riba, T. Hossain, P. Zhou, H.N. Jayatirtha, H.H. Kang, R.D. Vispute, M. Spencer, and K.A. Jones, MRS Internet J. Nitride Semicond. Res. 5S1 (2000) W 5.5.
85. Y. Shi, B. Liu, L. Liu, J.H. Edgar, E.A. Payzant, J.M. Hayes and M. Kuball, MRS Internet J. Nitride Semicond. Res. 6 (2000) 5.
86. L. Liu, B. Liu, Y. Shi and J.H. Edgar, MRS internet J. Nitride Semicond. Res. 6 (2001) 7.
87. Y. Shi, Z.Y. Xie, L. Liu, B. Liu, J.H. Edgar and M. Kuball, J. Crystal Growth 233 (2001) 177.
88. Y. Shi, B. Liu, L. Liu, J.H. Edgar, H.M. Meyer III, E.A. Payzant, L.R. Walker, N.D. Evans, J.G. Swadener and J. Chaudhuri, Phys. Stat. Sol. A 188 (2001) 757.
89. J.H. Edgar, L. Liu, B. Liu, D. Zhuang, J. Chaudhuri, M. Kuball and S. Rajasingam, J. Cryst. Growth, 246 (2002) 187.
90. B.M. Epelbaum, M. Bickermann and A. Winnacker, Mater. Sci. Forum 983 (2003) 433.
91. R. Dalmau, R. Schlessler, B.J. Rodriguez, R.J. Nemanich, Z. Sitar, J. Crystal Growth 281 (2005) 68.

92. E.N. Mokhov, O.V. Avdeev, I.S. Barash, T.Yu. Chemekova, A.D. Roenkov, A.S. Segal, A.A. Wolfson, Yu.N. Makarov, M.G. Ramm, H. Helava, J. Crystal Growth 281 (2005) 93.
93. S. Wang, B. Raghathamachar, M. Dudley, A.G. Timmerman, Materials Research Society Symposium Proceedings, 892 (2006) 775.
94. K. Balakrishnan, M. Banno, K. Nakano, G. Narita, N. Tsuchiya, M. Imura, M. Iwaya, S. Kamiyama, K. Shimono, T. Noro, T. Takagi, H. Amano, I. Akasaki, Materials Research Society Symposium Proceedings, 831 (2005) 607.
95. R. Schlessler, R. Dalmau, D. Zhuang, R. Collazo, and Z. Sitar, J. Crystal Growth 281 (2005) 75.
96. B. Liu, D. Zhuang and J.H. Edgar, Vacuum Science and Technology: Nitrides as Seen by the Technology, (Eds.) T. Paskova and B. Monemar, 43, Research Signpost, Trivandrum, India (2002) 327.
97. R. Dalmau, B. Raghathamachar, M. Dudley, R. Schlessler and Z. Sitar, Mat. Res. Soc. Symp. Proc. 798 (2004) Y 2.9.
98. J.H. Edgar, D. Zhuang and Z. Gu, unpublished.
99. G.L. Harris, in: G.L. Harris (Ed.), Properties of Silicon Carbide Inspec/IEE, 1995, p. 6.
100. N.W. Jepps, T.F. Page, in: P. Krishna (Ed.), Progress in Crystal Growth and Characterization, Vol. 7, Pergamon Press, New York, 1983, p. 259.
101. Z. Xie, in Surface Etching of 6H-SiC (0001) and Its Effects on Growth of GaN, AlN by MOCVD, and SiC by APCVD, Dissertation, 2000.

102. O. Kordina, Linköping Studies in Science and Technology, Dissertations, Vol. 352, Linköping University, http://www.ifm.liu.se/Matephys/new_page/research/sic/, 1994.
103. G.L. Harris, in: G.L. Harris (Ed.), Properties of Silicon Carbide Inspec/IEE, 1995, p. 4.
104. R.R. Reeber, K. Wang, Mater. Res. Soc. Symp. 622 (2000) T6.35.1.
105. G.L. Harris, in: G.L. Harris (Ed.), Properties of Silicon Carbide Inspec/IEE, 1995, p. 3.
106. R.C. Weast, M.J. Astle, W.H. Beyer (Eds), CRC Handbook of Chemistry and Physics, 66th Edition, CRC Press, Boca Raton, FL, 1986, p. E-99.
107. G.L. Harris, in: G.L. Harris (Ed.), Properties of Silicon Carbide Inspec/IEE, 1995, p. 9.
108. Kh.S. Bagdasarov, E.R. Dobrovinskaya, V.V. Pishchik, M.M. Chernik, Yu. Yu, A.S. Gershun, I.F. Zvyaginstseva, Sov. Phys. Crystallgr. 18 (1973) 242.
109. G.L. Harris, in: G.L. Harris (Ed.), Properties of Silicon Carbide Inspec/IEE, 1995, p. 8.
110. G.L. Harris, in: G.L. Harris (Ed.), Properties of Silicon Carbide Inspec/IEE, 1995, p. 15.
111. J.B. Casady, R.W. Johnson, Solid-State Electron. 39 (1996) 1409.
112. R.R. Siergiej, R.C. Clarke, S. Siram, A.K. Agarwal, R.J. Bojko, A.W. Morse, V. Balakrishna, M.F. MacMillan, A.A. Burk Jr., C.D. Brandt, Mater. Sci. Eng. B61/62 (1999) 9.
113. B.J. Baliga, Res. Soc. Symp. Proc. 512 (1998) 77.

114. J.B. Casady, R.W. Johnson, Solid-State Electron. 39 (1996) 1409.
115. Y.M. Tairov, V.F. Tsvetkov, J. Crystal Growth 43 (1978) 209.
116. C.D. Brandt, R.C. Clarke, R.R. SiergieJ, J.B. Cassady, S. Sriram, A.K. Agarwal, and A.W. Morse, *SiC for applications in high-power*, in SiC Materials and Devices, Y.S. Park ed. (Semiconductors and Semimetals vol. 52, Academic, New York, 1998) pp.195-236.
117. M.M. Rahman and S. Furukawa, IEEE, Circuits and Devices, 1 (1992) 22.
118. Cree Research Inc. 2810 Meridian Parkway, Suite 176, Durham, NC 27713.
119. Y.M. Tairov and V.F. Tsftetkov, J. Crystal Growth 36 (1976) 147.
120. G. Ziegler, P. Lanig, D. Theis and C. Weyrich, IEEE Trans. Electron Devices 30 (1983) 277.
121. J.A. Lely and Ber.Dt. Keram, Ges. 32 (1955) 229.
122. C.H. Carter Jr., L. Tang, and R.F.Davis, paper presented at the Fourth National Review Meeting on the Growth and Characterization of SiC, Raleigh, NC (1987).
123. H. Matsunami and T. Kimoto, Mater. Sci. Eng., A, R20 (1997) 125.
124. H.O. Pierson, in: H.O. Pierson (Ed.), Handbook of chemical vapor deposition, Inspec/IEE, 1999, Chapter 9, p. 15.
125. H. Tsuchida, I. Kamata, T. Jikimoto, T. Miyanagi and K. Izumi, Mater. Sci. Forum (2003) 433, (Silicon Carbide and Related Materials 2003) 131.
126. F. Wischmeyer, D. Leidich and E. Niemann, Mater. Sci. Forum (1998) 264, (Pt.1, Silicon Carbide, III-Nitrides and Related Materials) 127.
127. Y. Ishida, T. Takahashi, H. Okumura, K. Arai and S. Yoshida, Jpn. J. Appl. Phys., Part 1, 43 (8A) (2004) 5140.

128. S.M. Bishop, E.A. Preble, C. Hallin, A. Henry, L. Storasta, H. Jacobson, B.P. Wagner, Z.J. Reitmeier, E. Janzen and R.F. Davis, *Mater. Sci. Forum* (2004) 457 (Pt.1, Silicon Carbide and Related materials 2003) 221.
129. Y.J. Lee, D.J. Choi, J.Y. Park and G.W. Hong, *J. Mater. Sci.* 35 (18) (2000) 4519.
130. Q. Zhu, Z. Qiu and C. Ma, *Huagong Yejin* 19 (4) (1998) 289.
131. W.G. Zhang and K.J. Hüttinger, *Chem. Vap. Deposition* 7 (4) (2001) 167.
132. G.S. Myoung and S. Chun, *J. Vac. Sci. Technol. A* 6(1) (1988) 5.
133. Y.J. Lee and D.J. Choi, *J. Ceram. Processing Res.* 3 (3) (2002) 222.
134. S.N. Gorin and L.M. Ivanova, *Phys. Stat. Sol. (b)* 202 (1997) 221.
135. A.J. Steckl and H.E. Devrajan, *Appl. Phys. Lett.* 69 (25) (1996) 3824.
136. V.V. Zelenin, V.G. Solov'ev, S.M. Starobinets, S.G. Konnikov and V.E. Chelnokov, *Semiconductors* 29 (6) (1995) 581.
137. Z.Y. Xie, S.F. Chen, J.H. Edgar, K. Barghout and J. Chaudhuri, *Electrochem. Solid-State Lett.* 3 (8) (2000) 381.
138. D. Crippa, G.L. Valente, A. Ruggiero, L. Neri, R. Reitano, L. Calcagno, G. Foti, M. Mauceri, S. Leone, G. Pistone, G. Abbondanza, G. Abbagnale, A. Veneroni, F. Omarini, L. Zamolo, M. Masi, F. Roccaforte, F. Giannazzo and S. Di franco, *Mater. Sci. Forum* (2005) 67.
139. V.J. Jennings, A. Sommer, H. Chang, *J. Electrochem. Soc.* 113 (1966) 728.
140. W. Von Muench, I. Phaffeneder, *Thin Solid Films* 31 (1976) 39.
141. S. Yoshida, E. Sakuma, H. Okumura, S. Misawa, and K. Endo, *J. Appl. Phys.* 62 (1987) 303.

142. J.A. Powell, J.B. Petit, J.H. Edgar, I.G. Jenkins, L.G. Matus, J.W. Yang, P. Pirouz, W.J. Choyke, L. Clemen, M. Yoganathan, *Appl. Phys. Lett.* 59 (1991) 333.
143. Y. Matsushita, T. Nakata, T. Uetani, T. Yamaguchi, T. Niina, *Jpn. J. Appl. Phys.* 29 (1990) L343.
144. H.B. Bebb, and E.W. Williams, *Semiconductors and Semimetals*, (Ed.) R.K. Willardson, and A.C. Beer, 8, 181, Academic Press, New York (1972).

Nucleation of AlN on SiC substrates by seeded sublimation growth

P. Lu ^{a,*}, J.H. Edgar ^a, R.G. Lee ^b, J. Chaudhuri ^b

^a Department of Chemical Engineering, Kansas State University, Manhattan, KS-66506, USA

^b Department of Mechanical Engineering, Texas Tech University, Lubbock, TX-79409, USA

* Corresponding author: Peng Lu; Tel: 1-785-532-4325; Fax: 1-785-532-7372;

E-mail address: plu@ksu.edu

Abstract

The nucleation of aluminum nitride (AlN) on silicon carbide (SiC) seed by sublimation growth was investigated. Silicon-face, 8 ° off-axis 4H-SiC (0001) and on-axis 6H-SiC (0001) were employed as seeds. Initial growth for 15 minutes and extended growth for 2 hours suggested that 1850 °C was the optimum temperature of AlN crystal growth: on an 8 ° off-axis substrate, AlN grew laterally forming a continuous layer with regular “step” features; on the on-axis substrate, AlN grew vertically as well as laterally, generating an epilayer with hexagonal sub-grains of different sizes. The layer’s *c*-lattice constant was larger than pure AlN, which was caused by the compression of the AlN film and impurities (Si, C) incorporation. Polarity sensitive and defect selective etchings were performed to examine the surface polarity and dislocation density. All the samples had an Al-polar surface and no N-polar inversion domains were observed. Threading dislocations were present regardless of the substrate misorientation. Basal plane dislocations were revealed only on the AlN films on the 8 ° off-axis substrates. The total dislocation density was in the order of 10^8 cm^{-2} when the film was 20 – 30 μm thick.

1. Introduction

Aluminum nitride (AlN) is a direct wide band gap semiconductor ($E_g = 6.2$ eV) with high thermal conductivity and high thermal stability. Due to the small mismatch in thermal expansion coefficient and lattice constant with GaN, AlN is an ideal substrate for GaN based devices such as high-power UV lasers, UV photodetectors and blue light emitting diodes (LEDs).

Sublimation is the most successful growth method for bulk AlN, as demonstrated by Slack and McNelly [1,2], Bickermann [3], and others. Employing SiC as a seed to grow AlN was first reported by Balkas *et al.* [4]. SiC is a suitable substrate for AlN bulk crystal growth since it has a small *a*-lattice mismatch (0.96% for 6H-SiC and 1.2% for 4H-SiC) [5] with AlN. Dalmau *et al.* [6] grew 3 mm thick AlN layers on both on-axis 6H-SiC (0001) and off-axis 4H-SiC (0001). On Si-face of SiC, the AlN layers were primarily Al-polarity. Mokhov *et al.* [7] accomplished a 10-12 mm thick AlN layer on SiC substrates.

When SiC is employed as a seed crystal, optimal initial nucleation is required to ensure a high quality AlN crystal forms. Some studies have discussed the initial growth of AlN on SiC seeds. Shi *et al.* [8,9] reported the initial growth stage of AlN on SiC by sublimation in a tungsten furnace. At 1800 °C, after 15 and 45 minutes of growth, only individual AlN nuclei were formed, and after 120 minutes slow lateral growth was observed but the crystals were still in the form of individual grains not fully coalesced. AlN grown on on-axis and 3.5 ° off-axis 6H-SiC (0001) had similar nucleation mode and surface morphology; a higher temperature increased the growth rate of AlN but did not affect surface morphology. Yakimova *et al.* [10] stated that in the initial growth stage of

AlN on SiC, high temperature (1800 °C) and medium nitrogen pressure (300 mbar) promoted a continuous growth: columnar AlN crystals were obtained. Whereas, with decreasing temperature (1750 °C) and increasing nitrogen pressure (600 mbar) anisotropic growth became more pronounced: single crystal, needle-like AlN crystals were obtained. In the related work, Yamada *et al.* [11] investigated the nucleation of AlN deposited on on-axis 6H-SiC (0001) by metal-organic chemical vapor deposition (MOCVD): initially the AlN grew in the form of 3D islands, which subsequently coalesced to form sub-grains instead of a continuous film; the 3D growth mode was caused by the presence of energetic/kinetic barriers at the coalescence regions of the AlN islands.

The purpose of this study was to explore the nucleation mode of AlN over a wide temperature range (1800 °C – 1950 °C) on SiC seeds with different misorientation, i.e. 8° off-axis and on-axis. The surface morphology and the crystal quality of the deposited layer were characterized to evaluate the influences of the nucleation mode. The sublimation growth was carried out in a graphite furnace similar to those described in [6,7].

2. Experimental

The AlN crystals were grown by sublimation in a resistively heated graphite furnace, consisting of a growth chamber, a graphite heating element, graphite foam insulation and a temperature and pressure control system, as illustrated in [12]. The source was high purity AlN powder with less than 1 wt % oxygen and 0.06 wt % carbon. The SiC

substrate was supported 5 mm above the surface of the source by sintered AlN pieces. The substrate was about 10 – 15 °C lower in temperature than the source. The growth temperatures reported in this paper refer to the temperatures of the AlN source. Si-face 4H-SiC (0001) with an 8 ° mis-orientation toward $(11\bar{2}0)$ and on-axis 6H-SiC (0001) were employed as substrates. As-received wafers were cut into 1.5 cm x 1.5 cm pieces and cleaned in organic solvents in the sequence of trichloroethylene, acetone and methanol, rinsed with DI water and dried with nitrogen. The nucleation growths were performed for 15 minutes in UHP nitrogen at 800 torr and temperatures of 1800 °C, 1850 °C, 1900 °C and 1950 °C. In order to precisely control the nucleation, the temperature was gradually increased to 1600 °C, the maximum temperature for no nucleation, and then rapidly increased to the target temperature, at a rate of 40 – 50 °C/min. After nucleation finished the temperature was rapidly decrease to 1600 °C at the same rate. The optimum temperature was selected by comparing the surface morphology of the samples, which were characterized by optical, confocal and scanning electron microscopes. Subsequently, two hours growth was carried out at the optimized temperature. X-ray diffraction (XRD) was employed to characterize the crystal quality.

The polarity and structural dislocations in the AlN layers were explored by wet chemical etchings. First, the AlN samples were etched in an aqueous KOH solution (45 wt %) at 60 °C for 10 minutes. The N-polarity surface forms hexagonal hillocks after etching at this condition, while the more inert Al-polarity regions remain unchanged [13]. Second, the samples were etched in a molten KOH/NaOH eutectic alloy (59 wt % KOH / 41 wt % NaOH) at 300 – 310 °C for 5 minutes. In molten KOH/NaOH, both the N-polarity and the Al-polarity are etched: the N-polarity forms hexagonal hillocks and the

Al-polarity forms hexagonal etch pits. The type and the density of dislocations were revealed by the shape and density of the etch pits [13].

3. Results and discussion

3.1. Initial growth of 15 minutes

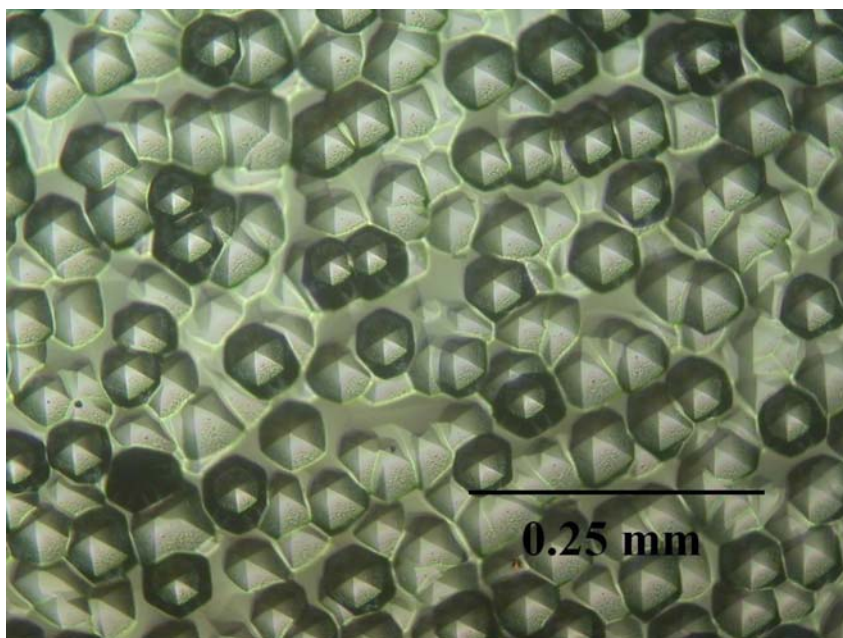
At 1800 °C, adsorbed AlN nucleated in 3-dimensions (3D) generating numerous hillocks covering most of the SiC substrate's surface in 15 minutes of growth, as shown in an optical micrograph Fig. 1 (a). These hillocks assumed the shape of regular point-topped pyramids [14], with hexagonal bases approximately 30 – 50 μm across, as shown in a SEM image Fig. 1(b). The distribution of hillocks was uniform with a density in the range of $1.2 - 1.5 \times 10^4 \text{ cm}^{-2}$. Some hillocks overgrew others.

At 1850 °C, adsorbed AlN nucleated in both 3- and 2-dimensions (2D). Scattered hexagonal hillocks were still observed, but with a reduced density of $0.2 - 0.5 \times 10^4 \text{ cm}^{-2}$.

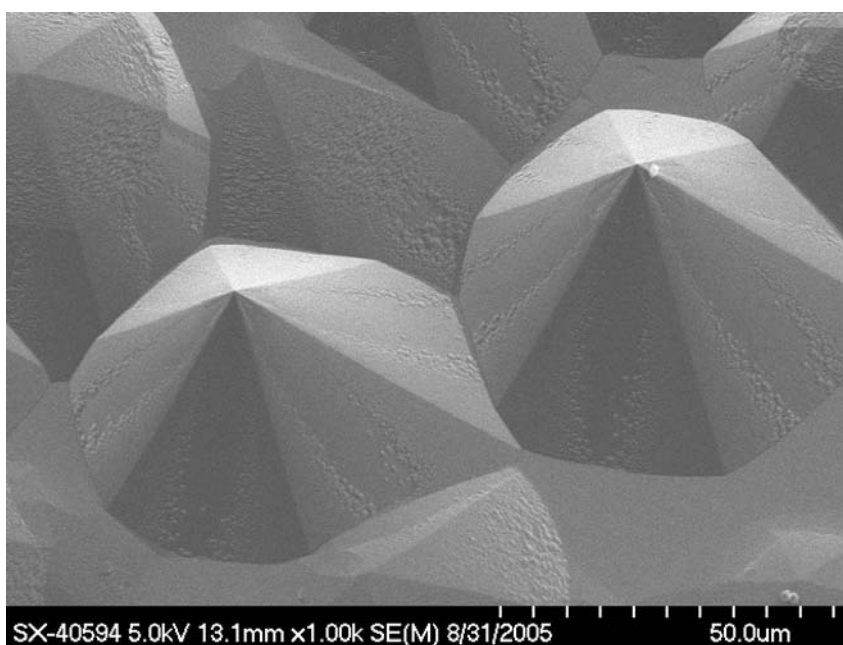
Among these hillocks, some crystals grew laterally toward the $[11\bar{2}0]$ direction, i.e. in the direction of the misorientation of the surface, forming irregularly shaped flakes (Fig. 2 (a)). Those flakes had a “step-flow growth mode” [15]. Thermal decomposition of the SiC generated micro-steps on the misoriented substrate surface. The step height and terrace width of 8 ° off-axis 4H-SiC substrate were 0.2 μm and 2 μm, respectively, as measured by confocal microscopy. The AlN tended to nucleate at the edges of the micro-steps and then grew laterally along the terraces. When a flake met a hillock, it either crossed or covered the hillock, (Fig. 2(b)).

At 1900 °C, all the adsorbed AlN grew in a pure 2D mode generating hexagonal flakes, (Fig. 3(a)). These flakes with the sizes of $40 \times 60 - 200 \times 300 \mu\text{m}^2$ were only attached at one end to underlying SiC and overlapped to each other, (Fig. 3(b)).

At 1950 °C, due to the accelerated sublimation rate of AlN source, much more AlN adsorbed on the substrate surface resulting in high growth rate: after 15 minutes, a thick layer, 30 – 50 μm thick, was deposited. However, the surface was very rough due to the misorientated growth crystals (off *c*-axis). Furthermore, several holes appeared on the backside of the SiC substrate indicating the SiC severely decomposed at this temperature.

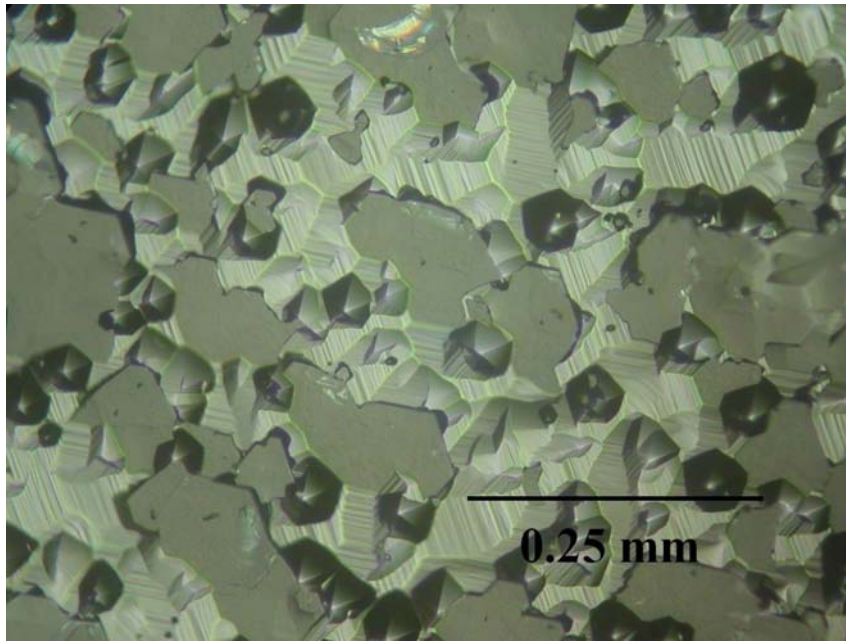


(a)

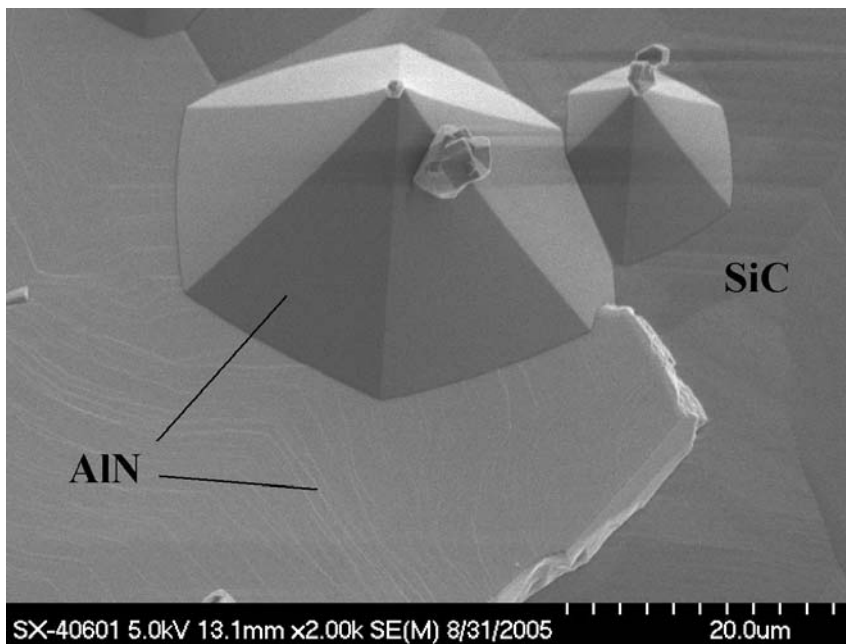


(b)

Fig. 1. AlN grown on 8 ° off-axis 4H-SiC (0001) at 1800 °C for 15 minutes:(a) optical micrograph and (b) SEM.

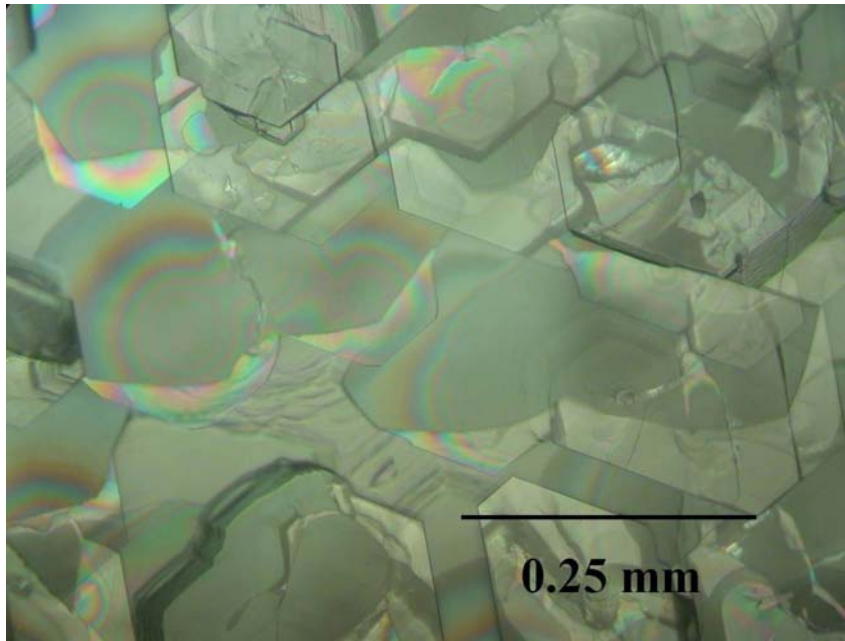


(a)

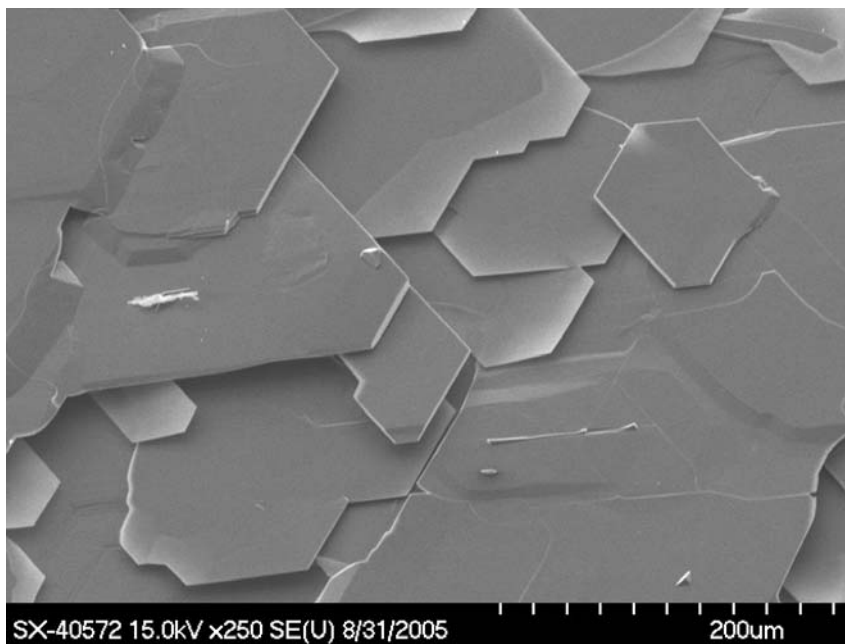


(b)

Fig. 2. AlN grown on 8 ° off-axis 4H-SiC (0001) at 1850 °C for 15 minutes:(a) micrograph and (b) SEM.



(a)



(b)

Fig. 3. AlN grown on 8 ° off-axis 4H-SiC (0001) at 1900 °C for 15 minutes:(a) micrograph and (b) SEM.

3.2. Two hours growth

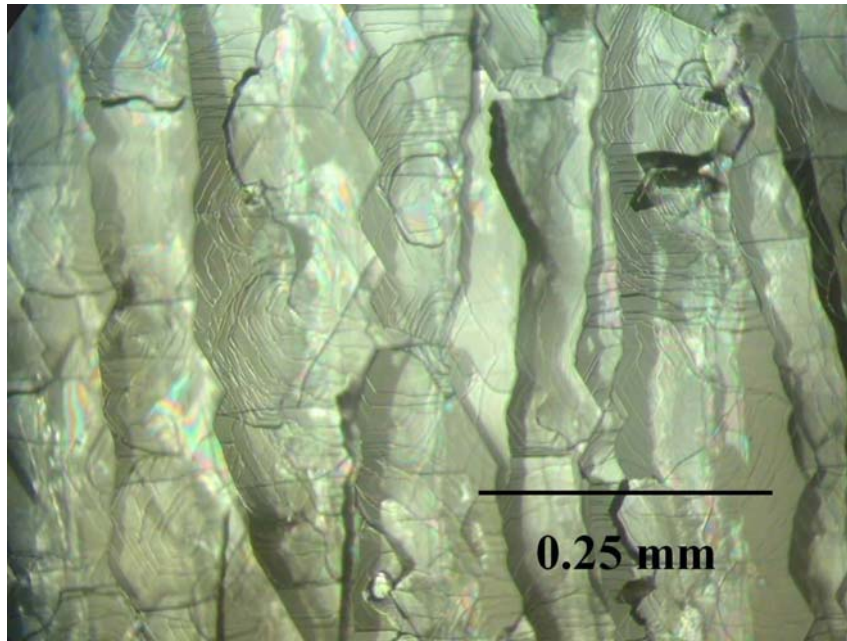
The initial growths suggested that 1850 °C and 1900 °C were suitable for AlN nucleation: partly 2D and completely 2D growth modes were observed. Hence, subsequent growths for two hours were carried out at these two temperatures. The growth at 1900 °C produced a rough layer composed of crystal clusters, due to the random growth and overlapping of the 2D flakes. In contrast, the growth at 1850 °C produced a continuous layer formed with regular steps implying the epitaxy of AlN, (Fig. 4(a)). The AlN initially nucleated in both 3D and 2D and then 2D growth became dominant as the film grew thicker.

The details of the steps in the AlN layer were studied in a 3D image by confocal microscope, Fig. 4(b). The steps had an approximately 8 ° angle relative to the sample holder plane indicating the crystals laterally grew toward the orientation of the 8 ° off-axis substrate. The terrace width of the steps was 100 – 150 μm, and the step height was 22 – 25 μm. Sub-grain were absent from the surface indicating most of the AlN had a coherent stacking sequence. The top view of this 3D image and the step height measurement are shown at upper left corner and the bottom of Fig. 4(b), respectively.

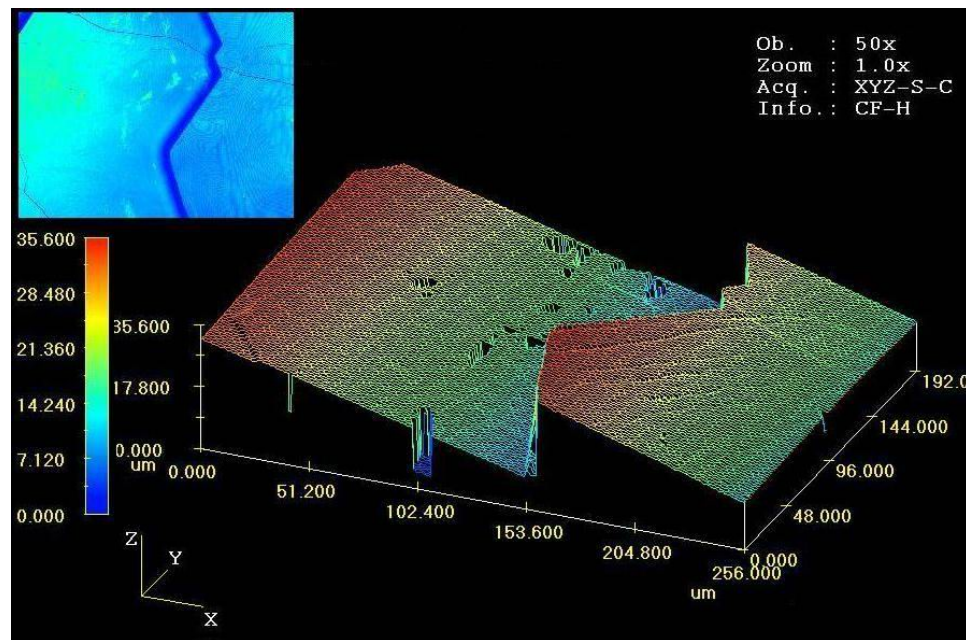
A complementary growth was performed on a Si-face on-axis 6H-SiC (0001) substrate at 1850 °C for 2 hours. For this orientation, the AlN layer contained hexagonal sub-grains of different sizes but no regular steps, as shown in a micrograph Fig. 5(a). Since the substrate was on-axis, i.e. the mis-orientation was less than 0.5 °, SiC thermal decomposition generated a surface morphology with larger terrace widths and smaller micro-step density [15]. Yamada *et al.* [11] reported that for AlN nucleation on on-axis 6H-SiC (0001) via MOCVD, 3D nuclei formed on the SiC terraces and coalesced to 2D

islands. Although in the present study this sample was grown by sublimation, the surface morphology matched their description. The 3D growth mode was dominant and the AlN layer was not fully coalesced, unlike the layer deposited on the 8 ° off-axis substrate. A confocal 3D image, Fig. 5(b), shows a hexagonal sub-grain was contained in a bigger grain and the thickness of the grains was different. The height measurement is shown at the bottom of Fig. 5(b). The heights of the 2D island at position 1 and 2 were 20 μm and 24 μm, respectively.

The mismatch in lattice constants and thermal expansions between the AlN layer and the SiC substrate generated stresses, resulting in cracks on both samples. Most of the cracks on the off-axis grown film, with a density of 80 – 100 cm⁻², were perpendicular to the step edge, Fig. 4 (a). More stress was generated along the step than across the step, since the step length, 2 – 5 mm, is much larger than the terrace width, 100 – 150 μm. The cracks on the on-axis grown film were randomly orientated with a much smaller density of 5 – 10 cm⁻², Fig. 5 (a), due to the release of the stress by the sub-grain boundaries.

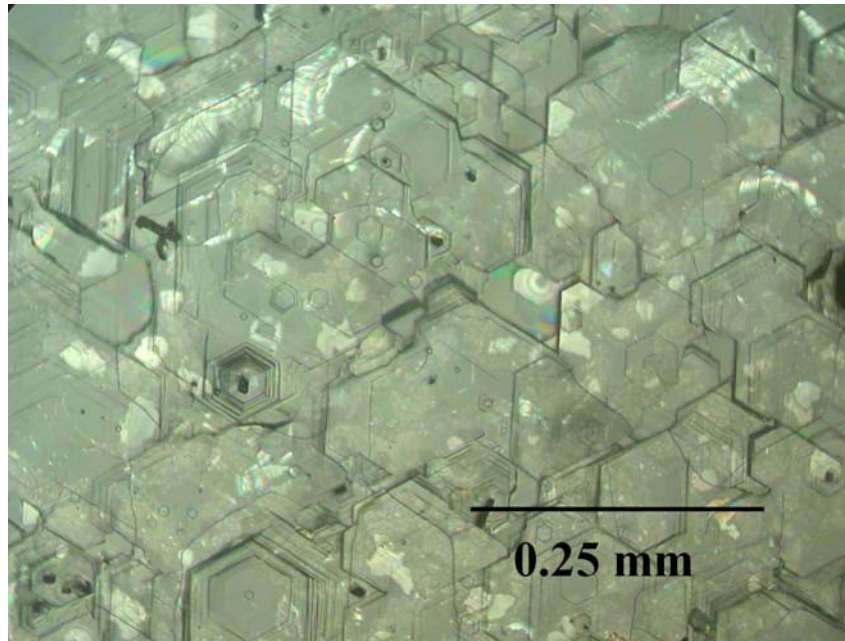


(a)

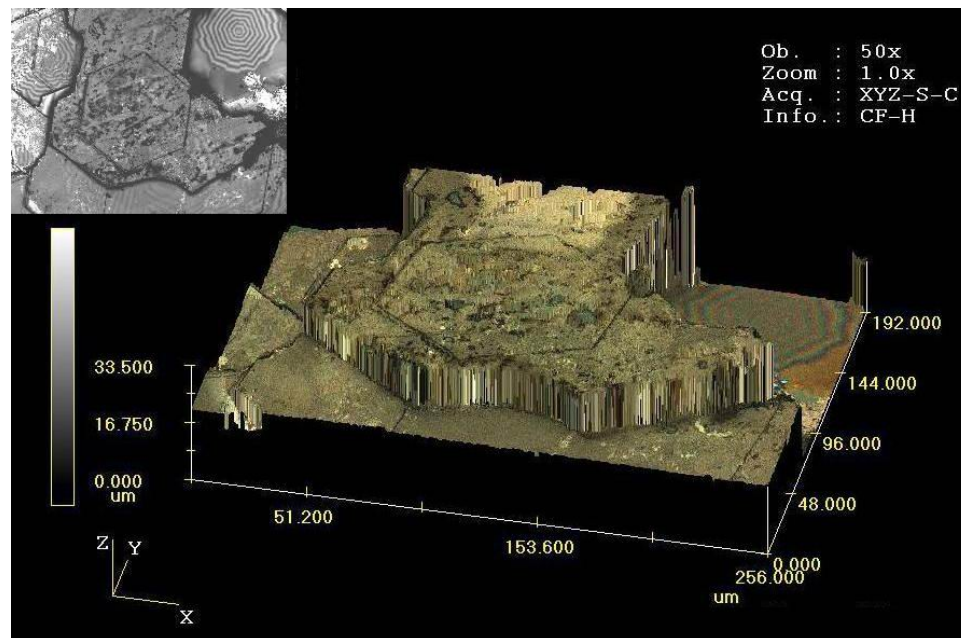


(b)

Fig. 4. AlN grown on 8 ° off-axis 4H-SiC (0001) at 1850 °C for 2 hours:(a) optical micrograph and (b) 3D image and step height measurement by confocal microscope.



(a)

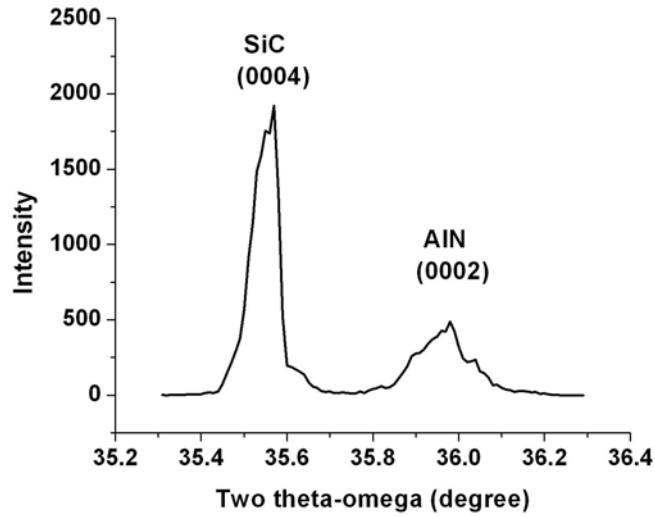


(b)

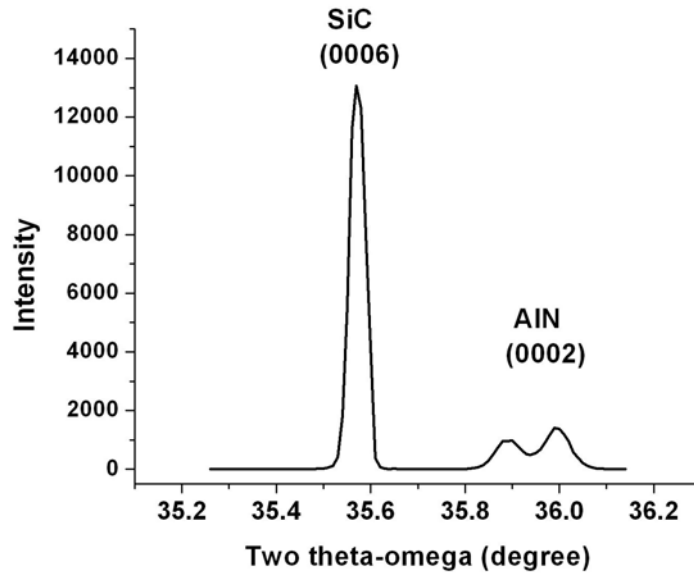
Fig. 5. AlN grown on on-axis 6H-SiC (0001) at 1850 °C for 2 hours:(a) micrograph and (b) 3D image and step height measurement by confocal microscope.

Fig. 6 (a) and (b) illustrate the conventional θ - 2θ x-ray diffraction patterns of the AlN films on 8° off-axis 4H-SiC and on-axis 6H-SiC grown at 1850°C for 2 hours. The symmetric AlN (0002) plane was characterized on both samples, indicating AlN grew along c -axis: AlN (0001) // SiC (0001). The 2θ value of AlN (0002) is in the range of $35.89 \sim 35.99^\circ$, which shifted from pure AlN, 36.04° toward 4H-SiC (0004), 35.67° , and 6H-SiC (0006), 35.75° . The calculated c -lattice constant of the AlN films is from 4.9860 to 5.0001, which is larger than that of the self-seeded growth AlN bulk crystal, 4.9795 Å [5]. The differences in the 2θ value and c -lattice constant were partially caused by the compression of the film, which was generated by the lattice mismatch between the AlN and SiC. Besides, using SiC as the seed could incorporate silicon and carbon into the AlN layer [7], changing its lattice constants. The SiC in the AlN may come from the volatile Si and C species generated by the decomposition of the SiC substrate during growth. For the AlN film grown on on-axis 6H-SiC, XRD characterized two peaks of AlN (0002), at 35.89° and 35.99° , respectively, resulting in two calculated c -lattice constants. The presence of multiple peaks implied that the AlN crystals were composed of multiple domains within the footprint of x-ray beam, which were slightly misoriented with respect to each other [16]. This phenomenon was well known in the sublimation growth of SiC boules [17]. The individual domains or sub-grains of crystal were separated by boundaries since they had different dislocation densities, difference stacking sequence, or a little basal-plane-tilt [16-19]. The FWHM (full width at half maximum) of AlN (0002) peak of the off-axis grown film, 576 arcsec, is much larger than that of the on-axis grown film, 218 and 246 arcsec. Since the stress was released by the sub-grain boundaries, the on-axis grown film suffered much less bending and less cracks than the

off-axis grown film resulting in better crystal quality. The XRD peak positions, FWHM, and the calculated c -lattice constants are reported in Table. 1. For comparison, data obtained for the SiC substrates are also presented in the same table.



(a)



(b)

Fig. 6. X-ray rocking curve of AlN films grown at 1850 °C for 2 hours: (a) on 8 ° off-axis 4H-SiC(0001), and (b) on on-axis 6H-SiC(0001).

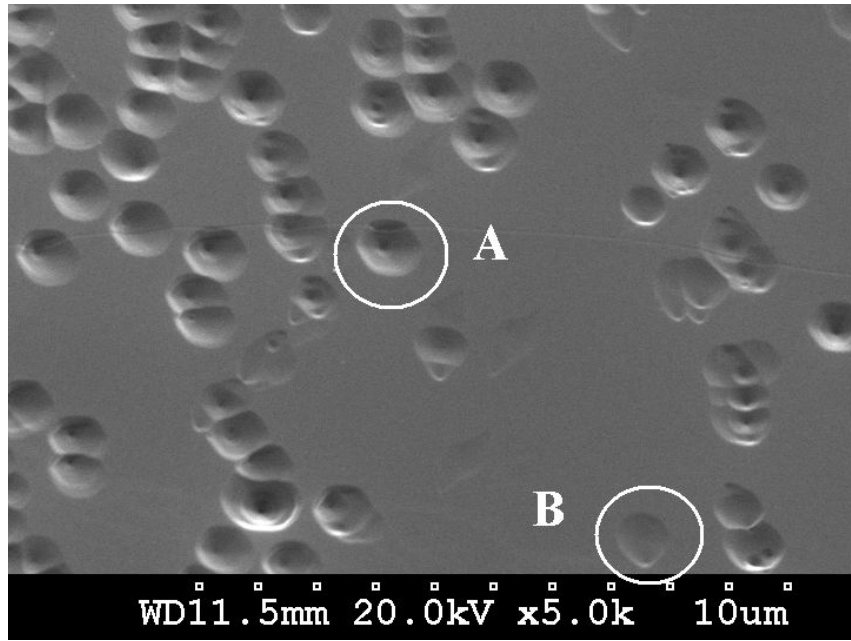
Table 1. Results of x-ray rocking curve of symmetric (0002) peaks of SiC substrates and AlN epilayers, and the lattice parameters of AlN epilayers.

Sample	AlN film thickness (μm)	SiC		AlN (0002)		<i>c</i> -lattice of AlN (\AA)
		2θ ($^\circ$)	FWHM (arcsec)	2θ ($^\circ$)	FWHM (arcsec)	
AlN grown on 8° off-axis 4H-SiC at 1845°C for 2 hrs.	Nonuniform 20 ~ 35	35.57	192	35.98	576	4.9890
AlN grown on on-axis 6H-SiC at 1850°C for 2 hrs.	Nonuniform 20 ~ 35	35.57	145	35.99	218	4.9860
				35.89	246	5.0001

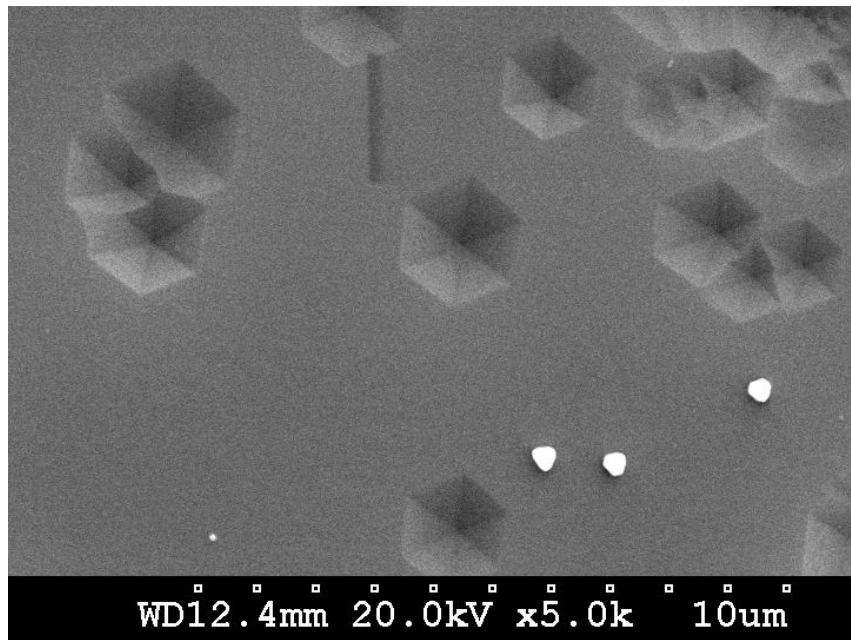
3.3. Wet chemical etching

The AlN films grown on the 8° off-axis 4H-SiC (0001) and the on-axis 6H-SiC (0001) were etched in aqueous KOH solution and molten KOH/NaOH eutectic alloy sequentially to characterize the polarity and dislocation densities. After the etching in the aqueous KOH solution, both samples' surfaces were unchanged indicating the Al-polarity on both surfaces. Then the molten KOH/NaOH etching was performed at 310°C for 5 minutes. Hexagonal etch pits and oval-shaped etch pits formed on the film grown on the 8° off-axis 4H-SiC. In Fig. 7 (a), a typical hexagonal pit and an oval-shaped pit were circled and denoted as A and B, respectively. The hexagonal etch pit related to a threading dislocations, which was perpendicular to *c*-plane. Some were caused by the propagation of dislocations from the SiC substrate into the AlN layer, approximately $10^4 - 10^5 \text{ cm}^{-2}$, and the rest were generated during the growth due to the lattice mismatch between AlN and the SiC substrate. The oval-shaped etch pit related to a basal plane dislocation (BPD), a slip in the basal plane, which was caused by the thermoelastic stress due to the

temperature distribution in growing crystals [16, 20, 21]. Since the substrate and the AlN film were misorientated 8° from the basal plane, BPDs interrupt the film surface and be observed after etching. On the surface of the AlN film grown on the on-axis 6H-SiC, most of the etch pits were regular hexagons, i.e. threading dislocations, and no oval-shaped pits were observed, as shown in Fig. 7.(b). Surface etching can not reveal the BPDs in the on-axis grown film since the BPDs are parallel to the c -plane and do not interrupt the surface. The total dislocation densities of the two samples were both in the range of $2 - 3 \times 10^8 \text{ cm}^{-2}$, calculated by counting the etch pits in a given area.



(a)



(b)

Fig. 7. SEM images of AlN after etched in molten KOH/NaOH at 310 °C for 5 minutes: (a) grown on 8 ° off-axis 4H-SiC (0001) and (b) grown on on-axis 6H-SiC (0001).

4. Conclusions

The nucleation of AlN on SiC seeds was highly dependent on growth temperature. The optimum growth temperature for AlN was 1850 °C confirmed by subsequent two hours' growth. On Si-face, 8 ° off-axis 4H-SiC, initially AlN grew in a mixed type of 3D and 2D. As the layer grew thicker, the 2D growth mode became dominant, and the film covered all the hillocks and finally becoming continuous with steps feature indicating the step control growth mode. On Si-face, on-axis 6H-SiC, the grown AlN layer contains hexagonal sub-grains caused by different dislocation density or a little basal-plane-tilt. The wet chemical etchings performed in aqueous KOH solution and molten KOH/NaOH eutectic alloy confirmed that the grown films surfaces were Al-polarity and no N-polarity region were observed implying the AlN was free of inversion domains.

References

1. G.A. Slack, T.F. McNelly, *J. Crystal Growth* 34 (1976) 263.
2. G.A. Slack, T.F. McNelly, *J. Crystal Growth* 42 (1977) 560.
3. M. Bickermann, B.M. Epelbaum, A. Winnacker, *J. Crystal Growth* 269 (2004) 432.
4. C.M. Balkas, Z. Sitar, T. Zheleva, L. Bergman, R. Nemanich, R.F. Davis, *J. Crystal Growth* 179 (1997) 363.
5. L. Liu, J.H. Edgar, *Mater. Sci. Eng.*, R37 (2002) 61.
6. R. Dalmau, R. Schlessler, B.J. Rodriguez, R.J. Nemanich, Z. Sitar, *J. Crystal Growth* 281 (2005) 68.
7. E.N. Mokhov, O.V. Avdeev, I.S. Barash, T.Yu. Chemekova, A.D. Roenkov, A.S. Segal, A.A. Wolfson, Yu.N. Makarov, M.G. Ramm, H.Helava, *J. Crystal Growth* 281 (2005) 93.
8. Y. Shi, B. Liu L. Liu J.H. Edgar, H.M. Meyer III, E.A. Payzant, L.R. Walker, N.D. Evans, J.G. Swadener, J. Chaudhuri, *Phys. Stat. Sol.* 188 (2001) 757.
9. Y. Shi, Z.Y. Xie, L.H. Liu, B. Liu, J.H. Edgar, M. Kuball, *J. Crystal Growth* 233 (2001) 177.
10. R. Yakimova, A. Kakanakova-Georgieva, G.R. Yazdi, G.K. Gueorguiev, M. Syväjärvi, *J. Crystal Growth* 281 (2005) 81.
11. S. Yamada, J. Kato, S. Tanaka, I. Suemune, *Appl. Phys. Lett.* 78 (2001) 3612.
12. B. Liu, J.H. Edgar, B. Raghathamachar, M. Dudley, J.Y. Lin, H.X. Jiang, A. Sarua, M. Kuball, *Mater. Sci. Eng.*, B 117 (2005) 99.
13. D. Zhuang, J.H. Edgar, B. Strojek, J. Chaudhuri, *Z. Rek, J. Crystal Growth* 262 (2004) 89.

14. J.L. Weyher, P.D. Brown, A.R.A. Zauner, S. Müller, C.B. Boothroyd, D.T. Foord, P.R. Hageman, C.J. Humphreys, P.K. Larsen, I. Grzegory, S. Porowski, *J. Crystal Growth* 204 (1999) 419.
15. H. Matsunami, T. Kimoto, *Mater. Sci. Eng., A* R20 (1997) 125.
16. S. Ha, M. Skowronski, W.M. Better, M. Dudley, *J. Appl. Phys.* 92 (2002) 778.
17. R.C. Glass, L.O. Kjellberg, V.F. Tsvetkov, J.E. Sundgren, E. Janzén, *J. Crystal Growth* 132 (1993) 504.
18. M. Tuominen, R. Yakimova, R.C. Glass, T. Tuomi, E. Janzén, *J. Crystal Growth* 144 (1994) 267.
19. J. Takahashi, N. Ohtani, M. Kanaya, *J. Crystal Growth* 167 (1996) 596.
20. W.M. Vetter, M. Dudley, *Philos. Mag. A*, 81 (2001) 2885.
21. D. Hull and D.J. Bacon, *Introduction to Dislocations*, 3rd ed. (Butterworth-Heinemann, Oxford, 1984), pp. 47-70.

Bulk AlN crystal growth on SiC seeds and defects study

P. Lu ¹, C. Cao ¹, J.H. Edgar ¹, K.Hohn ¹, R. Dalmau ², R. Schlessner ², and Z. Sitar ²

1. Department of Chemical Engineering, Kansas State University, Manhattan, KS 66506

2. Department of Materials Science and Engineering, North Carolina State University,
Raleigh, NC 27695

* Corresponding author: Peng Lu; Tel: 1-785-532-4325; Fax: 1-785-532-7372;

E-mail address: plu@ksu.edu

Abstract

Sublimation growth of AlN was performed on Si-face, 8 ° off-axis 4H-SiC (0001) and 3.5 ° off-axis 6H-SiC (0001) seeds. AlN layers 500 - 900 μm thick and 20 mm in diameter were grown at 1830 °C by consecutive growths and continuous growth. The *c*-axis growth rate was approximately 8 - 18 μm/hr. On both the 8 ° and 3.5° off-axis SiC substrates, “step” features formed on the AlN surface with uniformed terrace width and step density. The step heights and terrace widths increased as the AlN grew thicker. In addition, a single facet of 9 mm × 5 mm formed on the top of the layer grown on the 3.5 ° off-axis SiC. High resolution x-ray diffraction showed the AlN (00.2) 2θ value shifted from pure AlN toward SiC. Approximately 3 – 4 at% of SiC was detected at the surface of the AlN by XPS. Molten KOH/NaOH etching revealed that both samples had Al-polar surface with dislocation densities on the order of 10⁶-10⁷ cm⁻². The cross-section etching showed the re-nucleation layer and voids defects at the interfaces of the consecutive growths.

1. Introduction

Aluminum nitride (AlN) is a direct wide band gap semiconductor ($E_g = 6.2$ eV) with high thermal conductivity and high thermal stability. Due to its small lattice mismatch and small differences in thermal expansion coefficient with GaN, AlN is an ideal substrate for GaN based devices such as high-power UV lasers, UV photodetectors and blue light emitting diodes.

The most successful growth of bulk AlN is by the sublimation-recondensation method, as demonstrated by Slack and McNelly [1,2], Bickermann [3], and others. SiC crystals were first employed as seed crystals for bulk AlN growth by Campbell and Chang in 1967 [4]. SiC is a suitable substrate for AlN bulk crystal growth since it has a small a -lattice mismatch (0.96% for 6H-SiC and 1.2% 4H-SiC) [5] with AlN. Dalmau *et al.* [6] grew 3 mm thick single crystal AlN layers on both on-axis 6H-SiC (0001) and off-axis 4H-SiC (0001). On Si-face of SiC, the AlN layers were primarily Al-polarity. Mokhov *et al.* [7] successfully grew a 10-12 mm thick single crystal AlN layer on SiC substrates.

The nucleation of AlN on SiC has been studied in the author's previous paper [8]. Initial growth for 15 minutes and extend growth for 2 hours suggested that 1800 – 1850 °C was the optimum temperature range of AlN crystal growth. In this present work, long time growth, 20 – 50 hours growths were performed to deposit thick AlN layer on SiC substrates.

2. Experimental

AlN crystals were grown by sublimation in a resistively heated graphite furnace. The source material was AlN powder originally containing less than 1 wt % oxygen and 0.06 wt % carbon. Prior to growth, the AlN powders were purified by baking at 1850 – 1900 °C for 4 h, which reduced the oxygen concentration to less than 0.1 wt %, as measured by LECO analysis. Si-face, 8 ° off-axis 4H-SiC (0001) and 3.5 ° off-axis 6H-SiC (0001) were employed as seeds. As-received wafers were cut into 25 mm × 25 mm pieces and held on the top of the crucible, initially 5 mm above the surface of the AlN source. The seed temperature was 15 °C lower than that of the source. The AlN was grown at 1830 ± 10 °C (the source temperature) in UHP nitrogen at 800 torr. In one set of experiments, AlN was grown on one 8 ° off-axis 4H-SiC substrate for three consecutive 20 h periods with fresh baked source each time. In another experiment, the growth condition was modified: the temperature difference between the source and the seed was reduced to 5 – 10 °C and AlN was continuously grown on a 3.5 ° off-axis 6H-SiC substrate for 50 h. The crystal orientation was examined by high resolution x-ray diffraction (HRXRD).

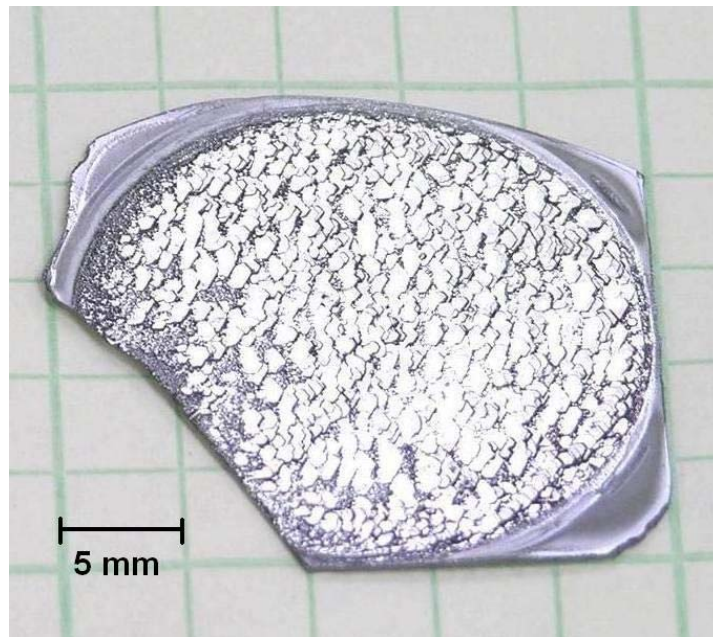
To explore the impurities in the crystal, the AlN layer grown on 8 ° off-axis 4H-SiC was characterized by x-ray photoelectron spectroscopy (XPS). The surface was sputtered by Ar ions for 1 hour to remove the oxidation layer and then scanned for 20 minutes.

The resulting AlN/SiC samples were etched in a molten KOH/NaOH eutectic alloy (59 wt % KOH / 41 wt % NaOH) at 300 – 310 °C for 5 minutes to examine the surface polarity and dislocation density. After etching, N-polar surface forms hexagonal hillocks

while the Al-polar surface forms etch pits at the dislocation sites. The type and the density of dislocations can be revealed by the shape and density of the etch pits [9].

3. Results and discussion

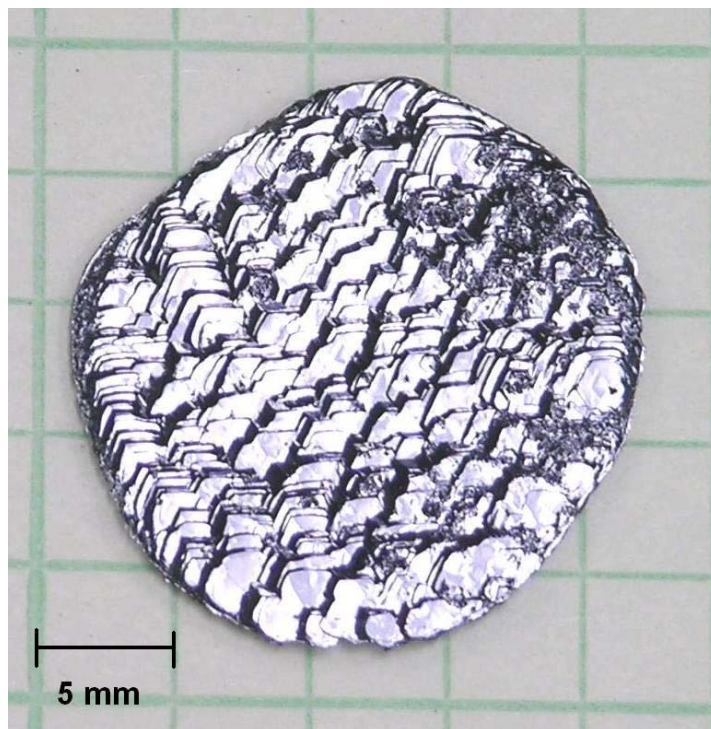
On 8° off-axis 4H-SiC substrate, an AlN layer with a diameter of 20 mm formed after the first 20 hours of growth. The surface consisted of “step” features with terrace width of 0.5 mm. As the AlN layer grew thicker during the second and third growths, and the terrace width enlarged to 1 mm and 1.5 – 2 mm, as shown in Fig. 1 (a) – (c), respectively. The total thickness of the AlN layer was 450 – 500 μm with the average growth rate of 8 $\mu\text{m}/\text{h}$. Some area near the edges became rough, caused by tilted growth of small AlN grains.



(a)



(b)



(c)

Fig. 1. Photographs of three consecutive growths on the same 8° off-axis 4H-SiC (0001): (a) after the first 20 h growth, (b) after the second 20 h growth, and (c) after the third 20 h growth.

On the 3.5° off-axis 6H-SiC substrate, an AlN layer with a diameter of 15 mm and a thickness of 800 – 900 μm formed after growth for 50 h, with an average rate of 15 – 18 $\mu\text{m}/\text{h}$. The surface consisted of “step” features with terrace of 0.2 – 0.5 mm. A single facet of $9\text{ mm} \times 5\text{ mm}$ was present of the top of the layer, as shown in Fig. 2.

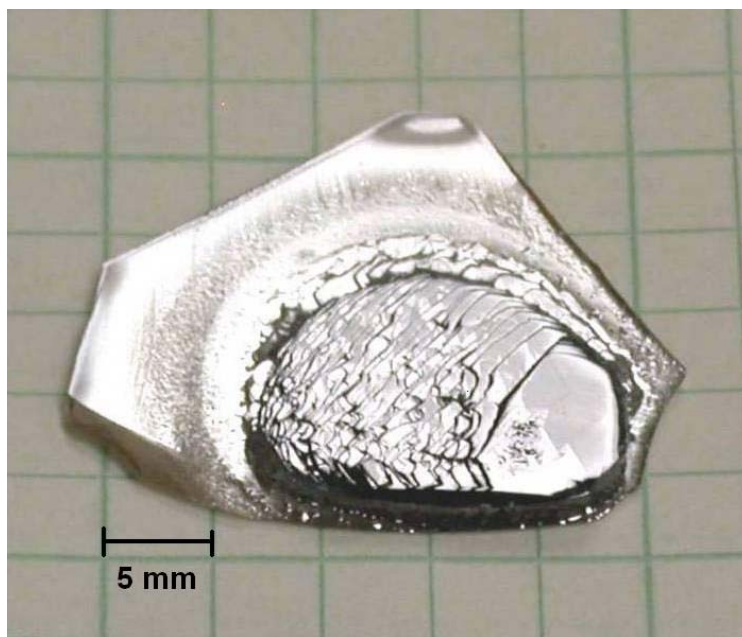
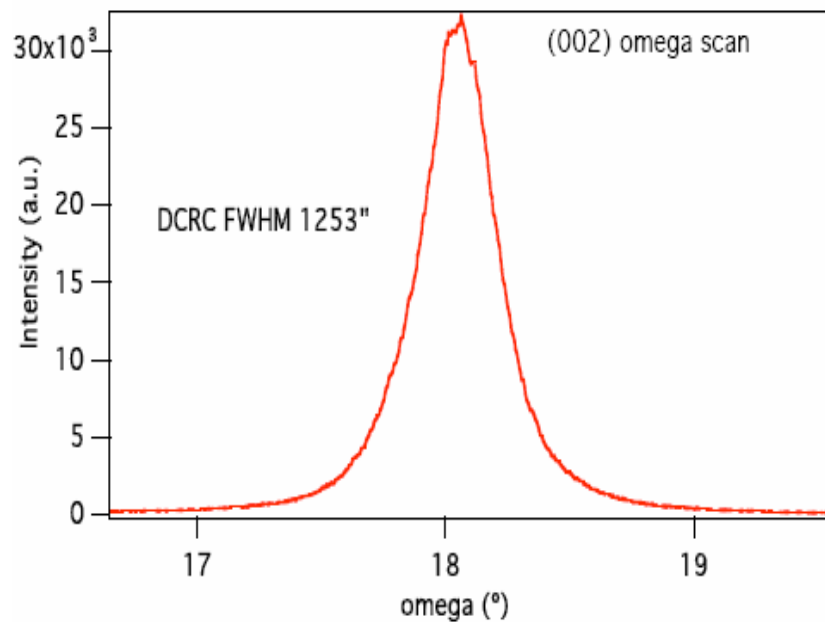


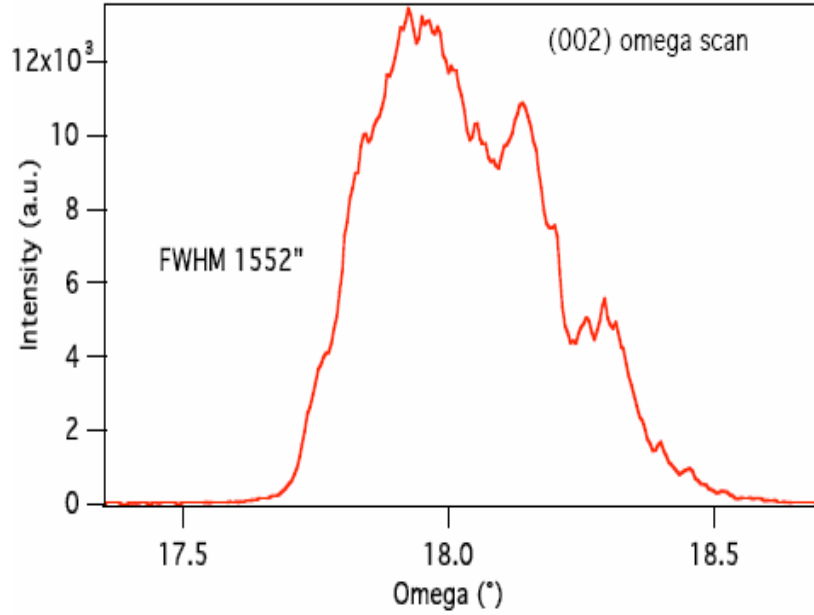
Fig. 2. Photograph of AlN on 3.5° off-axis (00.1) 6H-SiC substrate after growth for 50 h.

The crystal quality was examined by x-ray diffraction (XRD). The ω -scan double crystal rocking curves (DCRC) characterized the (00.2) AlN peak from the above two samples, illustrated in Fig. 3 (a) and (b). The full-width at half-maximum (FWHM) of the ω rocking curve (RC) are 1253 arcsec and 1552 arcsec for the films grown on the 8° off-axis 4H-SiC and 3.5° off-axis 6H-SiC substrates, respectively. Peak broadening could be

attributed to the presence of cracks in the AlN, bowing of the wafer due to the differential thermal expansion between AlN and SiC, and crystallographic tilt distribution of mosaic blocks. The precise Bragg peak 2θ angle was 35.97° for both films as determined by the high-resolution triple crystal (00.2) 2θ - ω scan. This value is shifted from the powder diffraction file (PDF) database value of AlN (36.04°) toward 4H-SiC (00.4) (35.67°) and 6H-SiC (00.6) (35.75°). The shift in the 2θ value was partially caused by the compression of the film due to the lattice mismatch between the AlN and SiC. In addition, the decomposition of SiC seed could generate volatile silicon and carbon species, which subsequently incorporate into the AlN layer, changing its lattice constants.



(a)



(b)

Fig. 3. (00.2) ω -scan double crystal rocking curves (DCRC) of the main diffraction peak from (a) AlN film grown on 8° off-axis 4H-SiC and (b) AlN film grown 3.5° off-axis 6H-SiC.

The XPS spectrum and the detected elements are shown in Fig. 4. Approximately 3.6 at% of silicon was detected, which came from the decomposition of SiC seed. 8.4 at% of carbon was detected, which came from both the SiC seed and the degradation of the graphite components of the furnace. The apparent oxygen concentration was 3.8 at%, but this value was higher than the actual value, a consequence of the strong affinity of the AlN surface toward oxygen. After the sputtering, the detected oxygen peak was really small, however during the scan the peak intensity gradually increased due to the re-deposition of the oxygen.

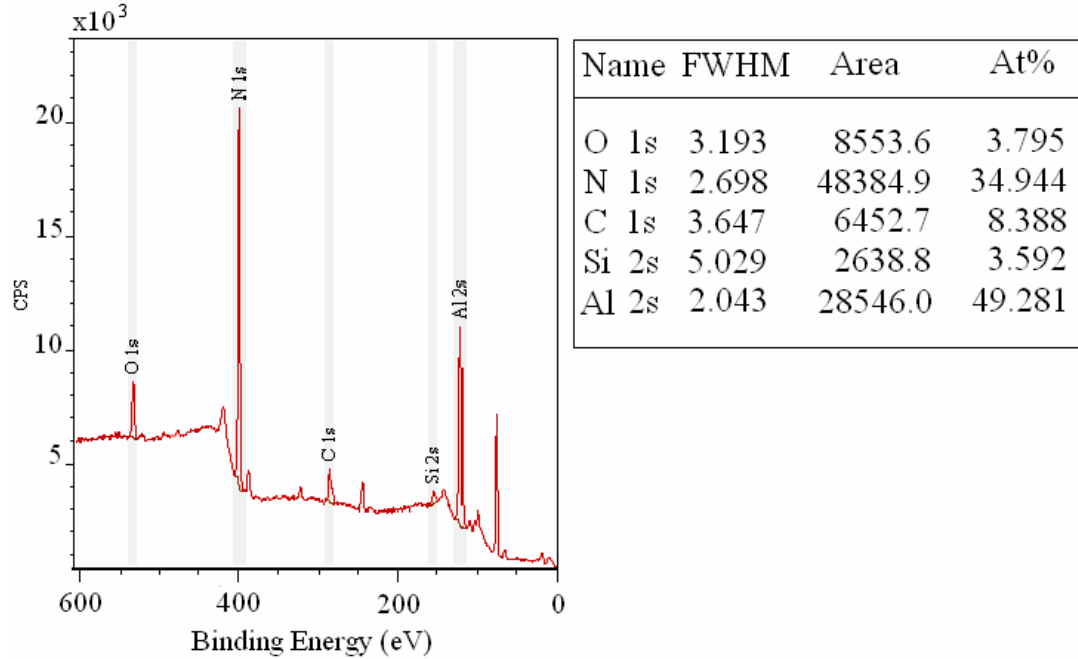
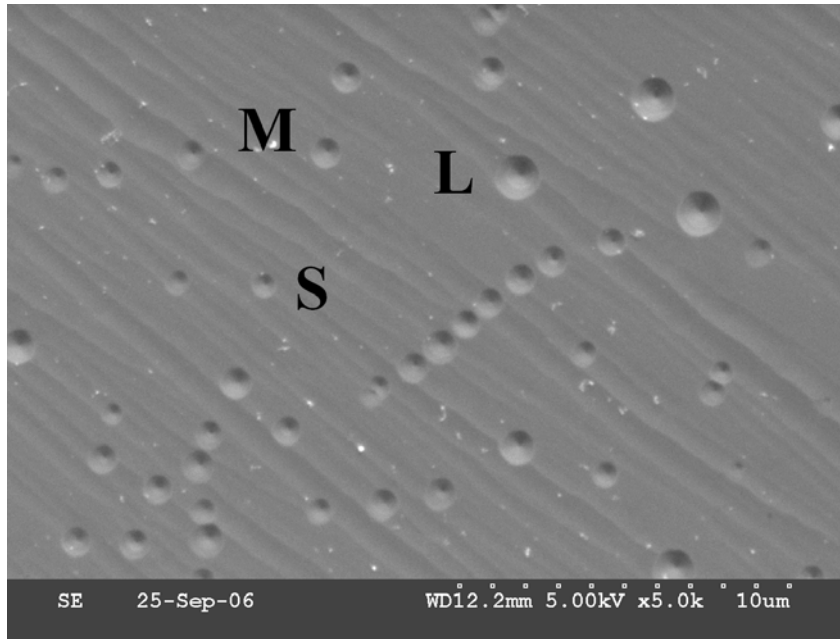


Fig. 4. XPS spectrum and analysis results of the AlN layer grown on 8° off-axis 4H-SiC for three consecutive growths for total 60 h.

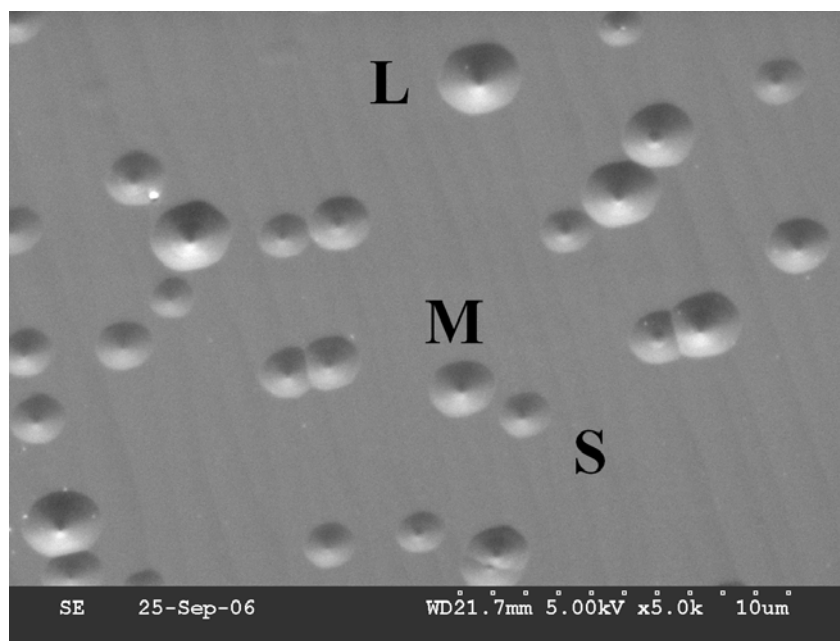
After defect selective etching, only pits appeared on the surfaces (no hillocks), indicating both layers have Al-polar surfaces and no N-polar inversion regions. Most of the etch pits on both surface were hexagonal shaped, related to threading dislocations, as shown in SEMs, Fig. 5 (a) and (b). Three etch pit sizes are clearly visible in these figures indicating the presences of three types of dislocations in the films. In Fig. 5, small, medium and large etch pits are pointed as S, M, and L, respectively. By investigating the molten KOH etching of GaN, Weyher [10] suggested that the small, medium, and large etch pits were associated with edge dislocations, mixed edge and screw dislocations, and screw dislocations respectively. Further work is underway to see if this association also holds true for AlN. The dislocation densities on the 500 μm thick film and the 900 μm thick film are $1.3 \times 10^7 \text{ cm}^{-2}$ and $4.3 \times 10^6 \text{ cm}^{-2}$, estimated by counting the etch pits in a given area. The author’s previous paper [8] reported the dislocation density in a 30 μm

thick AlN film grown on SiC was $2 - 3 \times 10^8 \text{ cm}^{-2}$. Clearly, the dislocation density decreased as the film thickness increased. It can also be observed from Fig. 5 that the terraces are not really flat, but are composed of smaller micro-steps, which are parallel to the macro-steps shown in Fig. 1 and Fig. 2.

The AlN layer grown on the 8° off-axis 4H-SiC was cleaved and its cross-section was etched in molten KOH/NaOH as the same condition as the growing surface. Interfaces created by interrupting growth are evident in the cross-sectional SEM, Fig. 6 (a). At the beginning of each consecutive growth, the AlN first re-nucleated, forming numerous hillocks, Fig. 6 (b); further growth in the *c*-axis direction produced a continuous solid layer. The re-nucleation layer might be caused by lower temperature nucleation and impurity incorporation, e.g. oxygen. In addition, voids, up to $1 \mu\text{m} \times 3 \mu\text{m}$, were also observed at the interfaces due to the incomplete coalescence of the re-nucleation layer, Fig. 6 (c). Clearly, the re-nucleation layer and the voids degraded the crystal quality and generate extra defects. Hence, long-time, continuous growth is preferable to produce better quality and less defects AlN crystal.



(a)



(b)

Fig. 5. SEM images of AlN layers after molten KOH/NaOH etching, (a) AlN layer grown on 8° off-axis 4H-SiC and (b) AlN layer grown on 3.5° off-axis 6H-SiC.

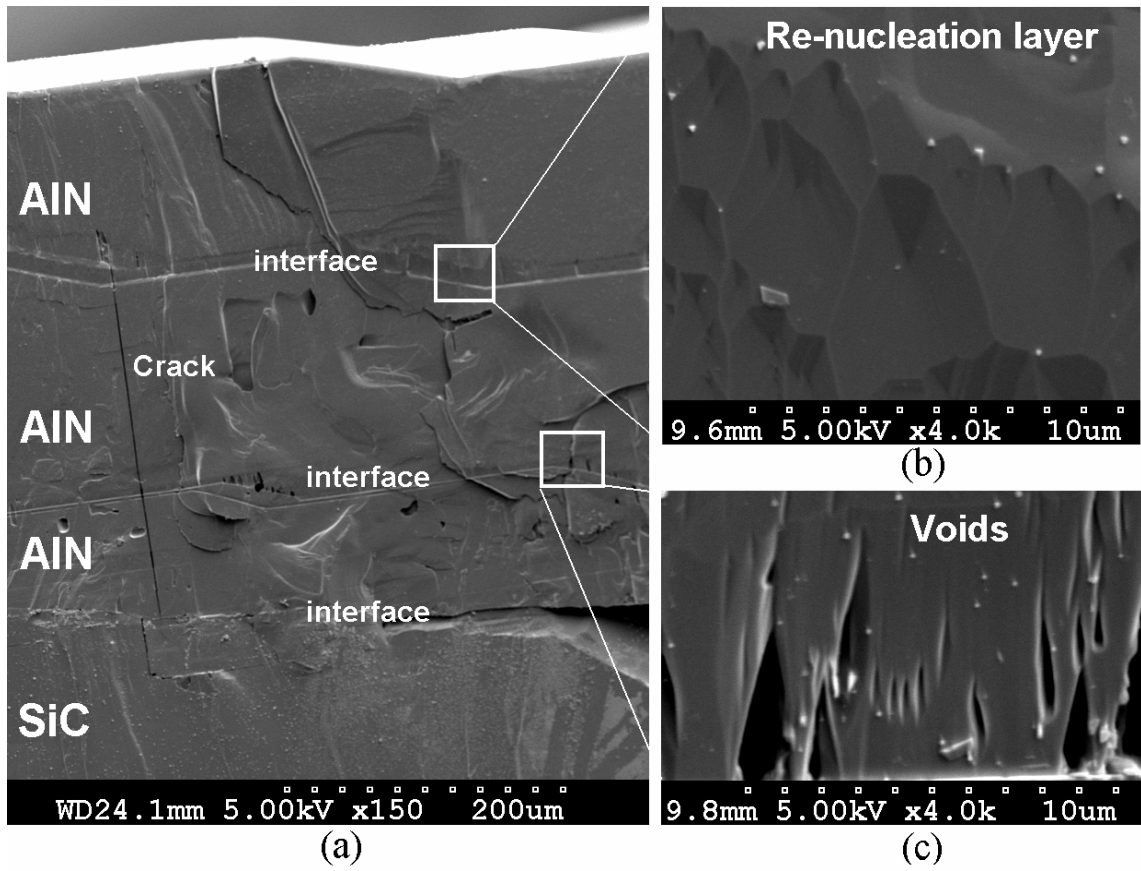


Fig. 6. Cross-section SEM images of the AlN layer grown the 8 ° off-axis 4H-SiC after molten KOH/NaOH etching: (a) the whole layer, (b) re-nucleation layer, and (c) voids defects.

4. Conclusions

AlN layers grown on 8 ° off-axis and 3.5 ° off-axis SiC seeds showed slightly different surface morphologies: uniformed “steps” feature were formed the 8 ° off-axis grown AlN film, while a single facet was present on top layer of the 3.5 ° off-axis grown AlN film. Presumably, on the 3.5 ° off-axis SiC seed, as the AlN layer grow thick enough, a single facet may cover the entire growing surface. Smaller temperature difference (5 – 10 °C) between the source the seed produce higher growth rate for AlN seeded growth on SiC. The dislocation densities are $1.3 \times 10^7 \text{ cm}^{-2}$ on the 500 μm thick AlN film and $4.3 \times 10^6 \text{ cm}^{-2}$ in the 900 μm thick AlN film. Long time, continuous growth is better than the short time consecutive growth due to the re-nucleation layer present at the each growth interface.

Acknowledgements

Support for this project from Hexatech Inc. and the National Science Foundation via award DMR 0408874 is greatly appreciated.

References

1. G.A. Slack and T.F. McNelly, *J. Cryst. Growth* 34, 263 (1976).
2. G.A. Slack and T.F. McNelly, *J. Cryst. Growth* 42, 560 (1977).
3. M. Bickermann, B.M. Epelbaum, and A. Winnacker, *J. Cryst. Growth* 269, 432 (2004).
4. R.B. Campbell and H.-C. Chang, *U.S. Govt. Res. Develop. Fed. Sci. Tech. Inform.*, (AD-815895), 164 (1969).
5. L. Liu and J.H. Edgar, *Mater. Sci. Eng.* R37, 61 (2002).
6. R. Dalmau, R. Schlessler, B.J. Rodriguez, R.J. Nemanich, and Z. Sitar, *J. Cryst. Growth* 281, 68 (2005).
7. E.N. Mokhov, O.V. Avdeev, I.S. Barash, T.Yu. Chemekova, A.D. Roenkov, A.S. Segal, A.A. Wolfson, Yu.N. Makarov, M.G. Ramm, and H. Helava, *J. Cryst. Growth* 281, 93 (2005).
8. P. Lu, J.H. Edgar, R.J. Lee and J. Chaudhuri, submitted to *J. Cryst. Growth*.
9. D. Zhuang, J.H. Edgar, B. Strojek, J. Chaudhuri, and Z. Rek, *J. Cryst. Growth* 262, 89 (2004).
10. J.L. Weyher, to be published in *Superlattices and Microstructures*.

Seeded growth of AlN on SiC substrates and defect characterization

P. Lu ^{a,*}, J.H. Edgar ^a, C. Cao ^a, K.Hohn ^a, R. Dalmau ^b, R. Schlessner ^b, and Z. Sitar ^b

^a Department of Chemical Engineering, Kansas State University, Manhattan, KS 66506

^b Department of Materials Science and Engineering, North Carolina State University,
Raleigh, NC 27695

* Corresponding author: Peng Lu; Tel: 1-785-532-4325; Fax: 1-785-532-7372;

E-mail address: plu@ksu.edu

Abstract

Sublimation growth of AlN was performed on Si-face, 3.5 °off-axis 6H-SiC (0001) seeds. AlN layers, each with 1 – 2 mm thick and 15 – 20 mm in diameter, were grown at 1830 °C. The *c*-axis growth rate was 15 - 20 μm/h. Step features formed on the surface with uniform terrace width and step density. In addition, a single facet of 9 mm × 6 mm formed on the top of the layer. High resolution x-ray diffraction showed the AlN (00.2) 2θ value shifted from pure AlN toward SiC. Both silicon and carbon were detected in the AlN by x-ray photoelectron spectroscopy. The layer with the higher concentrations of silicon (6 at%) and carbon (8 at%) exhibited a deep blue color, and the layer with lower concentrations of silicon (3 at%) and carbon (5.9 at%) exhibits transparent amber color. Molten KOH/NaOH etching revealed the grown layers had Al-polar surface and the dislocation density decreased from 10⁸ cm⁻² to 10⁶ cm⁻² as the film thickness increased from 30 μm to 2 mm.

1. Introduction

Aluminum nitride (AlN) is a direct wide band gap semiconductor ($E_g = 6.2$ eV) with high thermal conductivity and high thermal stability. Due to its small mismatch in coefficient of thermal expansion and lattice constants single crystal AlN is an ideal substrate for $\text{Al}_x\text{Ga}_{1-x}\text{N}$ epitaxial layers, as are used in high-power UV lasers diodes, UV photodetectors and blue light emitting diodes (LEDs). The benefits of AlN substrates was dramatically illustrated recently by Taniyasu *et al.* [1], who was able to prepare a silicon-doped AlN epitaxial layer with an extremely high room temperature electron mobility, $400 \text{ cm}^2/\text{V}\cdot\text{s}$, by using an AlN substrates with a low dislocation density.

Sublimation is the most successful growth method for bulk AlN single crystals, as demonstrated by Slack and McNelly [2, 3], Bickermann [4], and others [5-7]. SiC is a suitable substrate for AlN bulk crystal growth since it has a small a -lattice constant mismatch (0.96% for 6H-SiC and 1.2% 4H-SiC) [8] with AlN. Large area (up to 100 mm in diameter) and high quality single crystalline 4H- and 6H-SiC wafers are commercialized, providing high quality seeds for AlN. AlN crystals grown on 6H-SiC(0001) have a single crystallographic orientation to the c -axis [9]. Balkas *et al.* [10] obtained single crystalline AlN platelets ($2 \times 2 \text{ mm}^2$) in hexagonal shape in a temperature range of 2150 – 2250 °C with a growth rate up to 0.5 mm/hr. Contaminations of Si, C and O, and high density of screw dislocation and cracks were observed [10]. The cracking was caused by thermal expansion mismatch between AlN and SiC, which was also reported by others [11]. Edgar *et al.* [9, 12-14] designed a novel sublimation sandwich technique and utilized a tungsten resistively heating reactor to grow AlN on SiC. A

MOCVD layer of AlN/SiC alloy was deposited on SiC substrate prior to pure AlN growth to compensate the thermal expansion and lattice mismatch. Though cracks and stress were not completely eliminated, a freestanding AlN crystal ($4 \times 6 \text{ mm}^2$) was obtained after 100 hours growth [14]. The growth temperature, and thus the growth rate, was kept low to prevent the decomposition of SiC. Epelbaum *et al.* [15] reported the observations of three-dimensional growth of AlN on Si-face on-axis (0001) 6H-SiC. However, they produced fully coalesced AlN layers by employing a slightly off-axis substrate, where the step-flow growth mode was achieved [15].

Most recently, Dalmau *et al.* [16] obtained 3 mm thick single crystal AlN layers on both on-axis 6H-SiC (0001) and off-axis 4H-SiC (0001) by “two-step growth”. First a fully coalesced AlN layer was grown at a low temperature around 1850 °C with a growth rate of 10 – 30 $\mu\text{m/hr}$, covering the SiC substrate. Then the temperature was raised 100 – 200 °C to achieve a high growth rate of 70 $\mu\text{m/hr}$. As-grown surface were characterized by sharp hexagonal hillocks [16]. Wang *et al.* [17] and Balakrishnan *et al.* [18] carried out the AlN growth on C-face SiC substrates, and 650 μm and 300 μm thick AlN layers were obtained respectively. They claimed that C-face SiC can produce AlN layers with smoother surface [17] and higher growth rate [18] than Si-face SiC.

The author’s previous paper investigated the initial growth stage of AlN on SiC [19]. The optimum temperature of AlN is 1830 – 1850 °C: 20 – 30 μm thick single crystalline AlN layers were produced on 8 ° off-axis 4H-SiC and on-axis 6H-SiC for two hours growth. The off-axis grown film consisted of regular steps features on the surface, while the on-axis grown film contained hexagonal sub-grains with different sizes. In this

present work, long period growths (50 – 100 hours) were performed to grow thick and large AlN layers based on the optimum conditions obtained from the nucleation study.

2. Experimental

The AlN crystals were grown by sublimation in a resistively heated graphite furnace, consisting of a growth chamber, a graphite heating element, graphite foam insulation and a temperature and pressure control system, as illustrated in [20]. The source material was AlN powder originally containing less than 1 wt % oxygen and 0.06 wt % carbon. Prior to growth, the AlN powders were purified by baking at 1900 °C for 4 h, which reduced the oxygen concentration to less than 0.1 wt %, as measured by gas fusion technique. Si-face, 6H-SiC (0001) with an 3.5 ° mis-orientation toward $(11\bar{2}0)$ was employed as the substrate. As-received wafers were cut into approximately 25 × 25 cm² pieces and cleaned in organic solvents in the sequence of trichloroethylene, acetone and methanol, rinsed with DI water and dried with nitrogen. The substrate was held directly on the crucible top with 3 mm above the surface of the sintered source. The temperature of substrate was 5 – 10 °C lower than the source. All samples were grown at a source temperature of 1830 °C. The crystal orientation was examined by high resolution x-ray diffraction (HRXRD).

X-ray photoelectron spectroscopy (XPS) was employed to characterize the impurities in the grown crystal. The sample surface was sputtered by Ar ions for 1 h to remove the oxidation layer and then scanned for 20 minutes.

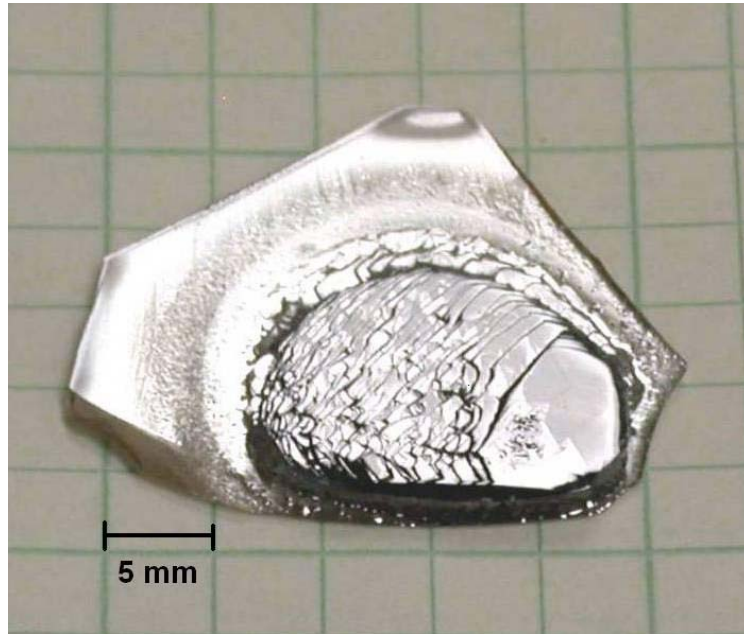
To explore the polarity and dislocation density of the grown AlN layers, the samples were etched in a molten KOH/NaOH eutectic alloy (59 wt % KOH / 41 wt % NaOH) at 300 – 310 °C for 5 minutes. In molten KOH/NaOH, both the N-polarity and the Al-polarity are etched: the N-polarity forms hexagonal hillocks and the Al-polarity forms hexagonal etch pits. The type and the density of dislocations were revealed by the shape and density of the etch pits [21].

3. Results and discussion

3.1 Surface morphology and crystal color

In this paper, two samples (A and B) are discussed. Sample A was grown for one period of 50 h, and sample B was grown for two consecutive 50 h periods. Between the two consecutive growths, the crucible was refilled with sintered AlN source. The two samples have similar surface morphologies: the surface consisted of step features, with the step width of 0.3 – 1 mm; a single facet was present on the top layer. The single facet of sample A is of 9 mm × 6 mm, as shown in Fig. 1 (a). The single facet of sample B enlarged from 9 mm × 3 mm after the first growth to 9 × 6 mm after the second growth, as shown in Fig. 1 (b) and (c). For both samples, the step terraces are smooth without any tilted growths or polycrystalline grains, indicating the superior epitaxy, as shown in Fig. 2. However, cracks still appeared on the surface, due to the mismatches in lattice constants and thermal expansion coefficient between the AlN and SiC. Sample A and B are approximately 0.9 – 1 mm and 1.7 – 2 mm thick, respectively, thus, the *c*-axis growth rate for both is approximately 15 – 20 μm/hr. The side view of sample B is shown in Fig.

3. Sample A exhibits a deep blue color, while sample B has a transparent amber color, implying they may contain different contamination levels.



(a)



(b)



(c)

Fig. 1. Images of:(a) sample A, grown at 1830 °C for 50 hours, (b) sample B, grown at 1830 °C for 50 hours, and (c) sample B, grown at 1830 °C for additional 50 hours.

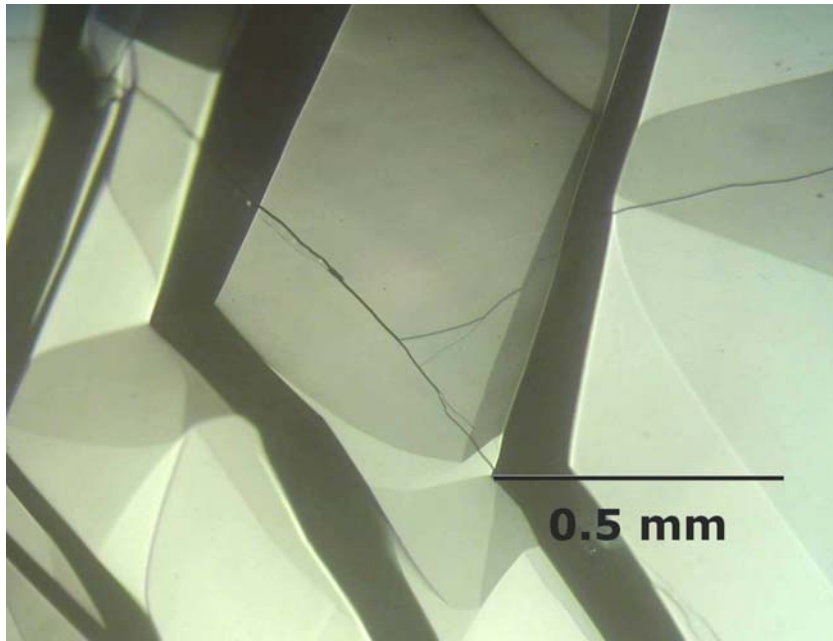


Fig. 2. A micrograph of sample B after the second growth.

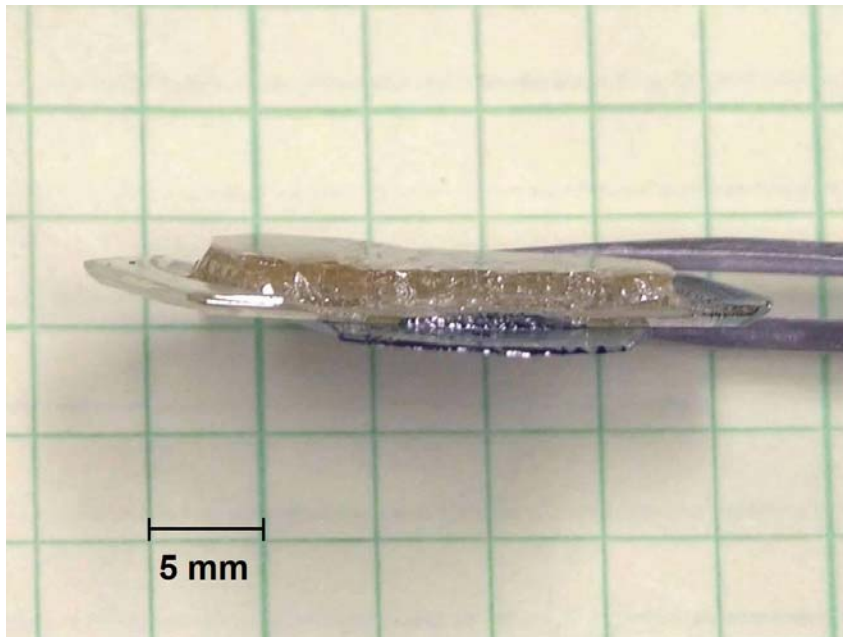


Fig. 3. Side-view image of sample B, showing the total AlN thickness of 1.7 – 2 mm.

3.2 Crystal quality characterization by high-resolution x-ray diffraction (HRXRD)

The ω -scan double crystal rocking curves (DCRC) characterized the AlN (00.2) peaks in both samples. The full-width at half-maximum (FWHM) of the ω rocking curve (RC) are 1552 arcsec and 444 arcsec for sample A and B, illustrated in Fig. 4 (a) and (b) respectively. Sample B has a better crystalline alignment than sample A. Peak broadening could be attributed to the presence of cracks in the AlN, bowing of the wafer due to the differential thermal expansion between AlN and SiC, and crystallographic tilt distribution of mosaic blocks. For comparison purpose, the backsides of the two samples (6H-SiC substrate without AlN) were also scanned by DCRC. The (00.6) DCRC of the SiC shows considerable peak broadening of a similar magnitude as the AlN layer for both samples, indicating the SiC wafer itself has a series of tilted mosaic blocks. The deposited AlN layer may replicate the mosaicity from the substrate. Thus, the AlN crystal quality is highly dependent on the quality of the SiC substrate underneath. For both samples the FWHM of (00.2) AlN peaks are smaller than the (00.6) SiC peaks from the back side of the substrate, implying that the grown AlN crystal quality may be as good or better than the SiC substrates. The FWHMs of the (00.2) AlN peaks and the (00.6) SiC are listed in Table 1.

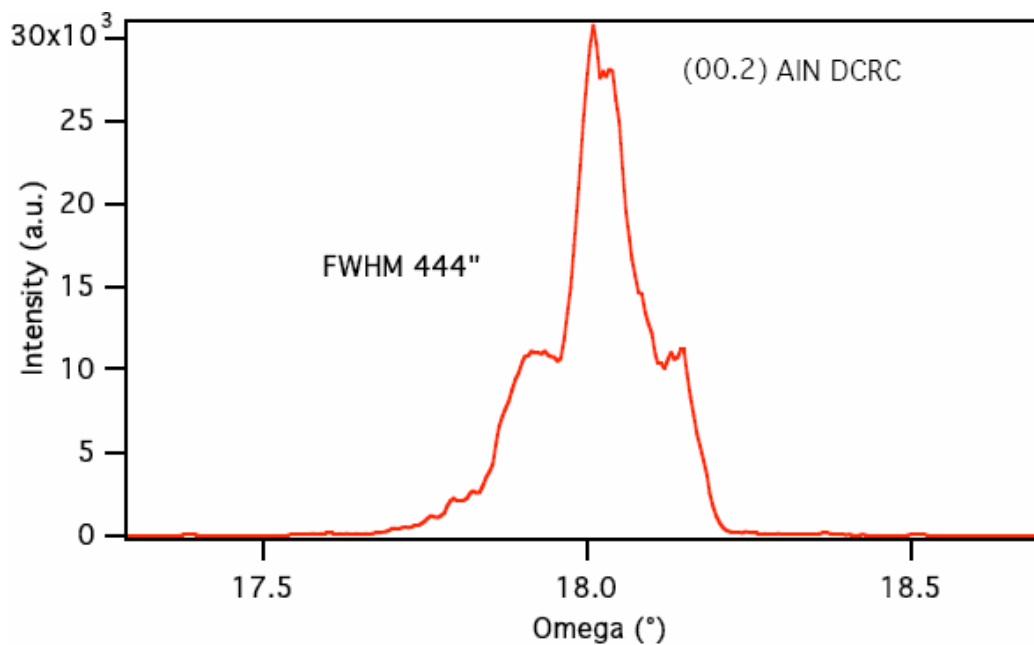
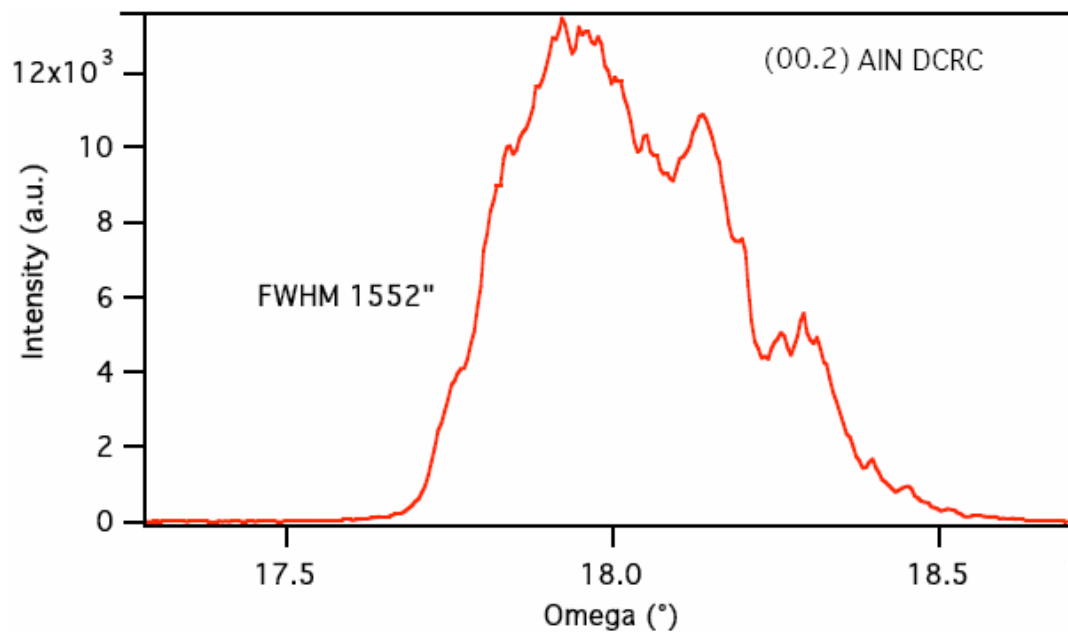


Fig. 4. The ω -scan double crystal rocking curves (DCRC) of the AlN (00.2) peak from (a) sample A, grown at 1830 °C for 50 hours, and (b) sample B, grown at 1830 °C for total 100 hours.

Table .1. FWHMs of the (00.2) AlN peaks and the (00.6) SiC peaks from the substrates

	Sample A		Sample B	
	AlN (00.2)	6H-SiC (00.6) (substrate)	AlN (00.2)	6H-SiC (00.6) (substrate)
FWHM	1552 ''	1690 ''	444 ''	577 ''

The precise Bragg peak 2θ angle was determined at 35.97° for both layers by the high-resolution triple crystal (00.2) 2θ - ω scan. This value shifted from the powder diffraction file (PDF) database value of AlN (36.04°) toward 6H-SiC (00.6) (35.75°). The shift in the 2θ value was partially caused by the compression of the film, which was generated by the lattice mismatch between the AlN and SiC. In addition, the decomposition of SiC seed could generate volatile silicon and carbon species, which subsequently incorporate into the AlN layer, changing its lattice constants.

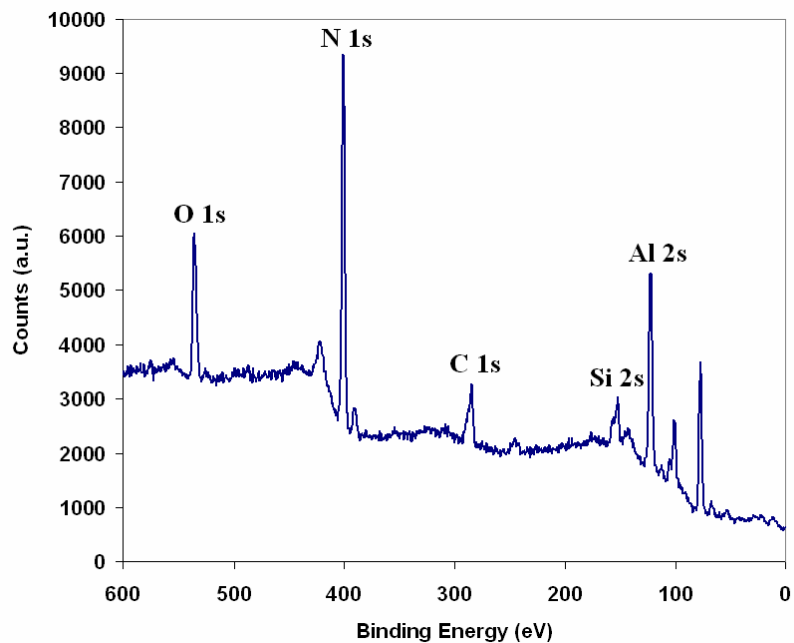
3.3 Impurities characterization by x-ray photoelectron spectroscopy (XPS)

The XPS spectrums of sample A and B are shown in Fig. 5 (b) and (b) and the detected elements and their atomic concentrations are listed in Table 2. The silicon in the crystals originated exclusively from the SiC seed, since there was no other silicon source in the furnace. The carbon in the crystals was from the SiC seed and the degradation of graphite components in the furnace. The impurities concentrations in sample A (Si: 6.0 at%, C: 8.1 at%) are higher than sample B (Si:3.0 at%, C: 5.9 at%). The differences in the silicon and carbon concentrations are believed to cause color difference in sample A and B.

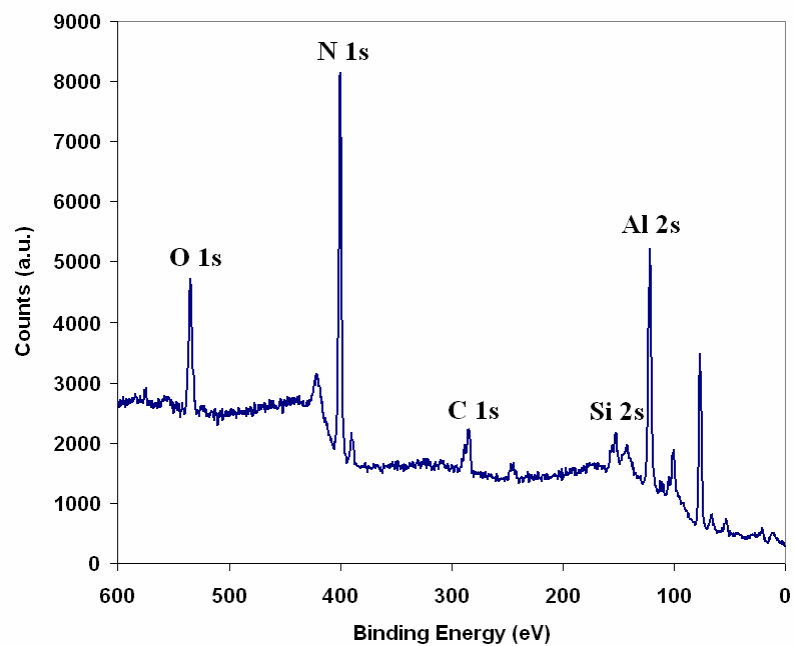
These two AlN layers were grown at nominally the same condition; however, unmeasured parameters might have affected the Si and C concentrations, such as unstable

growth temperature, crucible cracking and the condition of the heating element. In addition, the quality of the SiC substrate may influence the impurities in the AlN crystal. A SiC seed with a high micropipe density generates more volatile silicon and carbon than a seed with low micropipe density, since the decomposition at a micropipe is much faster than at a micropipe free region.

The oxygen concentrations in both samples were 8 – 9 at%., which were much higher than the actual values. Because of its strong affinity for oxygen, a native oxide layer forms on AlN whenever it is exposed to ambient air. Despite sputtering the sample before XPS measurements, oxygen was always detected, suggesting that oxidation occurs even under ultrahigh vacuum conditions. The oxygen concentration measured by XPS always exceeded the concentration of oxygen measured by LECO analysis (a bulk technique) of polycrystalline AlN grown by unseeded growth by two to three orders of magnitude. Since the AlN was grown on SiC substrates from similar source materials under similar conditions, we conclude that the high oxygen concentrations are limited to the surface of the samples.



(a)



(b)

Fig. 5. XPS spectrums of (a) sample A and (b) sample B.

Table .2. The detected elements and their atomic concentrations in sample A and B.

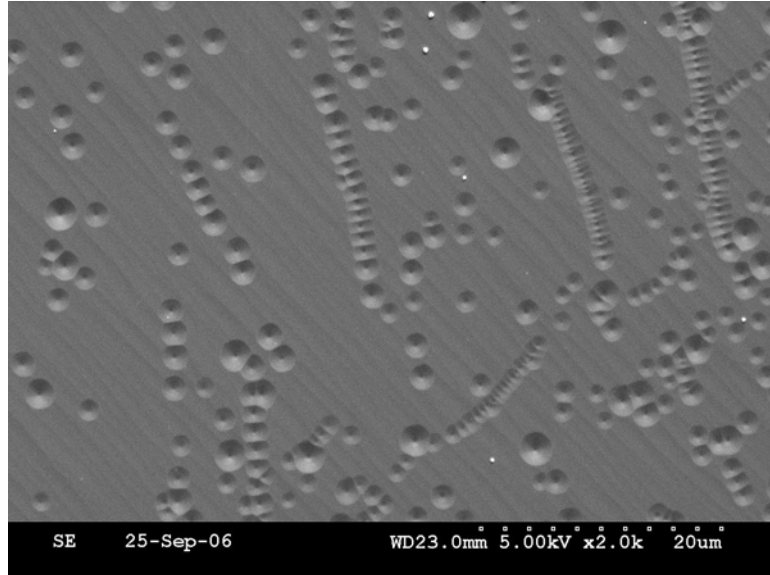
Elements	At % (Sample A)	At % (Sample B)
O 1s	9.3	8.5
N 1s	31.1	31.6
C 1s	8.1	5.9
Si 2s	6.0	3.0
Al 2s	45.5	51.0

3.4 Defect characterization by molten KOH/NaOH etching

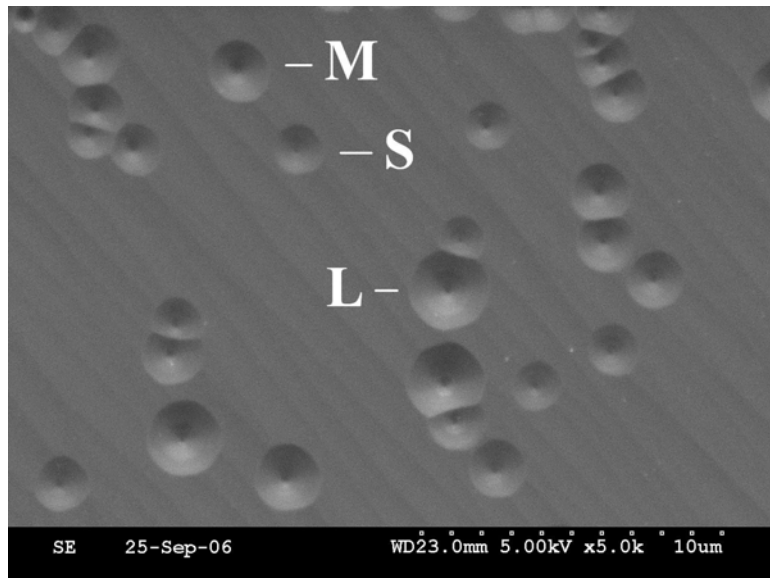
Molten KOH/NaOH etching revealed only etch pits (no hillocks) on sample A and B, indicating both layers have Al-polar surface without N-polar inversion regions. Most of the etch pits are hexagonal shaped, related to threading dislocations. SEM images of the surfaces after etching are shown in Fig. 6 (sample A: (a) and (b); sample B: (c) and (d)). Besides the scattered etch pits, some small etch pits aligned together forming pits arrays, which were referred to as low angle grain boundaries [22]. The low angle grain boundaries correspond to domain walls, which separate highly perfect crystal grains. The grains might be generated due to the different nucleation center or be slightly misorientated to each other. More low angle grain boundaries are observed on sample A (Fig. 6 (a)) than on sample B (Fig. 6(b)), implying sample A contained more crystal grains than sample B. Hence, sample B has better crystal quality since the crystal has more uniformed orientation with less crystal grains. This result is consistent with the xrd results shown In Fig. 4.

Three etch pit sizes are clearly visible in these figures indicating the presences of three types of dislocations in the films. In Fig. 6 (b) and (d), small, medium and large etch pits are demonstrated as S, M, and L, respectively. By investigating the molten KOH etching of GaN, Weyher [23] suggested that the smallest etch pits associated with edge dislocations, the largest pits associated with screw dislocations, and the medium pits associated with the mixed of edge and screw dislocations. Further work is underway to see if this association also holds true for AlN. The total dislocation densities on sample A (1 mm thick) and sample B (2 mm thick) are approximately $5 \times 10^6 \text{ cm}^{-2}$ and $3.5 \times 10^6 \text{ cm}^{-2}$, respectively, estimated by counting the etch pits in a given area. Combined with the author's previous work [19][24], a graph of dislocation density vs AlN layer thickness is plotted, Fig. 7. Apparently, as the AlN layer thickness increased from 0.03 mm to 1 mm, the dislocation density rapidly decreased from $2 \times 10^8 \text{ cm}^{-2}$ to $5 \times 10^6 \text{ cm}^{-2}$. At the initial growth stage, (less than 0.05 mm thick), the lattice mismatch between the SiC and AlN, the difference in thermal expansion and numerous nucleation centers created an extremely high density of dislocations. As the film grew thicker, the strain fields of dislocations interacted and the dislocations were drawn to each other and combined; the absorbed Al and N species recrystallized on the AlN surface instead of SiC surface achieving self-seeded growth; the grains with the same orientation might coalesce, reducing the density of growth centers. Due to the above reasons, a large part of dislocations disappeared, decreasing the total dislocation density. However, as the layer grew from 1 mm to 2 mm thick, the dislocation density decreased with a much slower rate. When the dislocation density was low, they were positioned so far apart that they did not interact, thus their combination becomes much less likely. In addition, a portion

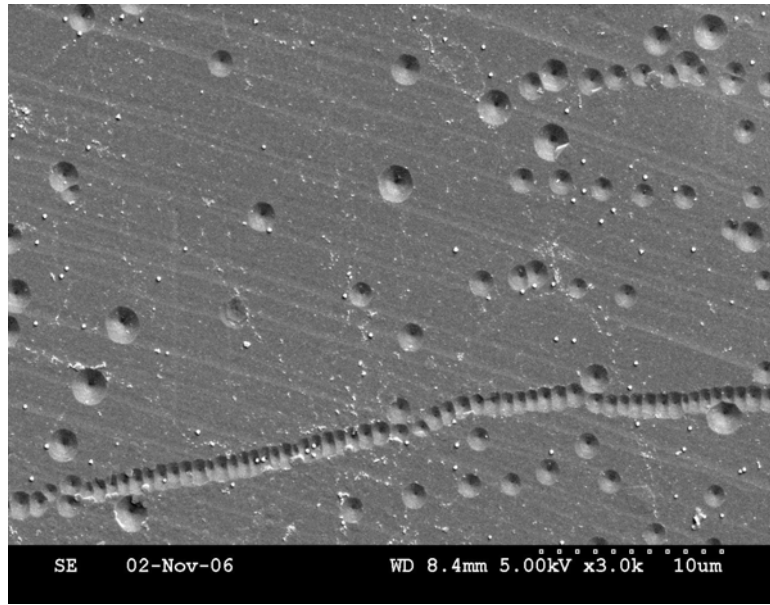
of dislocations were inevitable due to internal stress produced by the thermal gradient in the growth chamber, and misorientated crystal grains.



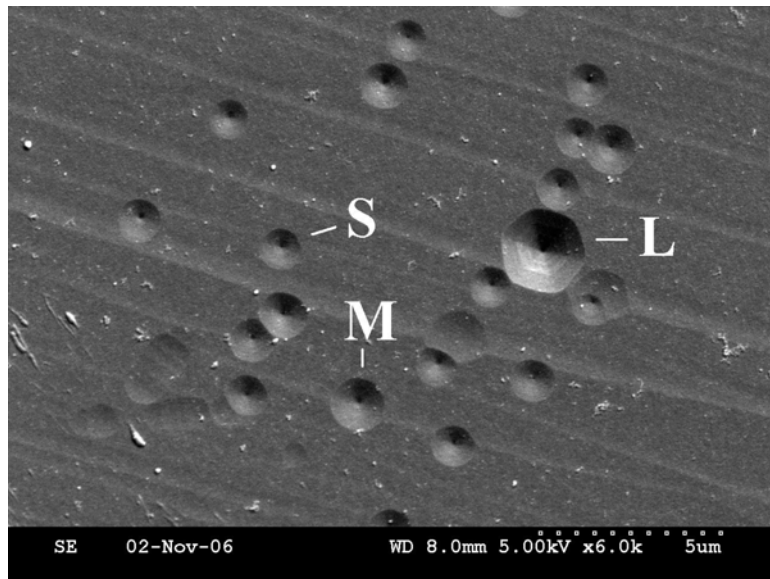
(a)



(b)



(c)



(d)

Fig. 6. SEM images of the AlN layers after molten KOH/NaOH etching: (a) sample A, 3kX, (b) sample A, 5kX, (c) sample B, 3kX, and (d) sample B, 6kX.

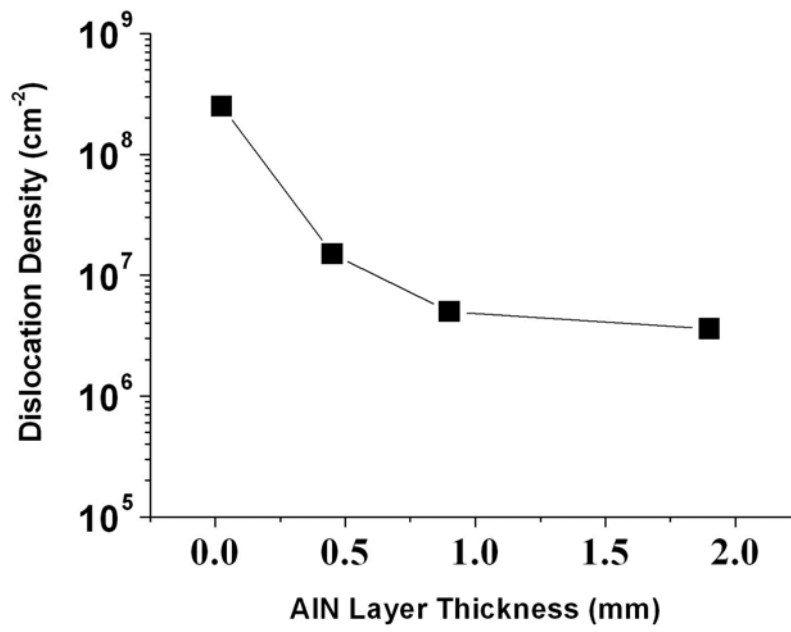


Fig. 7. The relationship of dislocation density and AlN layer thickness.

4. Conclusions

2 mm thick AlN layer with large area was grown on Si-face, 3.5 ° off-axis SiC (0001) seeds. The surface consisted of step features and a single facet. Presumably, as the AlN layer grow thick enough, a single facet may cover the entire growing surface. The crystal quality of the AlN layer is highly dependent on the quality of the SiC seeds. The tilted mosaic blocks in SiC impaired the AlN orientation and broadened the (00.2) AlN peak. The layer with deep blue color contains more SiC (6 at%) than the layer with transparent amber color (3 at%). The different contamination level might be caused by the unstable growth conditions and the different quality seeds. All the grown layers have Al-polar surface and no N-polar inversion domains were observed. As the film thickness increased from 30 μm to 2 mm, the dislocation density decreased from 10^8 cm^{-2} to 10^6 cm^{-2} .

References

1. Y. Taniyasu, M. Kasu, and T. Makimoto, *Appl. Phys. Lett.* 89 (2006) 182112.
2. G.A. Slack, T.F. McNelly, *J. Cryst. Growth* 34 (1976) 263.
3. G.A. Slack, T.F. McNelly, *J. Cryst. Growth* 42 (1977) 560.
4. M. Bickermann, B.M. Epelbaum, A. Winnacker, *J. Cryst. Growth* 269 (2004) 432.
5. E.N. Mokhov, O.V. Avdeev, I.S. Barash, T.Yu. Chemekova, A.D. Roenkov, A.S. Segal, A.A. Wolfson, Yu.N. Makarov, M.G. Ramm, and H. Heleva, *J. Cryst. Growth* 281 93 (2005).
6. D. Zhuang, Z. G. Herro, R. Schlessler, B. Raghothamachar, M. Dudley, and Z. Sitar, *J. Electron. Mater.* 35 1513 (2006).
7. L.J. Schowalter, S.B. Schujman, W. Liu, M. Goorsky, M.C. Wood, J. Grandusky, F. Shahedipour-Sandvik, *Phys. Stat. Sol. A* 203 1667 (2006).
8. L. Liu, J.H. Edgar, *Mater. Sci. Eng.* R37 (2002) 61.
9. J.H. Edgar, L. Liu, B. Liu, D. Zhuang, J. Chaudhuri, M. Kuball, S. Rajasingam, *J. Cryst. Growth* 246 (2002) 187.
10. C.M. Balkas, Z. Sitar, T. zheleva, L. Bergman, R. Nemanich and r.F. Davis, *J. Cryst. Growth* 179 (1997) 363.
11. W.L. Sarney, L. Salamanca-Riba, T. Hossain, P. Zhou, H.N. Jayatirtha, H.H. Kang, R.D. Vispute, M. Spencer, and K.A. Jones, *MRS Internet J. Nitride Semicond. Res.* 5S1 (2000) W 5.5.
12. L. Liu, B. Liu, Y. Shi and J.H. Edgar, *MRS Internet J. Nitride Semicond. Res.* 6 (2001) 7.

13. Y. Shi, Z.Y. Xie, L. Liu, B. Liu, J.H. Edgar and M. Kuball, *J. Cryst. Growth* 233 (2001) 177.
14. Y. Shi, B. Liu, L. Liu, J.H. Edgar, H.M. Meyer III, E.A. Payzant, L.R. Walker, N.D. Evans, J.G. Swadener and J. Chaudhuri, *Phys. Stat. Sol. A* 188 (2001) 757.
15. B.M. Epelbaum, M. Bickermann and A. Winnacker, *Mater. Sci. Forum* 983 (2003) 433.
16. R. Dalmau, R. Schlessler, B.J. Rodriguez, R.J. Nemanich, Z. Sitar, *J. Cryst. Growth* 281 (2005) 68.
17. S. Wang, B. Raghoeamachar, M. Dudley, A.G. Timmerman, *Mater. Res. Soc. Symp. Proc.* 892 (2006) 775.
18. K. Balakrishnan, M. Banno, K. Nakano, G. Narita, N. Tsuchiya, M. Imura, M. Iwaya, S. Kamiyama, K. Shimono, T. Noro, T. Takagi, H. Amano, I. Akasski, *Mater. Res. Soc. Symp. Proc.* 831 (2005) 607.
19. P. Lu, J.H. Edgar, R.G. Lee, J. Chaudhuri, submitted to *J. Cryst. Growth*.
20. B. Liu, J.H. Edgar, B. Raghoeamachar, M. Dudley, J.Y. Lin, H.X. Jiang, A. Sarua, M. Kuball, *Mater. Sci. Eng., B* 117 (2005) 99.
21. D. Zhuang, J.H. Edgar, B. Strojek, J. Chaudhuri, Z. Rek, *J. Cryst. Growth* 262 (2004) 89.
22. D. Hull and D.J. Bacon, *Introduction to Dislocations*, 3rd ed. (Butterworth-Heinemann, Oxford, 1984), pp. 13-16.
23. J.L. Weyher, to be published in *Superlatt. Microstruc.*
24. P. Lu, C. Cao, J.H. Edgar, K. Hohn, R. Dalmau, R. Schlessler, Z. Sitar, submitted to *Mater. Res. Soc. Symp. Proc.* (2006).

**High-speed homoepitaxy of SiC from methyltrichlorosilane by chemical vapor
deposition**

Peng Lu ^{1,*}, J.H. Edgar ¹, O.J. Glembocki ², P.B. Klein ², E.R. Glaser ², J. Perrin ³ and J. Chaudhuri ⁴.

1. Department of Chemical Engineering, Kansas State University, Manhattan, KS-66506, USA.
2. Naval Research Laboratory, 4555 Overlook Avenue SW, Washington DC-20375, USA.
3. Department of Mechanical Engineering, Wichita State University, 1845 Fairmount, Wichita, KS-67260, USA.
4. Department of Mechanical Engineering, Texas Tech University, Lubbock, TX-79409, USA.

PACS: 61.66

Keywords: A1. Crystal structure; A1. Substrates; A3. Chemical vapor deposition process

* Corresponding author: Peng Lu; Tel: 1-785-532-4325; Fax: 1-785-532-7372;

E-mail address: plu@ksu.edu

Abstract

Silicon carbide was deposited homoepitaxially at high growth rates (up to 90 $\mu\text{m/hr}$) with methyltrichlorosilane (MTS) as the precursor in chemical vapor deposition. The substrates were 6H- and 4H-SiC (0001) wafers with different misorientation ($< 0.5^\circ$, 3.5° and 8°) tilts toward $(11\bar{2}0)$. At a growth temperature of 1400 $^\circ\text{C}$, the grown film was composed of faceted grains and the surface was very rough. As the growth temperature increased, the crystal grains were enlarged and the films' surfaces became smoother and smoother. At 1600 $^\circ\text{C}$, on 8° misoriented substrate, a very smooth film with mirror-like surface was generated. Raman spectroscopy showed that the polytypes of the films were affected by the substrate misorientation. When the 6H-SiC substrates were well-oriented, i.e. with the offset angle of less than 0.5° , 3C-SiC was deposited with numerous triangular stacking faults (TSFs). When the offset angle of substrates was 3.5° , mixtures of 3C- and 6H-SiC polytypes were deposited. When the offset angle was 8° , the epitaxial growth perfectly replicated the substrates' polytypes, i.e. high quality 6H- and 4H-SiC epilayers were generated on the 6H- and 4H-SiC substrates, respectively. The full-width half-maximum (FWHM) of x-ray diffraction rocking curves for the c -plane of pure smooth 6H- and 4H-SiC layers was in the range of 15 to 20 arcsecs. Photoluminescence (PL) confirmed the polytypes of 6H- and 4H-SiC layers: Both exhibited clear near-band edge emission at room temperature. These results demonstrate that MTS is a suitable precursor for the rapid, high quality SiC epitaxy.

1. Introduction

Silicon carbide (SiC) is a wide-band gap semiconductor with remarkable properties including high chemical and thermal stability and radiation resistance [1]. These outstanding properties and controllable *p*- and *n*- type doping make SiC an excellent candidate for high-power, high-frequency and high-temperature devices [1-3].

SiC epitaxy is often performed by chemical vapor deposition (CVD) using silane (SiH₄) and propane (C₃H₈) as the precursors for silicon and carbon. Epitaxial films of 4H- and 6H-SiC have been deposited on commercial 4H- and 6H-SiC wafers respectively in cold wall reactors [1][3-6]. However, the growth rate of the current technology is slow, typically less than 10 μm/hr. Rates are limited in part by gas phase homogeneous nucleation of Si, due to the irreversible decomposition of silane. Consequently, with these precursors it is not practical to deposit uniform and thick (>150 μm) epilayers, which are required for high voltage, high power SiC transistors.

An alternative source for SiC CVD growth is methyltrichlorosilane CH₃SiCl₃ (MTS). The decomposition of MTS in hydrogen provides both the silicon and carbon needed for the formation of SiC. The overall reaction is:



MTS is widely employed to deposit polycrystalline 3C-SiC on graphite substrates as a protective coating against oxidation and etching [8-12]. In contrast, its use for SiC epitaxy is rare. Gorin *et al.* [7][13] employed MTS to grow single crystal 3C-SiC platelets (3mm×5mm×1.5mm) on graphite substrates at 1650° C to 1750° C. They produced very high quality crystals at extremely high growth rates of 500 μm/hr. Zelenin

et al. [14] deposited 6H-SiC epitaxial films on small misoriented ($0.5^\circ - 2^\circ$) 6H-SiC (0001) substrates. 3C-SiC inclusions and 6H-SiC stacking faults were evident in their films. They made no attempt to maximize the growth rate.

Compared to the combination of silane and propane, there are several advantages of MTS. First, MTS has low thermal stability. Its decomposition begins at less than 600°C and above 750°C its equilibrium is completely shifted toward the formation of SiC [7]. Second, MTS contains chlorine, and HCl is produced as the reactant decomposes. The presence of HCl during SiC epitaxy can produce a more regular step and terrace structure, decrease the surface supersaturation, and reduce undesired nucleation sites for 3C-SiC [15][16]. Third, it is a liquid, making it inherently safer than the gas sources more typically used. Lastly, inexpensive but high purity MTS is available, making it suitable for semiconductor synthesis. The disadvantage of MTS is the ratio of Si/C cannot be adjusted.

The present study of SiC homoepitaxy was undertaken to determine the maximum feasible growth rate in cold wall reactor while still maintaining good quality. The effects of the substrate misorientation and deposition temperature on the film quality were also examined.

2. Experimental

Epitaxy was performed in a vertical cold wall reactor. Commercial *n*-type 6H- and 4H-SiC (0001) wafers with different misorientations were employed as substrates. The offset angles included on-axis, 3.5° and 8° off-axis toward $(11\bar{2}0)$. 1cm x 1cm substrates

were placed on a resistively heated graphite susceptor. The films were deposited on the Si face. Liquid MTS was contained in a pyrex bubbler, which was held in an ice bath to maintain a constant vapor pressure of 6.67×10^3 Pa [14]. Hydrogen was the carrier gas for MTS. The main carrier gas was a mixture of 2 slm Ar and 1 slm H₂. Although H₂ does not participate in the main reaction as given by equation (1), it appears to take part in the intermediate stages and sharply decrease the amount of free carbon in the resulting films [7]. Nevertheless, H₂ can also react with the graphite susceptor at high temperature to generate hydrocarbons making the Si/C ratio uncontrollable; therefore Ar was also used as a dilution gas to minimize this reaction.

At the beginning of each experiment, the substrate was brought to 1600° C and etched by H₂ for 15 minutes to remove polishing scratches present on the as-received substrates. Then the temperature was adjusted to the growth temperature, and the MTS vapor was admitted into the reactor. Films were deposited over the temperature range from 1300° C to 1700° C. The pressure in the reactor was controlled at 100 torr. Depositions nominally lasted one hour.

The average film thickness was calculated using the density of SiC (≈ 3.2 g/cm³), the area and the mass change of the samples, and was confirmed by cross-sectional scanning electron microscopy (SEM) on selected films. Optical microscopy and SEM were employed to evaluate the morphologies of the deposited films. The crystal polytype and quality were characterized by micro-Raman spectroscopy, x-ray diffraction (xrd) rocking curves and photoluminescence (PL).

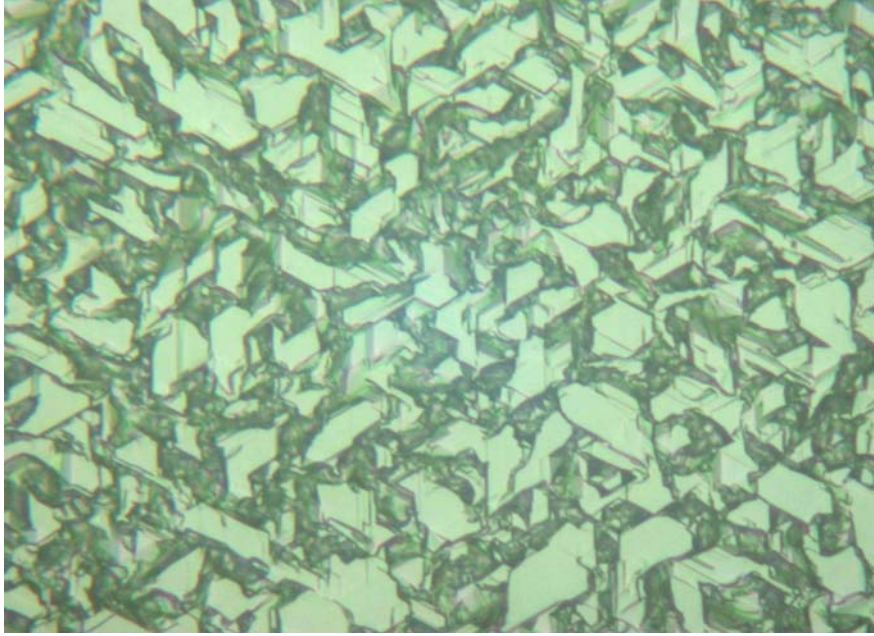
3. Results and discussion

3.1 Effect of temperature

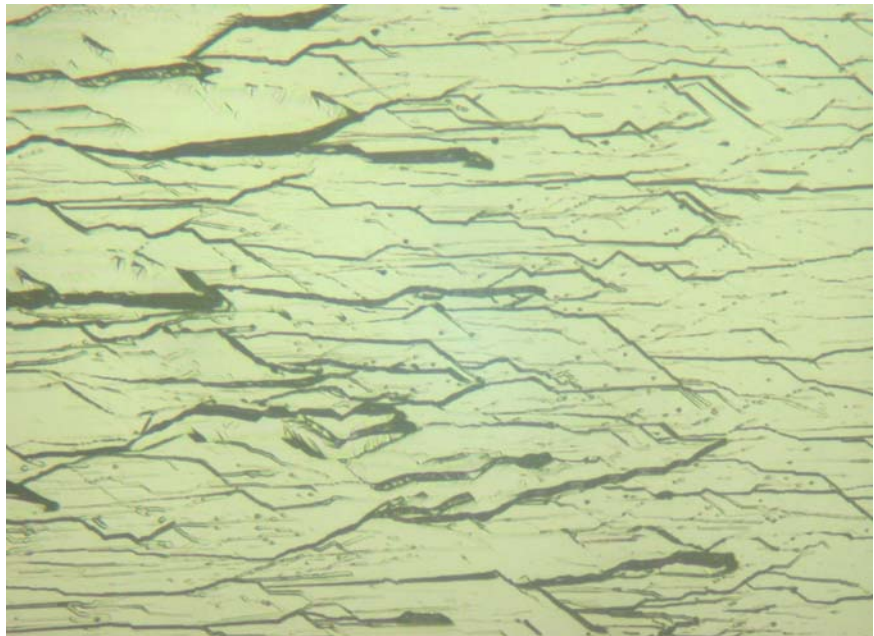
First, a series of experiments were performed to find the optimal growth temperature. The flow rate of the MTS carrier gas was fixed at 20 sccm and 3.5° off-axis 6H-SiC wafers were employed as the substrates. At a growth temperature of 1400°C, the deposited layer started to have crystalline features. The surface was very rough and composed of small crystal grains. At 1500°C, an oriented and continuous film formed, but the surface was full of inversion domain boundaries. When the growth temperature was in the range of 1600°C to 1650°C, the epilayer had a smooth and mirror-like surface with a few inversion domain boundaries. Above 1700°C, many particles formed on the epilayer surface, possibly due to Si nucleation in the gas phase at such high temperature. Thus, 1600°C was identified as the optimal growth temperature for the best surface morphology. Optical micrographs of films deposited at 1400°C, 1500°C and 1600°C with a constant growth rate 20 μm/hr are shown by Figs .1 (a), (b) and (c), respectively.

Subsequently, on-axis and 8° off-axis 6H-SiC and 8° off-axis 4H-SiC wafers were employed as substrates. At 1600°C, triangular stacking faults (TSFs) [17] formed in the epilayer grown on the on-axis substrate as shown in Fig. 2. (a). The TSFs originated from the faults in the stacking sequence, which were related to the formation of 3C-SiC. The epilayer grown on the 8° off-axis 6H-SiC surface was smoother than that grown on the 3.5° off-axis substrate and no inversion domain boundaries were observed. Its surface morphology is shown by optical micrograph in Fig. 2. (b).

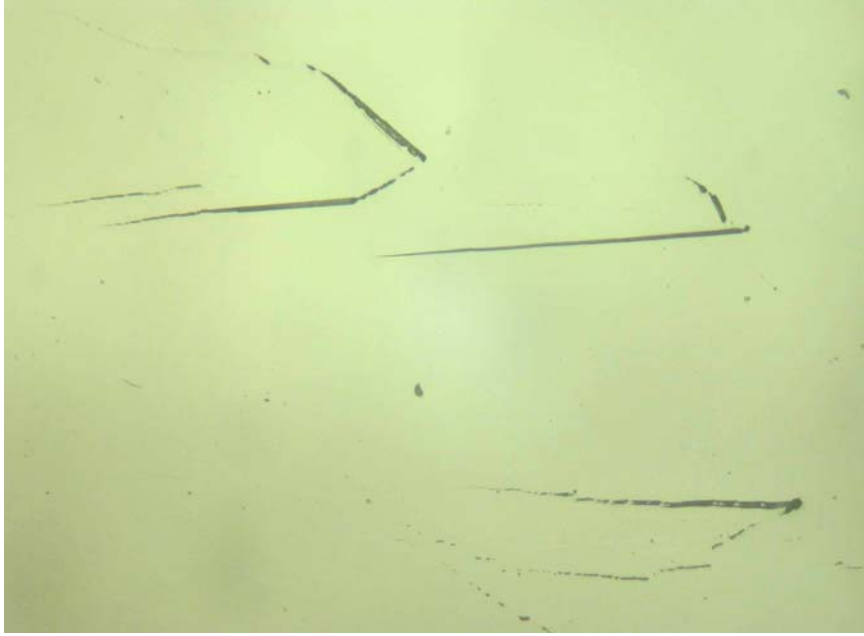
Powell *et al.* [18][19] stated that the epilayers of 4H-SiC were more susceptible than 6H-SiC to 3C-SiC inclusions because triangular patterns were more frequently seen in 4H epilayers than in 6H. His conclusion was based on the on-axis substrates. In our experiments, for misoriented substrates, especially those with the 8° off-axis angle, the quality of the epilayer deposited on the 4H-SiC substrate was similar to that deposited on 6H-SiC substrate; neither had visible TSFs patterns.



(a)

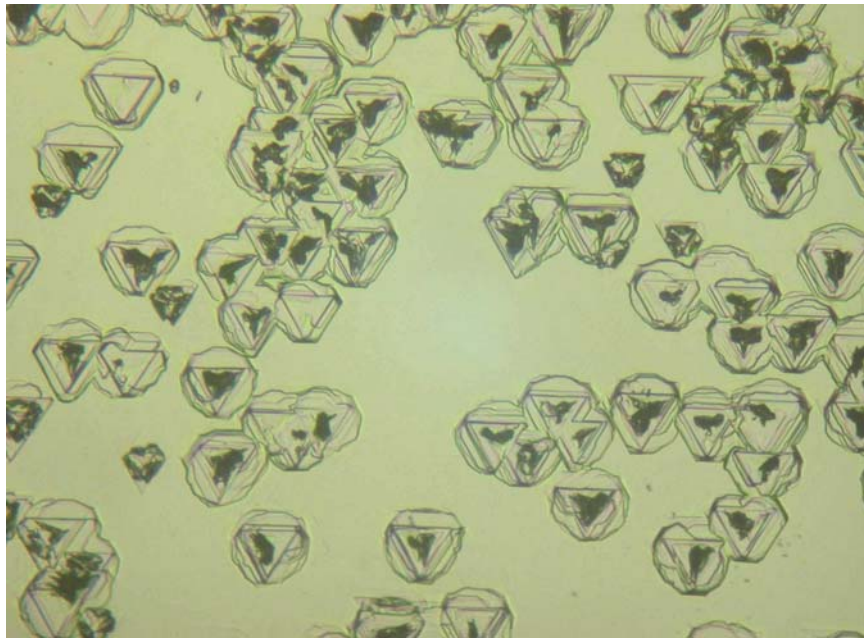


(b)



(c)

Fig. 1. Optical micrographs (160x) of films deposited on 3.5° off-axis 6H-SiC substrate at a constant growth rate 20 $\mu\text{m/hr}$: (a) at 1400°C, (b) at 1500°C and (c) at 1600°C.



(a)



(b)

Fig. 2. Optical micrographs (160x) of films deposited at 1600 °C: (a) on on-axis 6H-SiC substrate and (b) on 8° off-axis 6H-SiC substrates.

3.2 Effect of growth rate

Next, the effect of the growth rate on the epitaxial crystal quality was investigated. All of the samples described above were deposited with a fixed MTS carrier gas (H_2) flow rate of 20 sccm and a constant growth rate of $20\mu\text{m/hr}$. The growth rate was constant with temperature and different substrates, indicating that the reaction was carried out in the diffusion-controlled regime. In the next group of experiments, only the carrier gas flow rate to the MTS bubbler was changed; the temperature was fixed at 1600°C . Films were deposited on 8° off-axis 4H-SiC and 6H-SiC substrates; the growth rate was the same on both substrates.

The growth rate increased linearly from $20\mu\text{m/hr}$ to $90\mu\text{m/hr}$ as the flow rate was changed from 20 sccm to 100 sccm (Fig. 3.). All the films had smooth and mirror-like surface. Fig. 4. shows the SEM of the surface of the epilayer which was deposited at growth rate of $90\mu\text{m/hr}$. The epilayer's surface was composed of growth steps that were inherited from the 8° off-axis substrate. If the carrier gas flow rate was increased further, a growth rate over $100\mu\text{m/hr}$ could be achieved, but the surface quality suffered dramatically; many crystal particles formed on the epilayer surface. In this case, the MTS vapor concentration was so high that it caused severe gas phase nucleation.

By employing MTS as the precursor, epilayers with good surface quality were deposited at high growth rates ($80 \sim 90\mu\text{m/hr}$), which is much faster than that obtained with conventional SiH_4 and C_3H_8 sources.

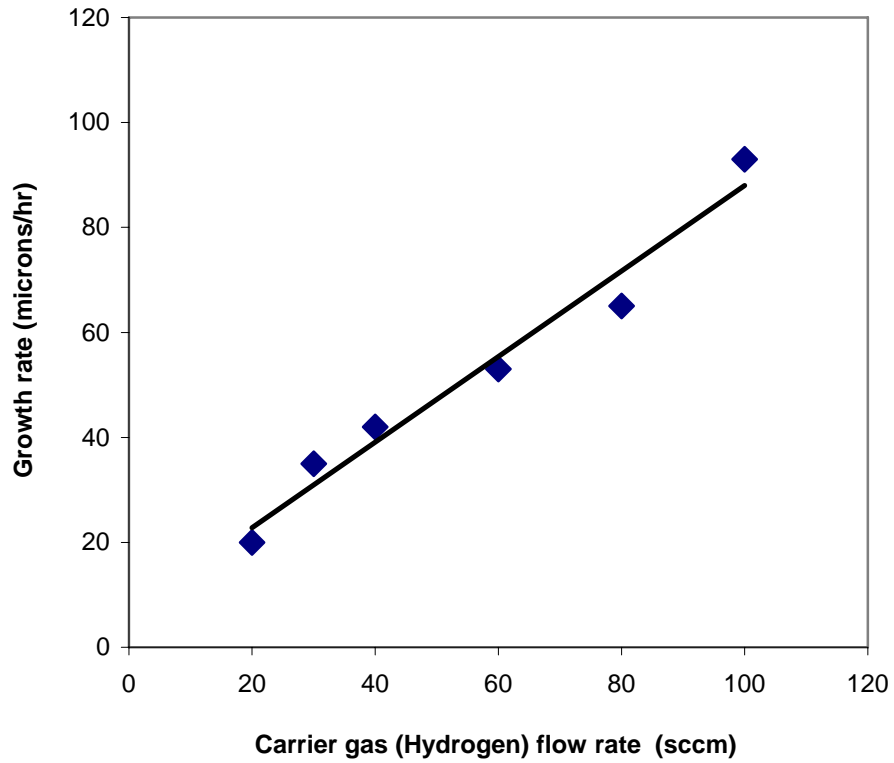


Fig. 3. The relationship between growth rate and carrier gas flow rate.

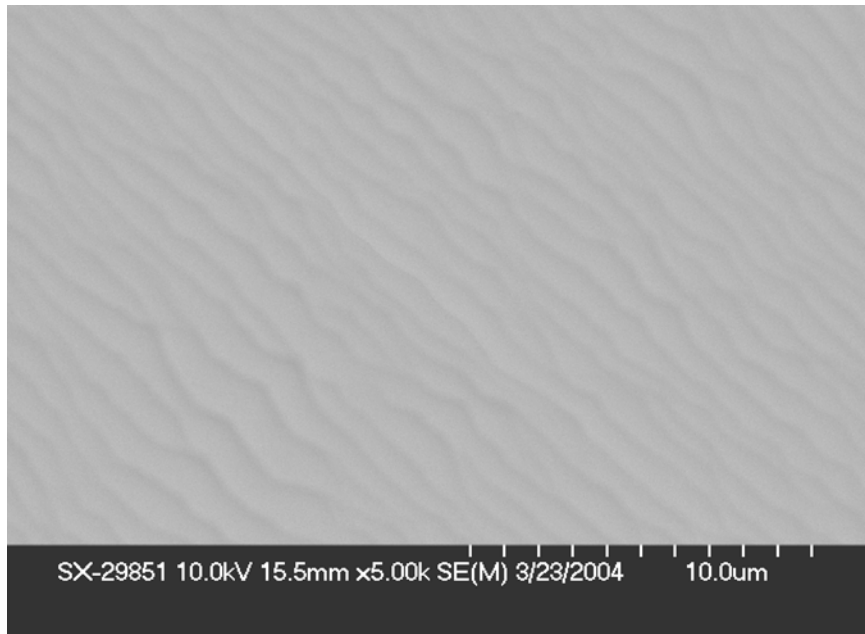


Fig. 4. SEM of the film deposited at 1600°C with high growth rate (90 μ m/hr) on 8° off-axis 6H-SiC substrates.

3.3 Polytypes of the grown epilayers

Micro-Raman spectroscopy was applied to determine the polytypes of the SiC epilayers, which were all grown at 1600°C and at the same growth rate of about 50 $\mu\text{m/hr}$. The Raman system was performed with SPEX Triplemate with CCD detector, Mitutoyo Microscope with 100x objective, and 10mW of 514.5nm laser light. The spatial resolution was 0.7 microns lateral and 15 microns in depth. Table. 1. lists the precise frequencies of the folded transverse optic (FTO) and longitudinal optic (FLO) modes from the literature [20]. Table. 2. lists the detected Raman modes' frequencies of the epilayers, and the polytype that the mode implies. The epilayer grown on on-axis 6H-SiC is mostly 3C with 6H inclusions. The epilayer grown on 3.5° off-axis 6H-SiC is mainly 6H but the inversion domain region (shown in Fig. 1.(c)) is 3C. The epilayers grown on 8° off-axis 6H-SiC and 4H-SiC are pure 6H and 4H polytypes, respectively.

The FTO modes linewidth (FWHM) of the pure 4H-SiC epilayer (on 8° off-axis 4H-SiC) is 2.54 cm^{-1} and that of the pure 6H-SiC epilayer (on 8° off-axis 6H-SiC) is 2.57 cm^{-1} , which compared well with those of commercial SiC wafers (about 2.55 ~ 2.75 cm^{-1}). Therefore, both epilayers are very good quality.

According to the micro-Raman results, the SiC epilayers perfectly replicate the polytype of the substrate when the substrate has an 8° offset angle. Pure 6H- and 4H-SiC epilayers were obtained by this method and their quality was as good as commercial SiC wafers. The 3.5° off-axis substrate cannot completely avoid the polytype mixing growth: 6H epilayer with 3C inclusions were detected.

This phenomenon can be explained by “step-controlled epitaxy” [11]. On the on-axis surface, the surface step density is very low and relative large terraces exist. Due to

the high supersaturation on the surface, the crystals start to nucleate on terraces and grow in two-dimensions. In this case, 3C-SiC is generated. The 6H-SiC substrate has the stacking order of ABCACB... and the deposited 3C-SiC may have two stacking orders of ABCABC... or ACBACB.... The difference in the stacking orders results in the stacking faults in the form of TSFs, which is shown by Fig. 2. (a). On the offset surface, a greater misorientation of substrate produced a higher step density and smaller terrace width. When the terrace is narrow enough, the adsorbed atoms could approach to steps where the potential is low. The nucleation will start from the step sites and grow in a step-flow mode to cover the terrace. At the step sites, bonds from the step uniquely control the stacking order of the adsorbed atoms. Therefore the deposited crystals will strictly replicate the polytype of the substrate. With our deposition rates, the 3.5° off-angle surface is insufficient to completely eliminate 3C-SiC nucleation. The inversion domain boundaries are observed in Fig. 1(c). The 3C-SiC inclusion is also detected by Raman spectra. The 8° off-axis surface can produce high enough step density and small enough terrace width to avoid 3C-SiC generation. Therefore the epilayers grown on the 8° off-axis 6H-SiC and 4H-SiC substrates have the pure polytype repetition.

Table 1. Raman frequencies of the FTO and FLO modes for typical SiC polytypes [20].

Mode (cm ⁻¹) Polytype	FTO-1	FTO-2	FTO-3	FLO-1	FLO-2
3C-SiC	-	-	796	-	972
4H-SiC	-	776	796	964	-
6H-SiC	767	789	797	965	-

Table 2. Raman modes' frequencies of the epilayers and polytypes conclusions.

Mode (cm ⁻¹) Polytype of Substrate	FTO-1	FTO-2	FTO-3	FLO-1	FLO-2	Polytype of Epilayer
On-axis 6H-SiC	767.1 6H (W)	787.6 6H (W)	795.6 3C (S)	964.7 6H (W)	974.2 3C (S)	Mainly 3C with 6H
3.5° off-axis 6H-SiC	766.5 6H (W)	789.2 6H (S)	795.6* 3C (W)	966.6 6H (S)	-	Mainly 6H With 3C
8° off-axis 6H-SiC	766.2 6H (W)	787.9 6H (S)	796.4 6H (W)	965.1 6H (S)	-	Pure 6H
8° off-axis 4H-SiC	-	776.6 4H (S)	-	964.1 4H (S)	-	Pure 4H

“ W ” – Weak intensity mode.

“ S ” – Strong intensity mode.

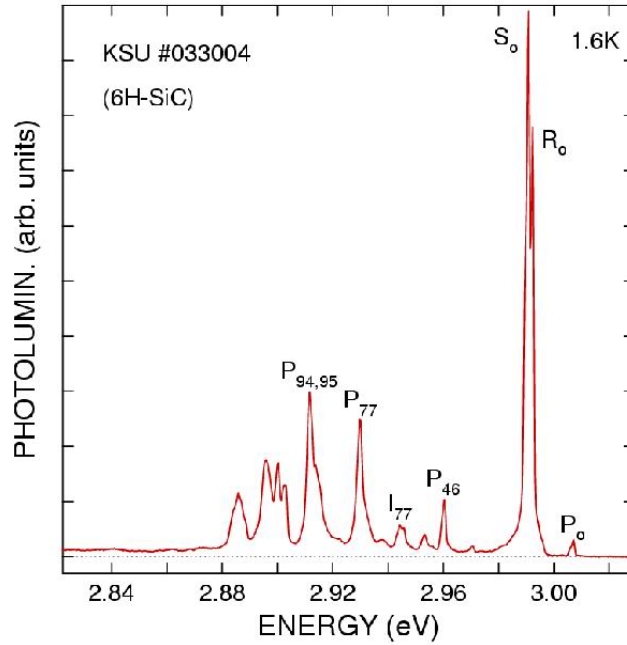
“ * ” – Mode from inversion domain region.

X-ray diffraction rocking curves were employed to characterize the grown epilayers having different polytypes. Area probed by x-ray was 2mm x 0.4mm. For each sample, the reflection peak from the *c*-plane is strong and sharp and the full-width at half-maximum (FWHM) is in the range of 15-20 arcsecs implying that all the epilayers strongly grew along the *c*-axis and had very high quality. The FWHMs are listed in Table. 3. The *c*-plane was different in different polytypes: (111) in 3C-SiC, (00.6) in 6H-SiC, and (00.4) in 4H-SiC.

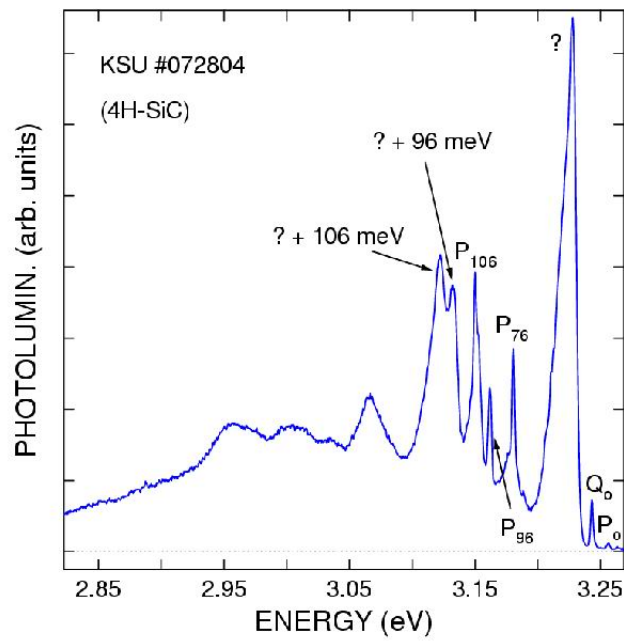
Table. 3. FWHMs of xrd rocking curves taken from different epilayers.

Epilayer Polytype	Substrate	<i>c</i> -Plane	FWHM (Arcsec)
3C-SiC (6H-SiC inclusion)	On-axis 6H-SiC	(111)	15
6H-SiC (3C-SiC inclusion)	3.5° off-axis 6H-SiC	(00.6)	17
6H-SiC	8° off-axis 6H-SiC	(00.6)	15
4H-SiC	8° off-axis 4H-SiC	(00.4)	18

The pure 6H and 4H-SiC epilayers on 8° misoriented substrates were investigated by photoluminescence (PL). The PL at 1.6K was excited by the 351 nm line of an Ar⁺ ion laser. The band edge emission was analyzed by a 0.25-m double-grating spectrometer and detected by a GaAs photomultiplier tube. At room temperature the 6H sample exhibits a clear peak near 425 nm, which is associated with shallow impurity emission. The 4H sample exhibits a very well defined near-edge emission near 390nm. Therefore, the PL confirms the polytypes of the films and demonstrates their good quality. The low temperature band edge photoluminescence in 6H layer exhibits a typical spectrum observed for *n*-type 6H-SiC, shown in Fig. 5. (a). Excitons bound to shallow nitrogen donors at hexagonal (P_O) and two cubic (R_O,S_O) lattice sites are found. P₄₆, P₇₇ and P_{94, 95} are phonon replicas. I₇₇ is phonon-assisted free exciton recombination. A nitrogen doping level of $1.7 \times 10^{16} \text{ cm}^{-3}$ is estimated from the (R_O + S_O)/I₇₇ PL ratio [21]. For the 4H sample, Fig. 5.(b), the band edge emission is dominated by a boron-related bound excitation at 3.23 eV, which is similar to PL reported for B-doped 4H-SiC [22]. This sample could be highly compensated or p-type. Both samples exhibit deep emissions that appear to also be related to boron. The boron impurity may come from the precursor or contamination of the CVD system.



(a)



(b)

Fig. 5. Low temperature near band edge photoluminescence spectrum of (a) 6H-SiC epilayer and (b) 4H-SiC epilayer.

4. Conclusions

Methyltrichlorosilane, CH_3SiCl_3 (MTS) was demonstrated as a good precursor for SiC epitaxy. High quality SiC epilayers were deposited in CVD at high growth rates (up to 90 $\mu\text{m/hr}$) with smooth, mirror-like surfaces. Micro-Raman spectroscopy proved that on 8° off-axis 4H- and 6H-SiC substrates, the epilayer perfectly replicates the polytype of the substrate; pure 6H- and 4H-SiC homoepitaxy was achieved. Growth on 3.5° off-axis 6H-SiC substrates cannot completely avoid polytype mixing growth; 6H- with 3C-SiC inclusions was detected by Raman spectra. Narrow high resolution x-ray diffraction and Raman spectra peaks confirmed the high quality of the films. Band edge photoluminescence emission was observed in the best quality films.

Acknowledgement

J. Perrin and J. Chaudhuri like to acknowledge National Science Foundation grant # DMR- 0408703

References

1. H. Matsunami and T. Kimoto, *Mater. Sci. Eng., A*, R20 (1997) 125.
2. B. Thomas, W. Bartsch, R. Stein, R. Schoerner and D. Stephani, *Mater. Sci. Forum* (2004), 457 (Pt. 1, Silicon Carbide and Related Materials) (2003) 181.
3. H. Tsuchida, I. Kamata, T. Jikimoto, T. Miyanagi and K. Izumi, *Mater. Sci. Forum* (2003) 433, (Silicon Carbide and Related Materials 2003) 131.
4. F. Wischmeyer, D. Leidich and E. Niemann, *Mater. Sci. Forum* (1998) 264, (Pt.1, Silicon Carbide, III-Nitrides and Related Materials) 127.
5. Y. Ishida, T. Takahashi, H. Okumura, K. Arai and S. Yoshida, *Jpn. J. Appl. Phys., Part 1*, 43 (8A) (2004) 5140.
6. S.M. Bishop, E.A. Preble, C. Hallin, A. Henry, L. Storasta, H. Jacobson, B.P. Wagner, Z.J. Reitmeier, E. Janzen and R.F. Davis, *Mater. Sci. Forum* (2004) 457 (Pt.1, Silicon Carbide and Related materials 2003) 221.
7. S.N. Gorin and L.M. Ivanova, *Phys. Stat. Sol. (b)* 202 (1997) 221.
8. Y.J. Lee, D.J. Choi, J.Y. Park and G.W. Hong, *J. Mater. Sci.* 35 (18) (2000) 4519.
9. Q. Zhu, Z. Qiu and C. Ma, *Huagong Yejin* 19 (4) (1998) 289.
10. W.G. Zhang and K.J. Hüttinger, *Chem. Vap. Deposition* 7 (4) (2001) 167.
11. G.S. Myoung and S. Chun, *J. Vac. Sci. Technol. A* 6(1) (1988) 5.
12. Y.J. Lee and D.J. Choi, *J. Ceram. Processing Res.* 3 (3) (2002) 222.
13. A.J. Steckl and H.E. Devrajan, *Appl. Phys. Lett.* 69 (25) (1996) 3824.
14. V.V. Zelenin, V.G. Solov'ev, S.M. Starobinets, S.G. Konnikov and V.E. Chelnokov, *Semiconductors* 29 (6) (1995) 581.

15. Z.Y. Xie, S.F. Chen, J.H. Edgar, K. Barghout and J. Chaudhuri, *Electrochem. Solid-State Lett.* 3 (8) (2000) 381.
16. D. Crippa, G.L. Valente, A. Ruggiero, L. Neri, R. Reitano, L. Calcagno, G. Foti, M. Mauceri, S. Leone, G. Pistone, G. Abbondanza, G. Abbagnale, A. Veneroni, F. Omarini, L. Zamolo, M. Masi, F. Roccaforte, F. Giannazzo and S. Di franco, *Mater. Sci. Forum* (2005) 67.
17. C. Hallin, A.O. Konstantinov, O. Kordina and E. Janzen, *Inst. Phys. Conf. Ser.* 142 (1) (1996) 85.
18. J.A. Powell, D.J. Larkin and P.B. Abel, *Inst. Phys. Conf. Ser.* 142 (1) (1995) 77.
19. J.A. Powell, D.J. Larkin and P.B. Abel, *J. Electron. Mater.* 24 (1995) 295.
20. S. Nakashima and H. Harima, *Phys. Stat. Sol. (a)* 162 (1997) 39.
21. I.G. Ivanov, C. Hallin, A. Henry, O. Kordina, and E. Janzén, *J. Appl. Phys.* 80, (1996) 3504.
22. S.G. Sridhara, L.L. Clemen, R.P. Devaty, W.J. Choyke, D.J. Larkin, H.S. Kong, T. Troffer and G. Pensl, *JAP* 83 (1998) 7909.

**The influence of the H₂/Ar ratio on surface morphology and structural defects in
homo-epitaxial 4H-SiC films grown with methyltrichlorosilane**

P. Lu ^{a)} and J.H. Edgar

Department of Chemical Engineering, Kansas State University, Manhattan, KS-66506,

USA

^{a)} Corresponding author's E-mail: plu@ksu.edu, Tel: 785-532-4325, and Fax: 785-532-7372

Abstract

Characterization of surface morphology and crystal defects are reported for homo-epitaxial 4H-SiC films grown at high rates (35 ~ 40 $\mu\text{m/hr}$) using methyltrichlorosilane (CH_3SiCl_3 , MTS) as single precursor. The ratio of hydrogen to argon (H_2/Ar) in the carrier gas was varied to determine the effect of hydrogen on the surface morphology and the crystalline defects. Due to hydrogen's reaction with the graphite heater, adjusting the H_2/Ar ratio effectively changed the C/Si ratio in the gas phase; thereby, influencing surface roughness and dislocation density. Low H_2/Ar ratios of 0.1 and 0.125 produced smooth surfaces without step-bunching. Higher H_2/Ar ratios of 0.2 and 0.33 enhanced the conversion of basal plane dislocations into threading edge dislocations, and reduced the density of basal plane dislocations to approximately 600 cm^{-2} . However, at these H_2/Ar ratios, macro-steps formed on the surface and the roughness increased. Micropipes from substrate dissociated into closed-core threading screw dislocations in the films grown with H_2/Ar ratio in the range 0.1 to 0.2. At H_2/Ar ratio of 0.33, micropipes propagated into the film, generating hollow-core threading screw dislocations.

1. Introduction

Silicon carbide (SiC) is an excellent semiconductor for high-power, high-frequency and high-temperature devices because of its remarkable properties including a wide bandgap (2.3 – 3.2 eV), high breakdown field ($> 2 \times 10^6 \text{ V cm}^{-1}$), high thermal conductivity ($3 - 5 \text{ W cm}^{-1} \text{ K}^{-1}$), and high electron saturation drift velocity ($2.0 \times 10^7 \text{ cm s}^{-1}$) [1, 2]

SiC epitaxy is usually performed by chemical vapor deposition (CVD) using silane (SiH_4) and propane (C_3H_8) as the sources, typically at growth rates less than $10 \text{ }\mu\text{m/hr}$ [3-6]. In contrast, using methyltrichlorosilane (CH_3SiCl_3 , MTS) as a novel precursor for SiC epitaxy we produced high-quality SiC epilayers with smooth mirror-like surfaces over a wide growth rate range ($20 - 90 \text{ }\mu\text{m/hr}$). Moreover, by employing SiC wafers misoriented 8° off the (0001) plane, (of both 6H and 4H polytypes), the epitaxial films perfectly replicated the polytype of the substrate without 3C-SiC inclusions [7]. Fully evaluating the 4H-SiC epilayers grown from MTS requires characterizations of their morphological and structural defects.

Common defects in 4H- and 6H-SiC epilayers include micropipes, triangular depressions, threading screw dislocations (TSDs), threading edge dislocations (TEDs) and basal plane dislocations (BPDs). Micropipes, each composed of a hollow-core perpendicular to the basal plane, are present in SiC substrates, and can propagate into the films during epitaxial growth. Triangular depressions are 3C-SiC inclusions in the epilayer caused by mixed polytype growth. Micropipes and triangular depressions degrade reverse voltage characteristics of *p-n* junction and Schottky barrier diodes [8-10].

Although progress in sublimation crystal growth has dramatically reduced their densities in commercial SiC wafers, the presence of micropipes still a major problem facing the current SiC technology. Triangular depressions can be reduced or eliminated by adding HCl into the reactor during the epitaxy [11] or employing SiC wafers with intentionally mis-orientated ($3 \sim 8^\circ$) off the (0001) plane [7, 12].

Basal plane dislocations (BPD) are slip dislocations in the basal plane, which are caused by the thermoelastic stress due to the temperature distribution in growing bulk crystals [13-15]. BPDs are attracting increasing attention since they degrade the forward voltage drop in SiC bipolar diodes [16]. BPDs provide the nucleation sites of the stacking faults, and the expansion of stacking faults cause the instability of forward voltage in high-voltage bipolar devices [16-18]. Therefore, reducing BPDs is a major objective in developing these devices. Typical density of BPDs in standard 8° off-axis SiC substrates is approximately 10^4 cm^{-2} [17].

During SiC epitaxy, 90% of BPDs in the substrate convert to threading edge dislocations (TEDs) in the epilayer to minimize the elastic energy of dislocation per unit growth length [19-21]. The remaining BPDs, with the density on the order of 10^3 cm^{-2} , can propagate from the substrates to the epilayer. The conversion of BPDs to TEDs is beneficial since BPDs cause severe damage to the performance of devices but TEDs do not. Considering the impact of growth conditions, Ohno *et al.* [21] demonstrated that the high C/Si ratio ($2 \sim 3$) and low growth rate ($3.6 \mu\text{m/h}$) reduced the fraction of BPDs propagating into the epilayer to 10% of the total BPDs in the substrate. Ohno *et al.* [21] theorized that the C-rich environment reduced the step-flow speed of silicon and carbon atoms and increased the conversion of BPDs to TEDs. In an alternate approach, Zhang *et*

al. [16,17] significantly enhanced the conversion of BPDs into TEDs in the epilayers by etching the SiC substrates in molten KOH before epitaxy.

In addition to these structural defects, the surface morphology may also degrade the performances of the SiC devices: step-bunching in particular causes problems. Step-bunching is the formation of macro-steps (multiple Si-C bilayers with the height up to 8 μm) on misoriented 4H- and 6H-SiC substrates during the SiC epitaxy [22]. In this manner, the surface energy is minimized by forming edges with a lower number of dangling bonds. For reasons not understood step-bunching enhances as the C/Si reactant ratio is increased [22]. Step-bunching is detrimental for electronic device performance, as the surface roughness causes interface scattering, reduces electron channel mobility in MOSFETs, and lowers blocking voltages in *p-n* junctions.

The C/Si ratio in the gas phase is an important factor in SiC epitaxy, as it determines the growth rate, the surface morphology and the dislocation density. Change in the C/Si ratio is usually imposed by changing the flow ratio of the reactants, i.e. C_3H_8 and SiH_4 . However, for MTS, the C/Si reactant ratio is unchangeable and fixed as 1. The overall reaction is



At first thought, this fixed C/Si ratio might be an impediment to produce epitaxial layer with low BPD density.

This present work reconsiders this thinking, by examining another important parameter, the composition of the carrier gas, and its effect on the gas phase C/Si ratio. Although H_2 does not appear in the overall deposition reaction, it is essential for preparing high quality SiC epitaxial layers, as it prevents the co-deposition of carbon

(graphite) [23]. Due to the high temperature applied in SiC epitaxy, H₂ can react with the graphite susceptor generating hydrocarbons into the gas phase. By adding inert gas Ar into the main carrier gas and adjusting the ratio of H₂/Ar, the H₂ – graphite reaction can be suppressed or promoted to reduce or increase the hydrocarbons, respectively. Consequently, the C/Si ratio is changeable in the single precursor MTS system: a low H₂/Ar flow ratio in main carrier gas produces a low C/Si ratio and vice versa. The influence of the H₂/Ar ratio on the surface morphology and defects in the grown films is reported in this work.

2. Experimental

Epitaxy was performed in a home-built vertical cold wall reactor. Commercial *n*-type 4H-SiC (0001) wafers intentionally misoriented 8 ° off-axis toward $[11\bar{2}0]$ were employed as substrates. 1cm×1cm substrates were placed on a resistively heated graphite susceptor. The liquid MTS was contained in a pyrex bubbler held in an ice bath to maintain a constant vapor pressure of 6.67×10^3 Pa [24]. H₂ was the carrier gas for MTS. Mixtures of H₂ and Ar were added into the reactor as the main carrier gas. The flow rate of Ar was fixed at 2 slm, and different H₂/Ar ratios (0.1, 0.125, 0.2, 0.33 and 0.5) were achieved by adjusting the flow rate of H₂ as 0.2 slm, 0.25 slm, 0.4 slm, 0.6 slm and 1 slm, respectively.

All films were grown at 1600 °C, 100 torr, under the different H₂/Ar ratios on Si – face of the substrates for one hour. The growth rate was controlled at 35 ~ 40 μm/hr by adjusting the flow rate of the H₂ carrier gas of MTS as 0.02 ~ 0.03 slm. Micro-Raman

spectroscopy and x-ray diffraction rocking curve (XRC) confirmed that all epilayers grown on the 8 ° off-axis 4H-SiC substrates were pure 4H-SiC polytype without 3C polytype inclusions. The films' crystal quality was comparable to commercial wafers. The residual nitrogen doping levels were about $1.5 \sim 2 \times 10^{16} \text{ cm}^{-3}$ as estimated by photoluminescence. These results were reported in our previous paper [7].

In this study, surface morphologies of the resulting films were examined in detail by tapping mode atomic force microscopy (AFM). For each sample, the root mean square (rms) of the roughness was measured five times in different areas. The films and a bare 4H-SiC substrate were etched in molten KOH/NaOH eutectic alloy (59 % wt. KOH / 41 % wt. NaOH) to identify the various dislocation types and measure their densities. Samples were etched in a platinum crucible at a temperature of 480 °C for 6 – 8 minutes. Etch pit shapes were observed by scanning electron microscopy (SEM) and the dislocation densities were measured by the counting the number of each type of etch pit in a given area using an optical microscope.

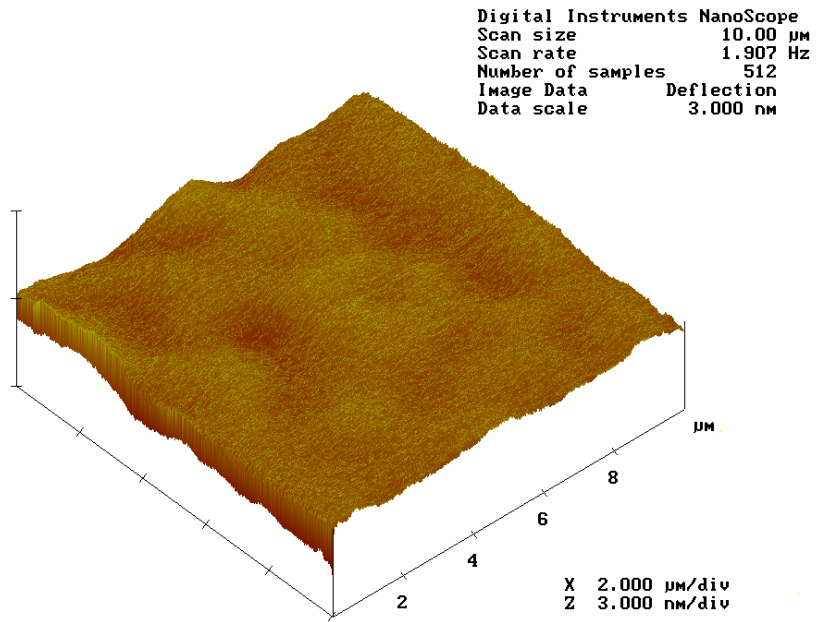
3. Results and discussion

3.1 The influence of the H₂/Ar ratio on the surface morphology and roughness

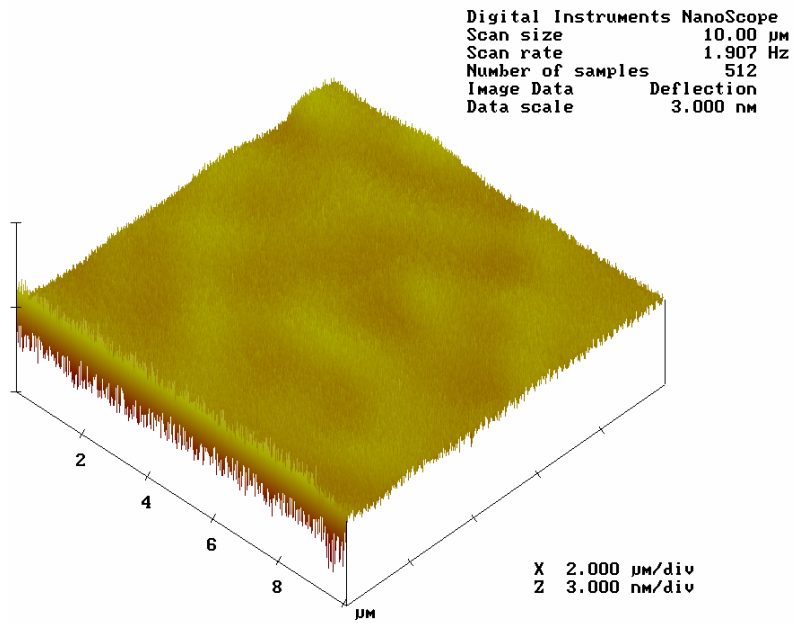
All the grown films had smooth and mirror-like surfaces when viewed under an optical microscope. Films were 35 to 40 μm thick, as confirmed by cross-section SEM. Pronounced difference in the surface morphologies were revealed by AFM. Fig. 1. (a) – (e) are the AFM images of the films grown at different H₂/Ar ratios: 0.1, 0.125, 0.2, 0.33 and 0.5. The average of rms for each sample was listed in Table 1.

At low H_2/Ar ratios of 0.1 and 0.125, the films' surfaces were smooth and without step structures, as shown in Fig. 1. (a) and (b), respectively. The average rms of the roughness for these two samples was around 3.5 nm. As the H_2/Ar ratios increases to 0.2, surface perturbations appeared. These protuberances were discontinuous and approximately 4 ~ 6 μm long, 1 ~ 1.5 μm wide, and 10 ~ 15 nm high, as shown in Fig. 1.(c). The average rms increases to 4.9 nm. At the H_2/Ar ratio of 0.33, the protuberances were elongated and formed steps parallel to $(11\bar{2}0)$, and crossed over each other. The step width and height were 0.7 ~ 0.9 μm and 15 ~ 20 nm, respectively. At the H_2/Ar ratio of 0.5, the steps were continuous across the surface and parallel to $(11\bar{2}0)$. Step width was reduced to 0.2 ~ 0.4 μm but the step height was unchanged, 15 ~ 20 nm. The average rms for these two samples was almost same around 6.1 nm.

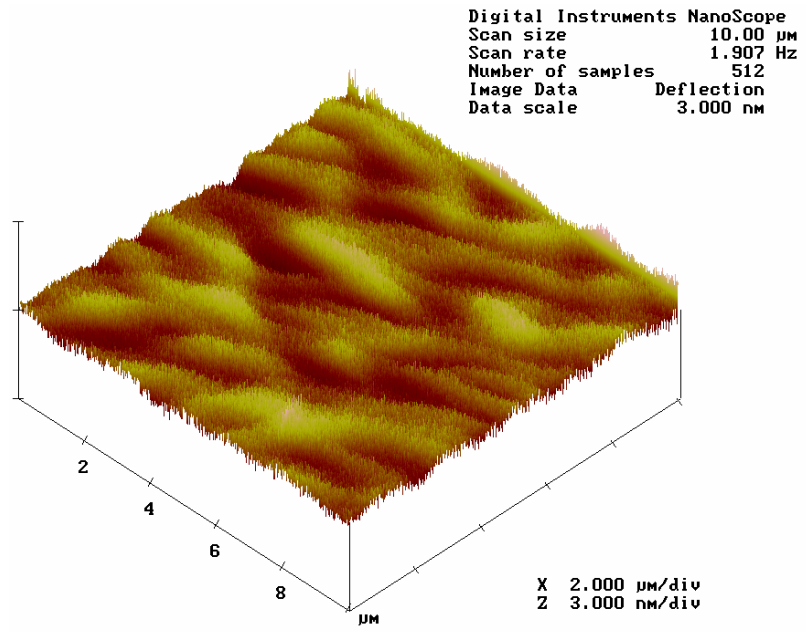
It is apparent that changes in H_2/Ar ratio varied the C/Si ratio in gas phase and consequently influenced surface morphology and roughness of the grown films. At the H_2/Ar ratios of 0.1 and 0.125, the C/Si ratio in gas phase was close to 1; small amount of H_2 did not generate much hydrocarbon by the reaction with graphite susceptor. Raising H_2/Ar ratio to 0.2, 0.33 and 0.5, clearly increases C/Si because of the H_2 – graphite reaction. AFM demonstrated that a C-rich environment, i.e. high C/Si ratio, promoted the formation the macro-steps and increased the surface roughness.



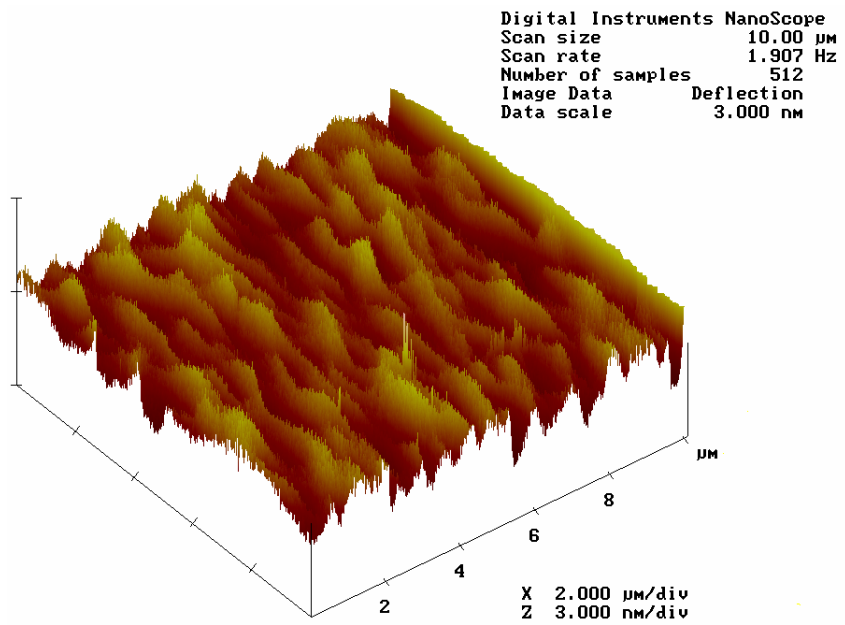
(a)



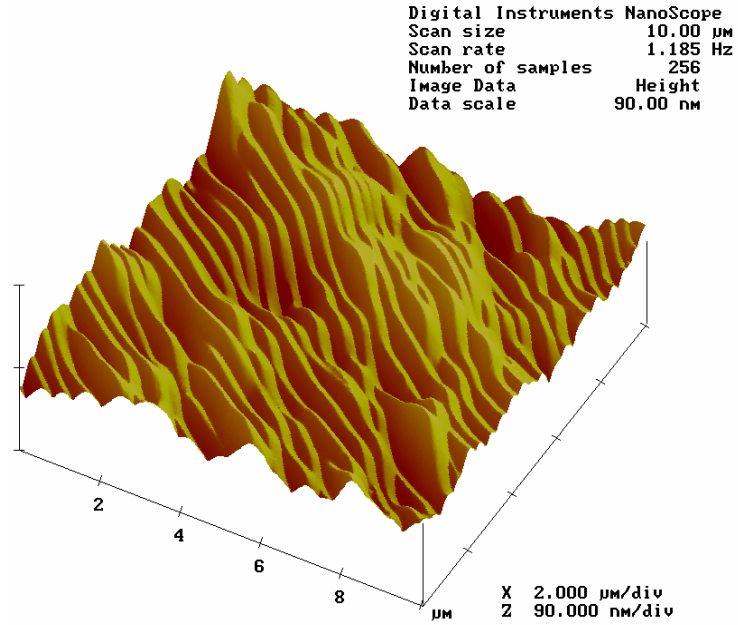
(b)



(c)



(d)



(e)

Fig. 1. AFM images of the films grown under different H_2/Ar ratios: (a) 0.1, (b) 0.125, (c) 0.2, (d) 0.33 and (e) 0.5.

Table 1. The average rms of the films grown under different H_2/Ar flow ratio.

H_2/Ar flow ratio	0.1	0.125	0.2	0.33	0.5
Average rms	3.48 nm	3.51 nm	4.87 nm	6.13 nm	6.15 nm

3.2 Dislocation type and density revealed by molten KOH/NaOH etching

Molten KOH/NaOH etching produced three types of etch pits in all of the grown films: large hexagonal pits, small hexagonal pits and shell-shaped pits, which correspond to threading screw dislocations (TSDs), threading edge dislocations (TEDs) and basal plane dislocations (BPDs), respectively [19-21]. Both hollow- and closed-core TSDs were observed [21], which were caused by the propagations of micropipes and TSDs from substrates respectively [17,18].

The bare 4H-SiC substrate, without any eiptaxial layer, was etched to assess the defects initially present. Micropipes appeared on the 4H-SiC substrate, with diameters of $4 \sim 6 \mu\text{m}$, and a density of $40 \sim 50 \text{ cm}^{-2}$. A high density of basal plane dislocations surrounded the micropipes with random orientations, as illustrated in SEM images, Fig. 2 (a) and (b).

On the films grown at the H_2/Ar ratios of 0.1, 0.125 and 0.2, all the TSDs were closed; no hollow-core TSDs were observed. Fig. 3. (a) shows a TED (left) and a closed-core TSD (right) on the film grown at H_2/Ar ratio of 0.1 and Fig. 3. (b) shows three or four closed-core TSDs that were surrounded by a high density of TEDs on the film grown at a H_2/Ar ratio of 0.2.

At the H_2/Ar ratio of 0.33, most of the TSDs were still closed but some hollow-core TSDs were also present. The diameter and density of the hollow-cores TSDs were about $4 \sim 6 \mu\text{m}$ and 50 cm^{-2} , respectively, matching those of the micropipe in the substrate. At the H_2/Ar ratio of 0.5, the amount of hollow-core TSDs increased dramatically, to 90% of the total TSDs. The density of hollow-core TSDs was much larger than that of the micropipes in the substrate. The hollow-core TSDs and TEDs on the film grown at the

H₂/Ar ratio of 0.5 are shown in SEM images, Fig. 4: (a) two hollow-core TSDs, and (b) two hollow-core TSDs are surrounded by high density of TEDs.

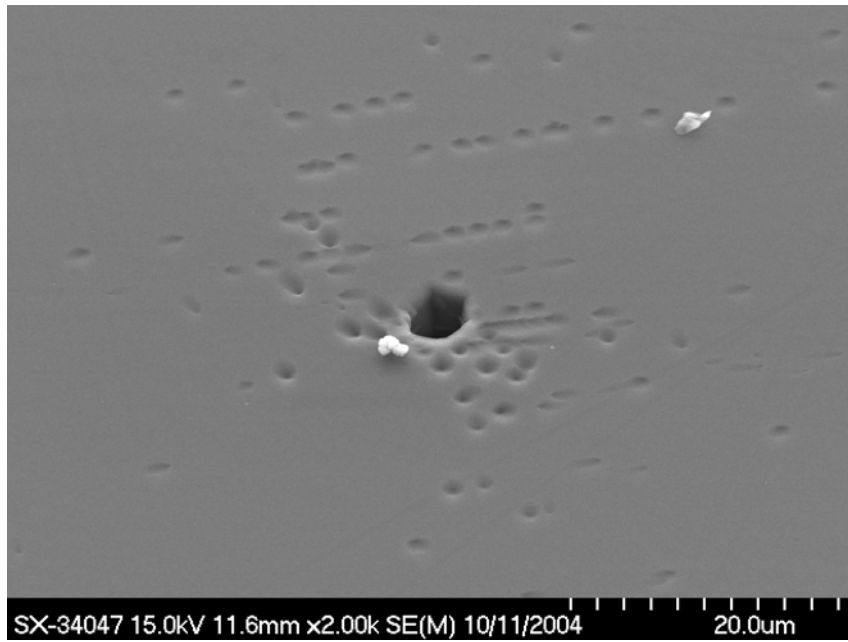
Kamata *et al.* [25] reported that a micropipe has a high probability of dissociating into several closed-core TSDs under relatively low C/Si ratio growth conditions. Nakamura *et al.* [26] observed that a low C/Si ratio enhances step flow growth and a high C/Si ratio enhances spiral growth around screw dislocation sites.

In our experiments, the C/Si ratio was changed from about 1 to C-rich by adjusting H₂/Ar ratio. SiC films grown at H₂/Ar ratios of 0.1, 0.125 and 0.2 show no hollow-core TSDs; most of the micropipes from the substrate dissociated into closed-core TSDs. The step flow speed is higher than the spiral step speed at these conditions. In Fig. 3.(b) a few closed-core TSDs are next to each other on a film, which were dissociated from a micropipe. The surrounded TEDs were converted from the high density of BPDs around a micropipe in the substrate, showed in Fig. 2. At the H₂/Ar ratio of 0.33, the densities of hollow-core TSDs in the film and micropipes in the substrate were the same, indicating that the flowing step speed was about the same as the spiral step speed and had no effect on the propagation of micropipes.

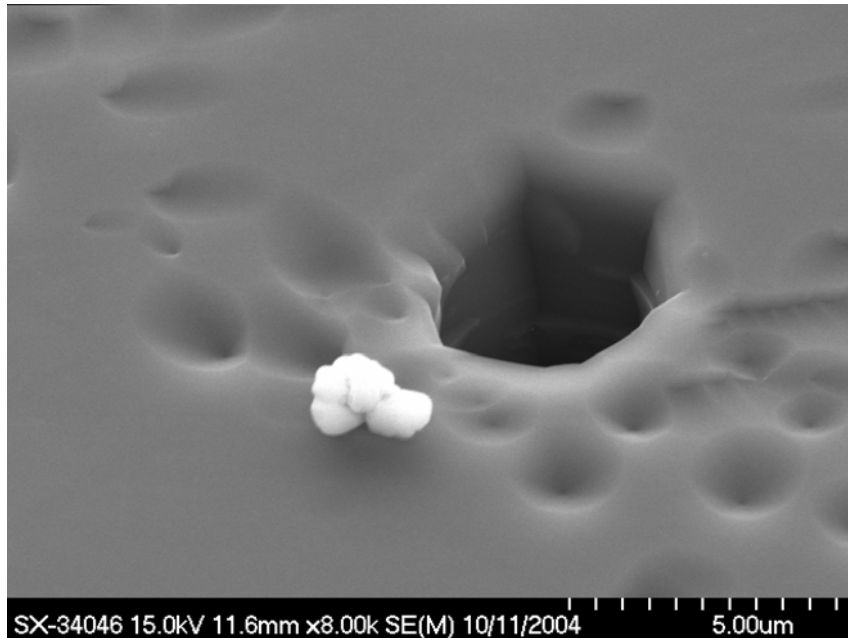
The above results match descriptions reported in the literature. The film prepared with a H₂/Ar ratio of 0.5 show the hollow-core TSDs with the density of hundreds cm⁻², much higher than the micropipe density in the substrates.

Basal plane dislocations (BPDs) appeared in all of the films regardless of the H₂/Ar ratios. Unlike the BPDs in the substrate, the BPDs in films have uniformed orientation toward the down-step, the off-axis cut orientation $[11\bar{2}0]$. A SEM image Fig. 5 (a) illustrates that on the film grown at the H₂/Ar ratio of 0.5, amongst a few TEDs were

three BPDs aligned on one same step all pointing the down-step direction. A single BPD is shown in a high magnification image Fig. 5 (b).

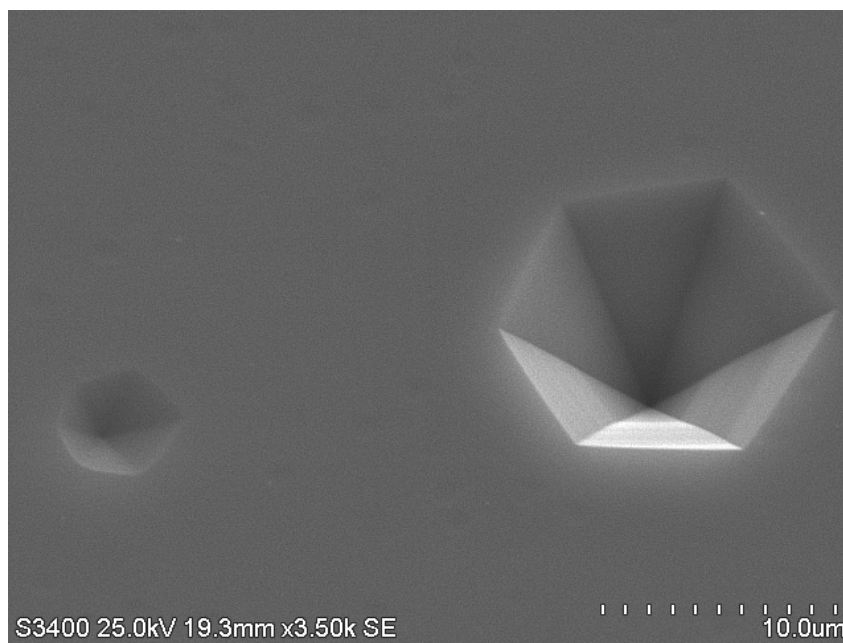


(a)

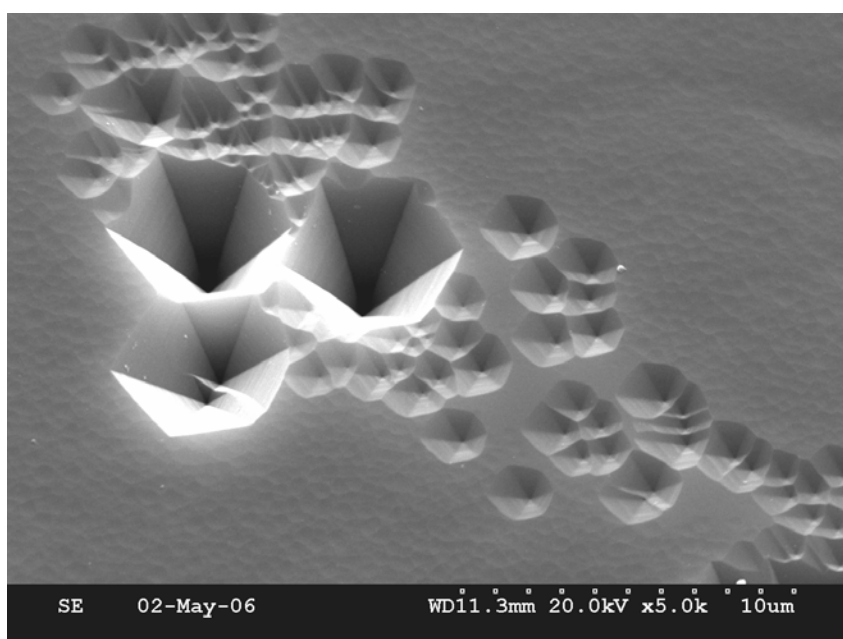


(b)

Fig. 2. SEM images of bare 4H-SiC substrate after molten KOH/NaOH etching, (a) 2kX, and (b) 8kX.

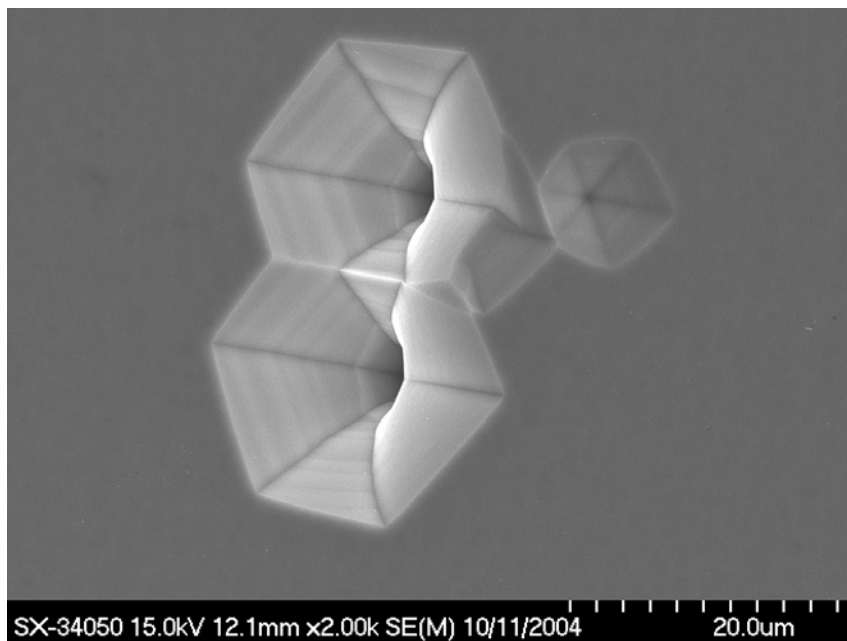


(a)

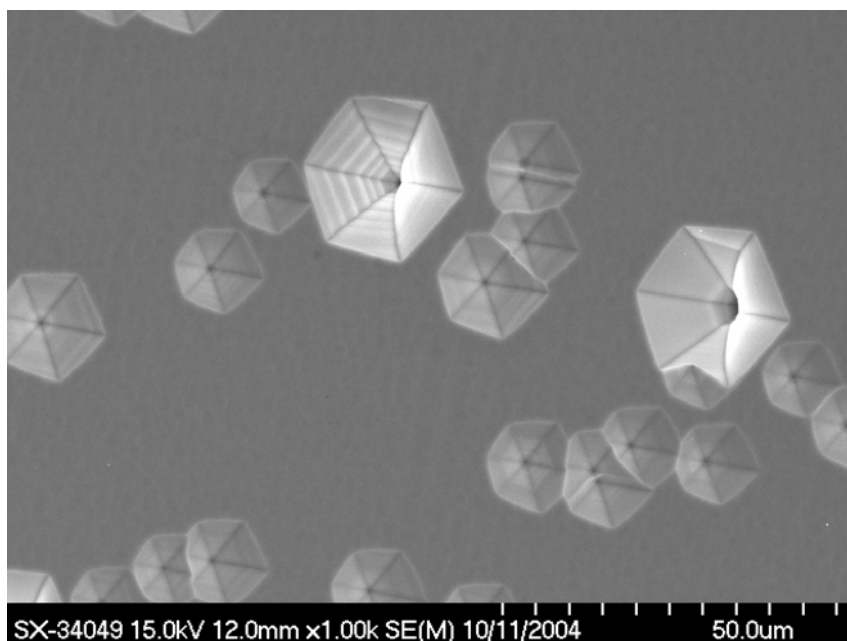


(b)

Fig. 3. (a) SEM image of the film grown at H_2/Ar ratio of 0.1 after etching: a TED and closed-core TSD, 3.5kX (b) SEM image of the film grown at H_2/Ar ratio of 0.2 after etching: closed-core TSDs surrounded by TEDs, 5kX.

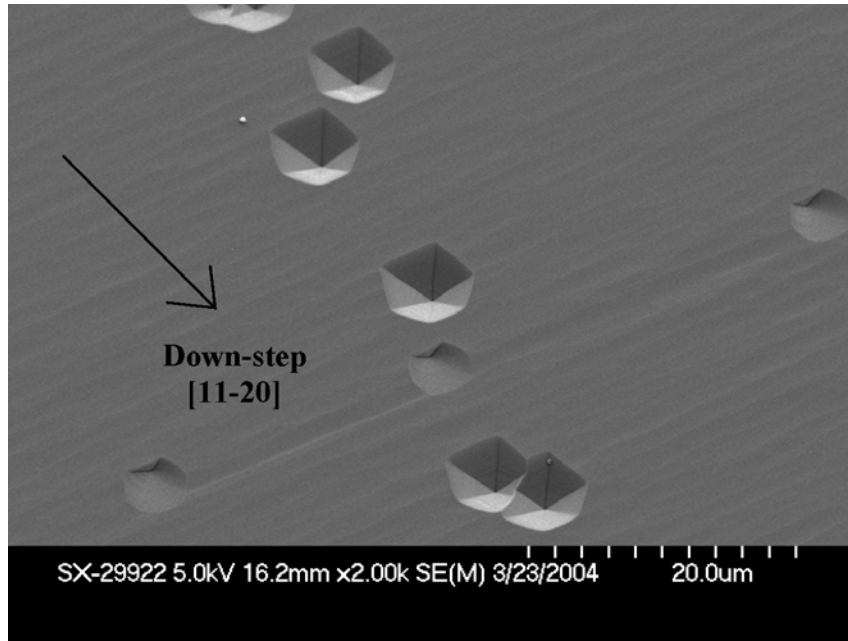


(a)

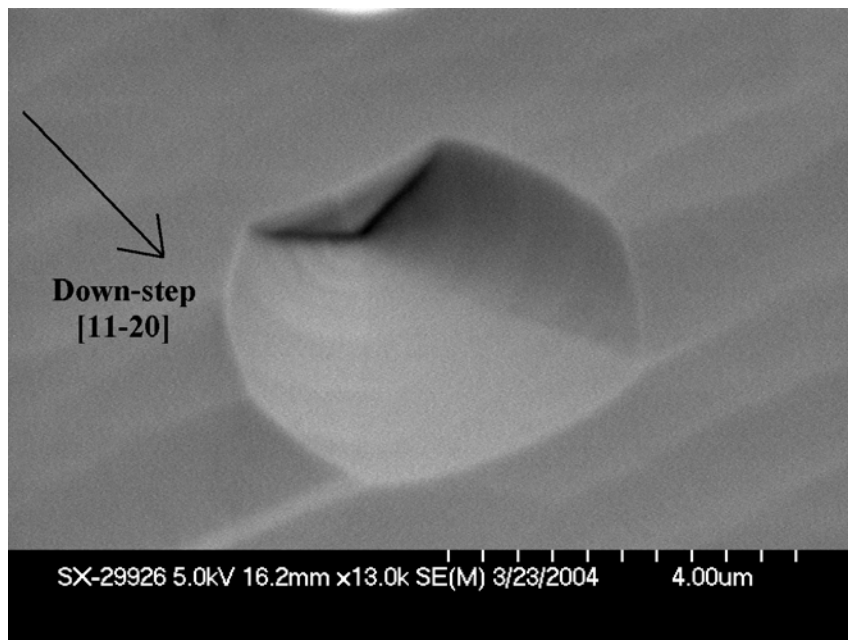


(b)

Fig. 4. SEM images of the film grown at the H_2/Ar ratio of 0.5: (a) two adjacent hollow-core TSDs, 2kX, and (b) two separated hollow-core TSDs are surrounded by high density of TEDs, 1kX.



(a)



(b)

Fig. 5. SEM images of the film grown at the H_2/Ar ratio of 0.5: (a) several TEDs and three BPDs aligned on one same step all pointing the down-step direction, 2kX, and (b) a single BPD, 13kX.

Fig. 6. summarizes the dislocation densities on all the grown films as a function of the H₂/Ar ratios. The BPDs density was about $2 \times 10^3 \text{ cm}^{-2}$ with H₂/Ar ratios of 0.1 and 0.125, but decreased to $500 \sim 800 \text{ cm}^{-2}$ for H₂/Ar ratios larger than 0.2. The BPDs density in the substrate was about $2.5 \times 10^4 \text{ cm}^{-2}$. The percent of the BPDs propagating from the substrate to the film decreased from 10 % to 2 %. The rest of the BPDs in the substrates might convert to TEDs in the grown films [18-21]. Klapper *et al.* [27] depicted that a dislocation, ending at a growing surface, will proceed into a newly grown layer in such a direction that the elastic energy of dislocation per unit growth length is minimum. Ohno *et al.*[20] calculated that the elastic energy per unit growth length of a BPD and a TED on the epilayer grown on the 4H-SiC with 8 ° off-axis towards $[11\bar{2}0]$ were $1.46 \times 10^{-7} \text{ J m}^{-1}$ and $2.30 \times 10^{-8} \text{ J m}^{-1}$, respectively. Since the elastic energy per unit growth length of a BPD is much larger than that of a TED, BPDs tend to convert to TEDs during the growth of the epilayer. Only a small portion of BPDs could propagate into the film and their orientations were all toward the down-step direction, as is shown in Fig. 5. At the low H₂/Ar ratios of 0.1 and 0.125, i.e. the C/Si ratio in the gas phase close to 1, the step flowing speed was relatively high, enhancing the probability that the BPDs will propagate from the substrate to the film. At the H₂/Ar ratios of 0.2 and higher, i.e. the C-rich gas phase, spiral growth around the dislocation sites was enhanced, [26] which restrained the propagation of BPDs and promotes the conversion of BPDs to TEDs.

As the H₂/Ar ratio increases from 0.1 to 0.5, the TED density decreased first and then increased, and the TSD density kept decreasing, as shown in Fig. 6. The lowest total dislocation density was obtained at the H₂/Ar ratio of 0.2, about $3 \times 10^4 \text{ cm}^{-2}$.

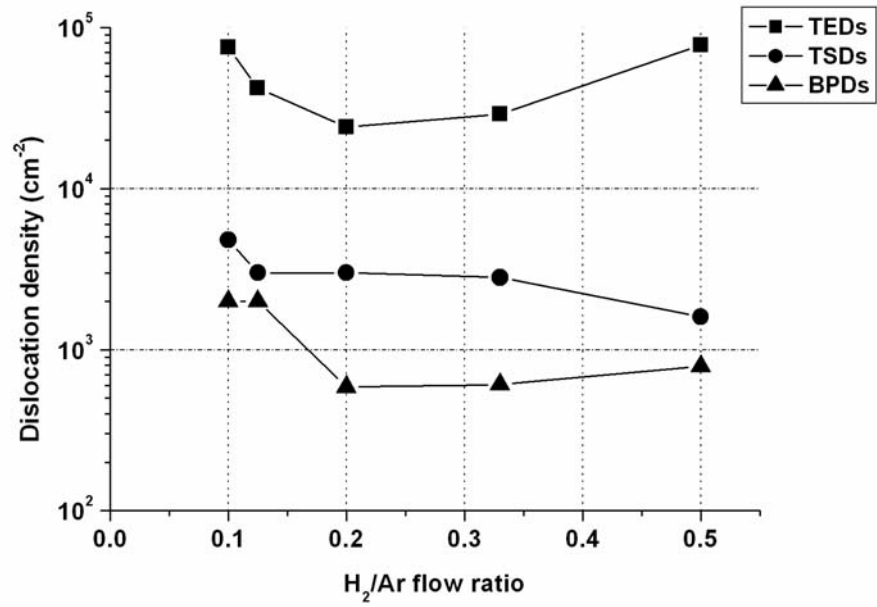


Fig. 6. Dislocation densities on the films grown at different H₂/Ar ratios.

4. Conclusions

In 4H-SiC homoepitaxial growth with MTS as the single precursor, the C/Si ratio in the gas phase can be changed by adjusting the H₂/Ar ratio in the main carrier gas. The optimum H₂/Ar flow ratio for SiC epitaxy was around 0.2: only 2% of BPDs in the substrate propagated into the epitaxial film, and most of the micropipes from the substrate dissociated into closed-core TSDs in the film. At the lower H₂/Ar ratio of 0.1 and 0.125, the resulting films were smooth and free of step-bunching, but more BPDs, about 10% in substrate, propagated into the epitaxial films. At a higher H₂/Ar ratio of 0.5, the regular macro-steps formed across the surface of the grown film increasing the surface roughness. Furthermore, the micropipes could propagate from the substrate into the film and many more hollow-core TSDs were generated during the epitaxy, which may dramatically degrade the electrical properties of the film. The change in the dislocation densities may be caused by the relationship between the step flowing speed and the spiral growth speed around screw dislocation sites under different C/Si ratio.

Acknowledgements

Support from the Office of Naval Research through Grant No. N000140610899 is gratefully appreciated.

References

1. B.J. Baliga, Res. Soc. Symp. Proc. 512, 77 (1998).
2. J.B. Casady and R.W. Johnson, Solid-State Electron. 39, 1409 (1996).
3. H. Tsuchida, I. Kamata, T. Jikimoto, T. Miyanagi and K. Izumi, Mater. Sci. Forum, 433 (2003), 131 (Silicon Carbide and Related Materials 2003).
4. F. Wischmeyer, D. Leidich and E. Niemann, Mater. Sci. Forum, 264 (1998), 127 (Pt.1, Silicon Carbide, III-Nitrides and Related Materials).
5. Y. Ishida, T. Takahashi, H. Okumura, K. Arai and S. Yoshida, Jpn. J. Appl. Phys., Part 1, 43 (8A), 5140 (2004).
6. S.M. Bishop, E.A. Preble, C. Hallin, A. Henry, L. Storasta, H. Jacobson, B.P. Wagner, Z.J. Reitmeier, E. Janzen and R.F. Davis, Mater. Sci. Forum, 457 (2004), 221 (Pt.1, Silicon Carbide and Related materials 2003).
7. P. Lu, J.H. Edgar, O.J. Glembocki, P.B. Klein, E.R. Glaser, J. Perrin and J. Chaudhuri, J. Crystal Growth 285, 506 (2005).
8. J.A. Powell, D.J. Larkin, and P.B. Abel, J. Electron. Mater. 24, 295 (1995).
9. J.A. Powell and D.J. Larkin, Phys. Stat. Sol. b 202, 529 (1997).
10. T. Kimoto, N. Miyamoto and H. Matsunami, IEEE Trans. Electron. Dev. 46, 471 (1999).
11. Z.Y. Xie, S.F. Chen, J.H. Edgar, K. Barghout, and J. Chaudhuri, Electrochem. Solid State Lett. 3, 381 (2000).
12. H. Matsunami and T. Kimoto, Mater. Sci. Eng Rep. 20, 125 (1997).
13. S. Ha, M. Skowronski, W.M. Better and M. Dudley, J. Appl. Phys. 92, 778 (2002).

14. W.M. Vetter and M. Dudley, *Philos. Mag. A*, 81, 2885 (2001).
15. D. Hull and D.J. Bacon, *Introduction to Dislocations*, 3rd ed. (Butterworth-Heinemann, Oxford, 1984), pp. 47-70.
16. Z. Zhang, and T.S. Sudarshan, *Appl. Phys. Lett.* 87, 161917 (2005).
17. Z. Zhang, and T.S. Sudarshan, *Appl. Phys. Lett.* 87, 151913 (2005).
18. W. Chen and M.A. Capano, *J. Appl. Phys.* 98, 114907 (2005).
19. S. Ha, P. Mieszkowski, M. Skowronski and L.B. Rowland, *J. Crystal Growth* 244, 257 (2002).
20. T. Ohno, H. Yamaguchi, S. Kuroda, K. Kojima, T. Suzuki and K. Arai, *J. Crystal Growth* 260, 209 (2004).
21. T. Ohno, H. Yamaguchi, S. Kuroda, K. Kojima, T. Suzuki and K. Arai, *J. Crystal Growth* 271, 1 (2004).
22. T. Kimoto, A. Itoh, H. Matsunami, and T. Okano, *J. Appl. Phys.* 81, 3494 (1997).
23. S.N. Gorin and L.M. Ivanova, *Phys. Stat. Sol. (b)* 202, 221 (1997).
24. V.V. Zelenin, V.G. Solov'ev, S.M. Starobinets, S.G. Konnikov and V.E. Chelnokov, *Semiconductors* 29 (6), 581 (1995).
25. I. Kamata, H. Tshuchida, T. Jikimoto and K. Izumi, *Jpn. J. Appl. Phys.* 41, L1137 (2002).
26. S. Nakamura, T. Kimoto and H. Matsunami, *Jpn. J. Appl. Phys.* 42, L846 (2003).
27. H. Klapper and H. Küppers, *Acta Cryst. A* 29, 495 (1973).